Sādhanā Vol. 28, Parts 3 & 4, June/August 2003, pp. 495–562. © Printed in India

Laser processing of materials

J DUTTA MAJUMDAR and I MANNA*

Metallurgical and Materials Engineering Department, Indian Institute of Technology, Kharagpur 721 302, India
e-mail: imanna@metal.iitkgp.ernet.in

Abstract. Light amplification by stimulated emission of radiation (laser) is a coherent and monochromatic beam of electromagnetic radiation that can propagate in a straight line with negligible divergence and occur in a wide range of wavelength, energy/power and beam-modes/configurations. As a result, lasers find wide applications in the mundane to the most sophisticated devices, in commercial to purely scientific purposes, and in life-saving as well as life-threatening causes. In the present contribution, we provide an overview of the application of lasers for material processing. The processes covered are broadly divided into four major categories; namely, laser-assisted forming, joining, machining and surface engineering. Apart from briefly introducing the fundamentals of these operations, we present an updated review of the relevant literature to highlight the recent advances and open questions. We begin our discussion with the general applications of lasers, fundamentals of laser–matter interaction and classification of laser material processing. A major part of the discussion focuses on laser surface engineering that has attracted a good deal of attention from the scientific community for its technological significance and scientific challenges. In this regard, a special mention is made about laser surface vitrification or amorphization that remains a very attractive but unaccomplished proposition.

Keywords. Laser processing; laser–matter interaction; laser surface vitrification.

1. Introduction

Laser, an acronym for light amplification by stimulated emission of radiation, is essentially a coherent, convergent and monochromatic beam of electromagnetic radiation with wavelength ranging from ultra-violet to infrared [1]. Laser can deliver very low (∼mW) to extremely high (1–100 kW) focused power with a precise spot size/dimension and interaction/pulse time (10^{-3} to 10^{-15}s) on to any kind of substrate through any medium [1–4]. Laser is distinguished from other electromagnetic radiation mainly in terms of its coherence, spectral purity and ability to propagate in a straight line. As a result, laser has wide applications from very mundane (bar code scanner) to most sophisticated (3-dimensional holography), mere commercial (audio recording) to purely scientific (spectroscopy), routine (printer) to futuristic (optical

*References in this paper have not been cited or prepared in journal format

computer), and life saving (surgery) to life threatening (weapons/guide). Laser is useful in metrology (length/velocity/ roughness measurement), entertainment (laser light show), medical diagnostics and surgery/therapy and optical communication/computation. From printer to pointer, surgery to spectroscopy, isotope separation to invisible surveillance and medical to material treatment, laser finds a ubiquitous presence mainly for some unique combination of properties. These important properties that justify the use of laser in such a wide spectrum of applications are (a) spatial and temporal coherence (i.e., phase and amplitude are unique), (b) low divergence (parallel to the optical axis), (c) high continuous or pulsed power density, and (d) monochromaticity [1–10].

Figure 1 presents a brief overview of the application of laser in different fields with diverse objective [1]. Though the list is not exhaustive, it serves to show the diversity of application of laser. In some applications, the power output is of main concern, e.g. atomic fusion and isotope separation. Sometimes, the main reason for using laser lies in its spectral purity and coherence (pollution detection, length/velocity measurement, interferometry, etc.), low divergence (laser show, pointer/guide, audio-player), or a combination of all of them (communication, holography, metrology). Accordingly, a host of lasers capable of delivering a wide variety of wavelength, energy, temporal/spectral distribution and efficiency have been developed over the last several decades [1].

In the present contribution, we would confine ourselves to only laser material processing. The intense heat that laser may produce on solid matter enables several types of ultrafast, novel and economical processing of material that are distinctly advantageous from the quality, productivity and efficiency point of view than that possible with their conventional counterparts. We will, at first, review the history of laser and enlist the main types of commercial laser used in material processing before introducing the working principle of the most

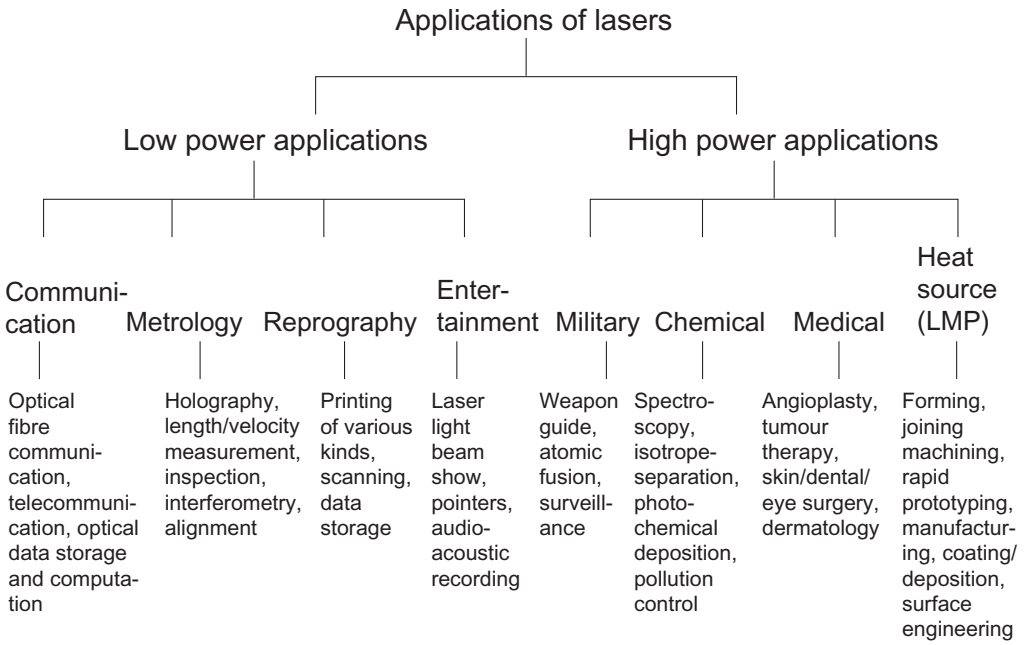

Figure 1. Application spectrum of lasers.

commonly used ones. Before embarking upon reviewing the current status of laser material processing, we will discuss the physics of laser–matter interaction and classify the different types of laser processing of materials. Finally, we will present a comprehensive update of the studies on different types of laser material processing and highlight the scientific and technological aspects of importance. In order to confine ourselves to the prescribed limit, we have deliberately reviewed the literature published from 1995 onwards. This cut-off, even though arbitrary, was unavoidable due to restriction on the length of the paper. However, this restriction applies only to the cited literatures but not to discussing the fundamentals of the subject. For further details on laser material processing, the textbook by Steen [1] is the most comprehensive source of information.

2. History of laser and its application

Laser is surely one of the greatest innovations of 20th century. Its continued development has been an exciting chapter in the history of science, engineering and technology. As a versatile source of pure energy in a highly concentrated form, laser has emerged as an attractive tool and research instrument with potential for applications in an extraordinary variety of fields.

The initial foundation of laser theory was laid by Einstein [11]. Subsequently, Kopfermann & Ladenburg [12] presented the first experimental confirmation of Einstein's prediction. In 1960, Maiman [13] developed a ruby laser for the first time. This was followed by much basic development of lasers from 1962 to 1968. Almost all important types of lasers including semiconductor lasers, Nd:YAG lasers, CO_2 gas lasers, dye lasers and other gas lasers were invented in this era. After 1968, the existing lasers were designed and fabricated with better reliability and durability. By mid 1970s more reliable lasers were made available for truly practical applications in the industrial applications such as cutting, welding, drilling and marking. During the 1980s and early 1990s the lasers were explored for surface related applications such as heat treatment, cladding, alloying, glazing and thin film deposition.

Table 1 summarises commercially available lasers and their main areas of application. Depending on the type of laser and wavelength desired, the laser medium is solid, liquid or gaseous. Different laser types are commonly named according to the state or the physical properties of the active medium. Consequently, we have crystal, glass or semiconductor, solid state lasers, liquid lasers, and gas lasers. The latter (gas lasers) can be further subdivided into neutral atom lasers, ion lasers, molecular lasers and excimer lasers. The typical commercially available lasers for material processing are (a) solid state crystal or glass laser – Nd:YAG, Ruby, (b) semiconductor laser – AlGaAs, GaAsSb and GaAlSb lasers, (c) dye or liquid lasers-solutions of dyes in water/alcohol and other solvents, (d) neutral or atomic gas lasers – He–Ne laser, Cu or Au vapour laser, (e) ionized gas lasers or ion lasers – argon (Ar^+) and krypton (Kr^+) ion lasers, (f) molecular gas lasers – CO_2 or CO laser, and (g) excimer laser – XeCl, KrF, etc. Wavelengths of presently available lasers cover the entire spectral range from the far-infrared to the soft X-ray.

3. Generation of laser

Laser is a coherent and amplified beam of electromagnetic radiation or light. The key element in making a practical laser is the light amplification achieved by stimulated emission due to the

Table 1. Commercially available lasers and their industrial applications.

Laser	Year of discovery	Commercialised since	Application
Ruby	1960	1963	Metrology, medical applications, inorganic material processing
Nd-Glass	1961	1968	Length and velocity measurement
Diode	1962	1965	Semiconductor processing, biomedical applications, welding
He–Ne	1962		Light-pointers, length/velocity measurement, alignment devices
Carbon dioxide	1964	1966	Material processing-cutting/joining, atomic fusion
Nd-YAG	1964	1966	Material processing, joining, analytical technique
Argon ion	1964	1966	Powerful light, medical applications
Dye	1966	1969	Pollution detection, isotope separation
Copper	1966	1989	Isotope separation
Excimer	1975	1976	Medical application, material processing, colouring

incident photons of high energy. A laser comprises three principal components, namely, the gain medium (or resonator), means of exciting the gain medium into its amplifying state and optical delivery/feed back system. Additional provisions of cooling the mirrors, guiding the beam and manipulating the target are also important. The laser medium may be a solid (e.g. Nd:YAG or neodymium doped yttrium–aluminum–garnet), liquid (dye) or gas (e.g. CO_2, He, Ne, etc.). For gas and diode lasers, the energy is usually introduced directly by electric-current flow, whereas, an intense flash of white light produced by incandescent lamps introduces the excitation energy in solid state crystal lasers. The sudden pumping of energy causes the laser medium to fluoresce and produce intense monochromatic, unidirectional (parallel/convergent) and coherent rays [1,2]. Among the commercially available lasers, CO_2-laser seems one of the earliest developed and most popular lasers for material processing because they are electrically more efficient (15–20%) and produce higher powers (0·1–50 kW) than other lasers in the continuous mode. Despite being less efficient in energy coupling with metals due to longer wavelength (10·6 μm), the higher wall plug ($\sim$ 12%) and quantum ($\sim$ 45%) efficiency and output power level of CO_2 lasers more than compensate for the poor laser–matter energy coupling capability. On the other hand, Nd:YAG and Ruby lasers possess shorter wavelength and are more suited to pulsed mode of applications requiring deeper penetration, smaller area coverage and precision treatment of materials for specific purposes.

As illustrated in figure 2a, the CO_2-laser device consists of three main parts – a gain or laser medium, an optical resonator or cavity with two mirrors, and an energizing or pumping source that supplies energy to the gain medium. The chemical species in the gain medium determines the wavelength of the optical output. Between the two mirrors, one is a fully reflecting and the other a partially reflecting one. From the quantum mechanical principle, when an external energy is supplied to an atom, the irradiated atom attains an excited state

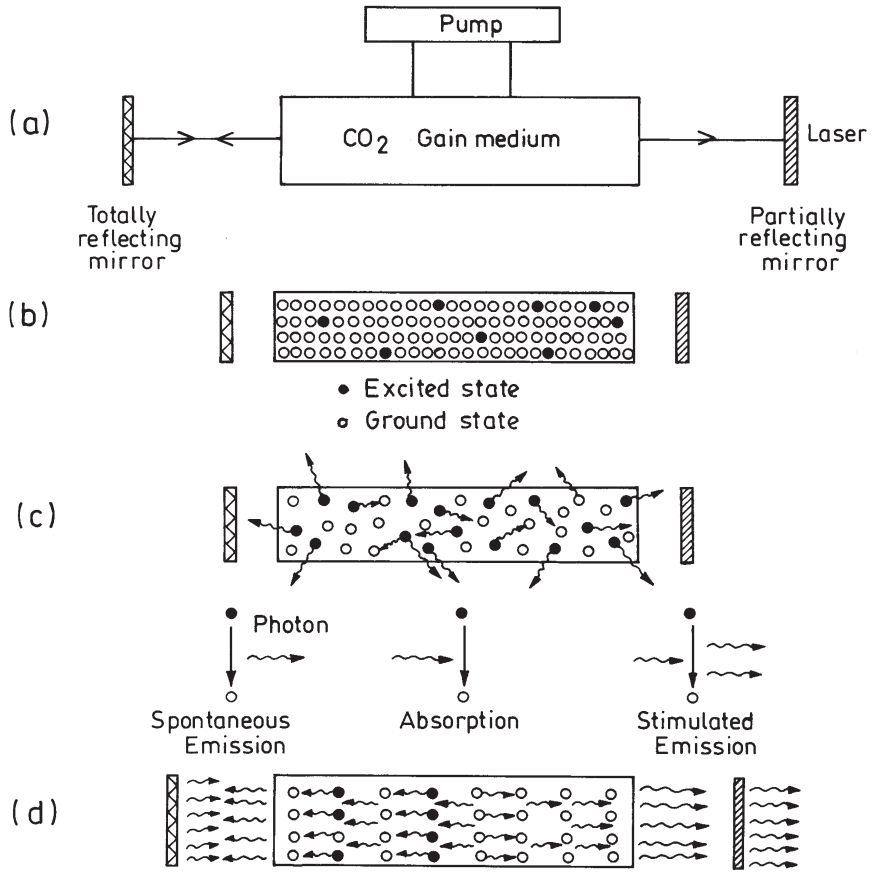

Figure 2. Schematic set-up of continuous wave CO_2 laser. **(a)** The major constituents of the machine, **(b)** initial stage of energy pumping, **(c)** excitation and de-excitation of the atoms in the medium leading to emission of laser and **(d)** stimulated emission and formation of laser beam.

(figure 2b). The excited atom spontaneously returns to the ground state (E_1) from the higher energy state (E_2) by emitting the energy difference as a photon of frequency (ν):

$$\nu = (E_2 - E_1)/h, \tag{1}$$

where, h is the Planck's constant. This phenomenon is known as spontaneous emission (figure 2c). A spontaneously emitted photon may in turn excite another atom and stimulate it to emit a photon by de-exciting it to a lower energy level. This process is called stimulated emission of radiation (figure 2c). The latter is coherent with the stimulating radiation so that the wavelength, phase and polarization between the two are identical. A photon interacting with an unexcited atom may get absorbed by it and excite it to higher energy state. This situation, called 'population inversion' is created by the pumping source. The photons moving along the optic axis interact with a large number of excited atoms, stimulate them and by this process get amplified. They are reflected back and forth by the resonator mirrors and pass through the excited medium creating more photons. In each round trip, a percentage of these photons exit through the partially transmitting mirror as intense laser beam (figure 2d). Finally, the

laser beam is either guided on to the work-piece by using reflecting mirrors or delivered at the desired site through optical fibres.

Figure 3 shows a schematic outline of a solid state neodymium doped yttrium aluminum garnet (Nd:YAG). The generation of high average power in Nd–YAG laser systems is accomplished by combining several individually pumped laser rods in a single resonator. Pumping is performed with arc lamps mounted in a close coupling optical geometry that ensures the maximum possible absorption of visible pump radiation by the laser rod. This optimizes both pumping efficiency and energy extraction efficiency. Energy pumping selectively energizes the Nd ions that subsequently lead to a cascading effect and stimulated emission of light. These days, energy pumping is also done with diode lasers of appropriate frequency. Nd:YAG laser has 40% quantum efficiency. However, the overall electrical efficiency of YAG lasers is low. The ratio of laser output power to electrical input power lies in the range 0·5–3%. The major advantages of Nd–YAG laser over CO_2 laser lie in its smaller wavelength (1·06 μm) and ability to deliver laser radiation through optical fibers.

4. Laser–matter interaction in material processing

The input of energy or energy deposition process from a pulsed/continuous wave laser beam into the near-surface regions of a solid involves electronic excitation and de-excitation within an extremely short period of time [8–10]. In other words, the laser–matter interaction within the near-surface region achieves extreme heating and cooling rates (10^3–10^{10} K/s), while the total deposited energy (typically, 0·1–10 J/cm^2) is insufficient to affect, in a significant way, the temperature of the bulk material. This allows the near-surface region to be processed under extreme conditions with little effect on the bulk properties.

4.1 *Lattice heating*

The initial stage in all laser-metal processing applications involves the coupling of laser radiation to electrons within the metal. This first occurs by the absorption of photons from the

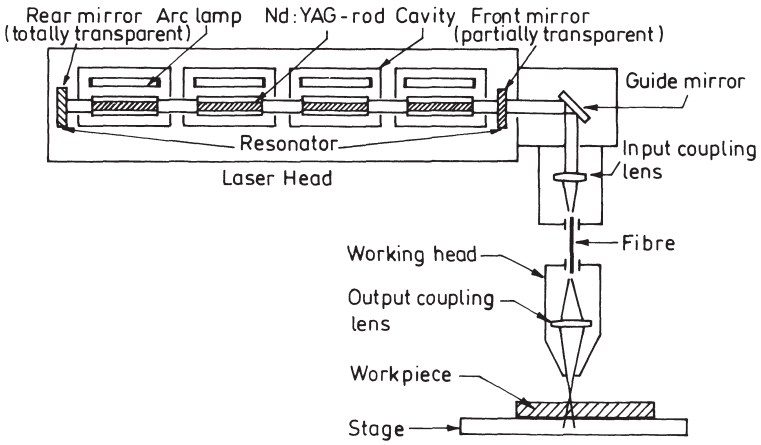

Figure 3. Schematic set-up of pulsed solid state neodymium–doped yttrium–aluminum–garnet (Nd:YAG) laser.

incident laser beam promoting electrons within the metal to states of higher energy. Electrons that have been excited in this manner can divest themselves of their excess energy in a variety of ways. For example, if the photon energy is large enough, the excited electrons can be removed entirely from the metal. This is the photoelectric effect and usually requires photon energies greater than several electron volts. Most laser processing applications, however, utilize lasers emitting photons with relatively low energy. The energy of CO_2 laser photons is only 0·12 eV while the photons obtained from the Nd:YAG laser have about 1·2 eV of energy. Electrons excited by absorption of CO_2 or Nd:YAG laser radiation do not therefore have enough energy to be ejected from the metal surface. Such electrons must, nevertheless, lose energy to return to an equilibrium state after photon excitation. This occurs when excited electrons are scattered by lattice defects like usual non-crystalline regions in a crystal such as dislocations and grain boundaries such as the lattice deformation produced by photons. In either case, the overall effect is to convert electronic energy derived from the beam of incident photons into heat. It is this heat that is useful (indeed necessary) in all surface treatment applications.

4.2 *Energy absorption*

Figure 4 describes the process that is important in electron excitation and excited carrier relaxation process involved during laser–matter interaction [8]. Photon interaction with matter occurs usually through the excitation of valence and conduction band electrons throughout the wavelength band from infrared (10 μm) to ultraviolet (0·2 μm) region. Absorption of wavelength between 0·2–10 μm leads to intra-band transition (free electrons only) in metals and inter-band transition (valence to conduction) in semiconductors. Conversion of the absorbed energy to heat involves (a) excitation of valence and/or conduction band electrons, (b) excited electron-phonon interaction within a span of 10^{-11}–10^{-12} s, (c) electron-electron or electron-plasma interaction, and (d) electron-hole recombination within 10^{-9}–10^{-10} s (Auger process). Since free carrier absorption (by conduction band electrons) is the primary route of energy absorption in metals, beam energy is almost instantaneously transferred to the lattice by electron-phonon interaction.

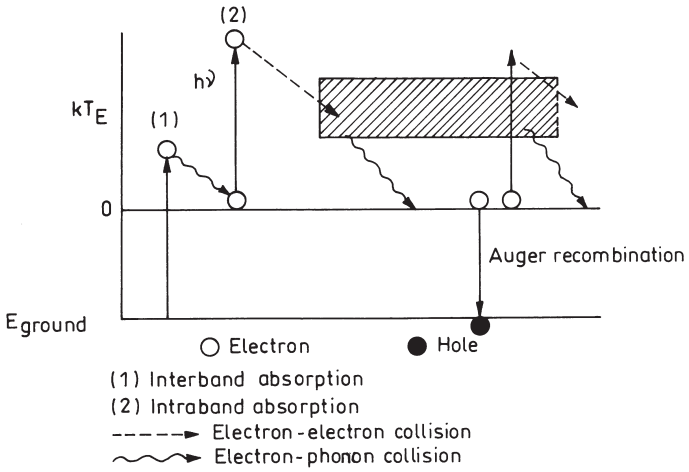

Figure 4. Schematic diagram depicting electron excitation and carrier relaxation process in materials subjected to intense laser irradiation.

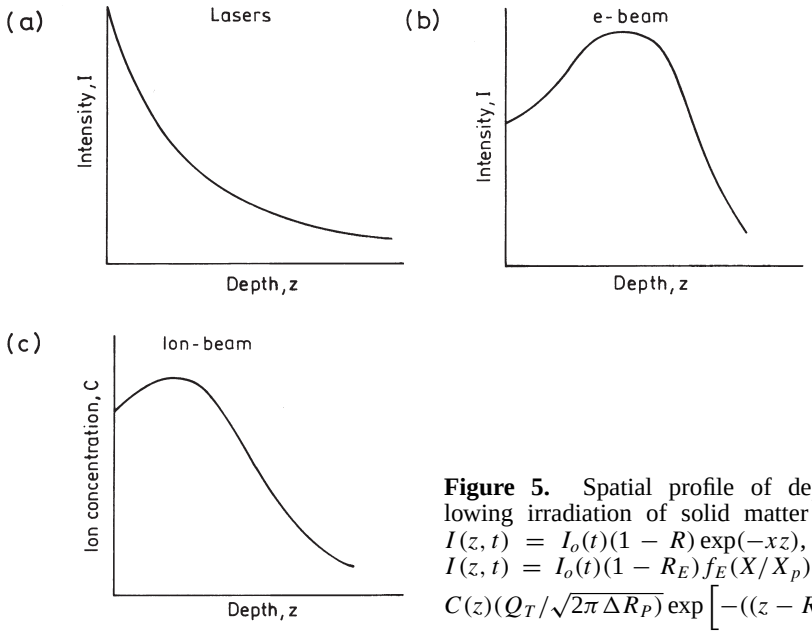

Figure 5. Spatial profile of deposited energy following irradiation of solid matter by **(a)** laser beam $I(z,t) = I_o(t)(1-R)\exp(-xz)$, **(b)** electron beam– $I(z,t) = I_o(t)(1-R_E)f_E(X/X_p)$, and **(c)** ion beam– $C(z)(Q_T/\sqrt{2\pi\Delta R_P})\exp\left[-((z-R_P)/\sqrt{\sqrt{2}\Delta R_P})\right]$.

4.3 *Spatial distribution of deposited energy*

The spatial profile of deposited energy from laser beam is illustrated in figure 5a. For laser irradiation, the beam intensity I at a depth z for the normally incident beam of initial intensity I_o (in W/m^2) is given by [8]

$$I(z,t) = I_o(t)(1-R)\exp(-\alpha z), \tag{2}$$

where, I_o is the incident intensity, t is time, R and α are the reflectivity and absorption coefficients, respectively. Since α is very high ($\sim 10^6\,\mathrm{cm}^{-1}$) for metals, light is totally absorbed within a depth of 100–200 Å. The efficiency of optical coupling is determined by the reflectivity (R). R for metals is relatively low at short wavelengths, rises abruptly at a critical wavelength (related to the plasma frequency of the free electron plasma), and then remains very high at long wavelength [8].

For comparison, the deposited energy profile from the other two important directed-energy-sources, namely electron and ion beams, are also shown in figure 5b and figure 5c, respectively. The energy deposition profile for electron beam irradiation of matter is given by a gaussian function,

$$I(z,t) = I_o(t)(1-R_E)f_E(x/x_P), \tag{3}$$

where, R_E is the reflectivity for e-beam, x_P is the distance (x) that coincides with the peak intensity and $f_E(x/x_P)$ is the spatial energy deposition profile. The deposition profile depends on the energy loss hence on incident energy and atomic number. Thus, electron beam is more suited to deep penetration welding than surface engineering applications. Similarly, the concentration of the implanted species in ion beam irradiation does not coincide with the top surface but lies underneath the surface (4):

$$C(z) = \left[Q_T/(2\pi)^{1/2}\Delta R_P\right]\left\{\exp\left[-\left(\frac{z-R_P}{\sqrt{2}\Delta R_P}\right)^2\right]\right\}, \tag{4}$$

Here, $C(z)$ is the concentration of a given species at a vertical distance z, R_p is the projected range/distance and Q_T is the dose.

4.4 *Heating due to laser irradiation*

Usually, the deposited energy of laser irradiation is converted into heat on a time scale shorter than the pulse duration or laser interaction time [8]. The resulting temperature profile depends on the deposited energy profile and thermal diffusion rate during laser irradiation. Thermal diffusivity (D) is related to thermal conductivity (k) and specific heat (C_P) as follows:

$$D = k/(\rho C_P), \tag{5}$$

where, ρ is the density. The vertical distance (z) over which heat diffuses during the pulse duration (t_p) is given by, $z = (2Dt_p)^{1/2}$. Here, z in comparison to α^{-1} determines the temperature profile. The condition of $\alpha^{-1} \ll z$ is applicable typically for laser irradiation of metals.

Under the one dimensional heat flow condition, the heat balance equation may be expressed as [5]:

$$\rho c_p \frac{\partial T(z,t)}{\partial T} = Q(z,t) + \frac{\partial}{\partial z}k\frac{\partial T(z,t)}{\partial z} \tag{6}$$

where, T and Q are the temperature and power density at a given vertical distance of depth (z) and time (t), respectively. Q follows a functional relation with z same as (2). The heat balance equation (6) may be solved analytically if the coupling parameters (α and R) and materials parameters (ρ, k and c_P) are not temperature and phase dependent. However, phase changes are unavoidable except in solid state processing. Thus, the heat balance equation is solved by numerical techniques like finite difference/element methods.

Depending on the temperature profile, the irradiated material may undergo only heating, melting or vapourization. For surface melting and subsequent re-solidification, the solid-liquid interface initially moves away from and then travels back to the surface with the velocity as high as 1–30 m/s. The interface velocity is given by $v \propto (T_m - T_i)$, where T_m and T_i are the melting and interface temperatures, respectively [8]. Further details on mathematical modelling of heat transfer in laser material processing may be obtained in several textbooks [5,6].

5. Laser material processing

The increasing demand of laser in material processing can be attributed to several unique advantages of laser namely, high productivity, automation worthiness, non-contact processing, elimination of finishing operation, reduced processing cost, improved product quality, greater material utilization and minimum heat affected zone [1–10]. Figure 6 shows a general classification of the laser material processing techniques. In general, application of laser to material processing can be grouped into two major classes, (a) applications requiring limited energy/power and causing no significant change of phase or state, and (b) applications

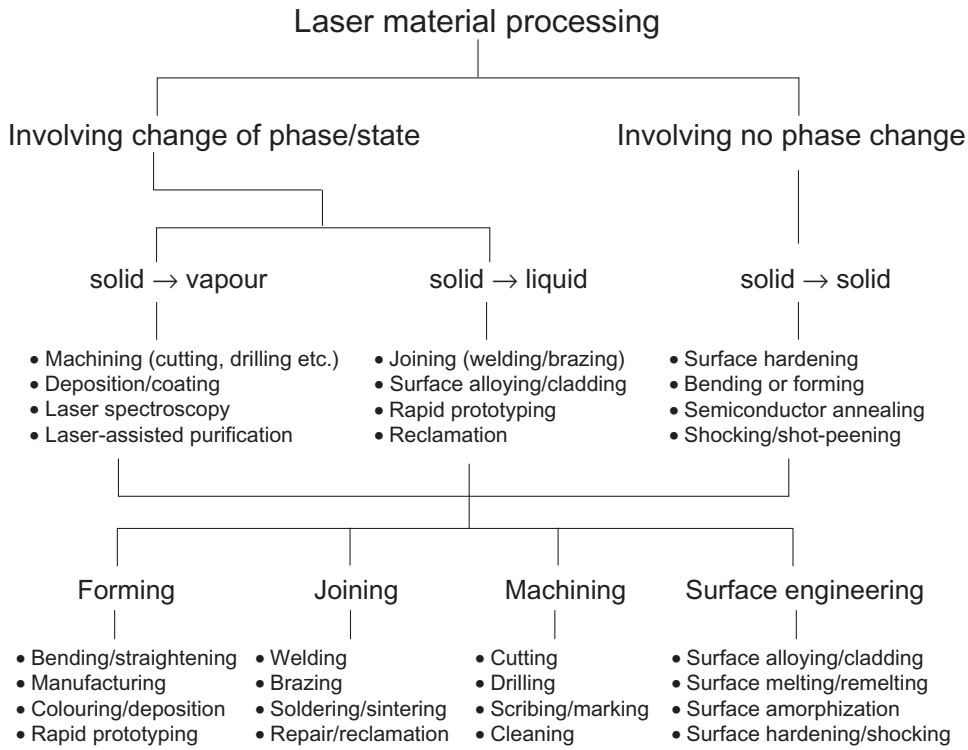

Figure 6. Classification of laser material processing.

requiring substantial amount of energy to induce the phase transformations. The first category includes semiconductor annealing and etching, polymer curing, scribing/marking of integrated circuit substrates, etc. The second type of application encompasses cutting, welding, fusion, heat treatments, etc. The average power and efficiency of lasers are not that important for the former category that involves no change in phase or state. Lasers suitable for this group of applications include (but not limited to) excimer lasers (KrF, ArF), ion lasers (Ar^+, Kr^+), metallic vapour lasers (cadmium, selenium, copper, gold), solid state lasers (Nd–YAG, Nd–glass), semiconductor lasers (gallium aluminum arsenide, etc.), and molecular lasers (CO_2, CO, etc.). For the second category, laser power/efficiency and interaction-time are crucial as the processes involve single or multiple phase changes within a very short time. Because of high-energy requirement, for this class of operations, CO_2 and Nd–YAG lasers are practically the only choice.

The classification based on phase changes or no phase changes is too academic to be of real use to the end users. From the true application point of view, laser material processing can be broadly divided into four major categories, namely, forming (manufacturing of near net-shape or finished products), joining (welding, brazing, etc.), machining (cutting, drilling, etc.) and surface engineering (processing confined only to the near-surface region) [1–20]. Figure 6 presents this classification in the lower half of the figure mentioning a few representative examples from each category of application. However, this classification is based on the general definition and scope of the processes as understood in conventional practice, but is certainly not sacrosanct.

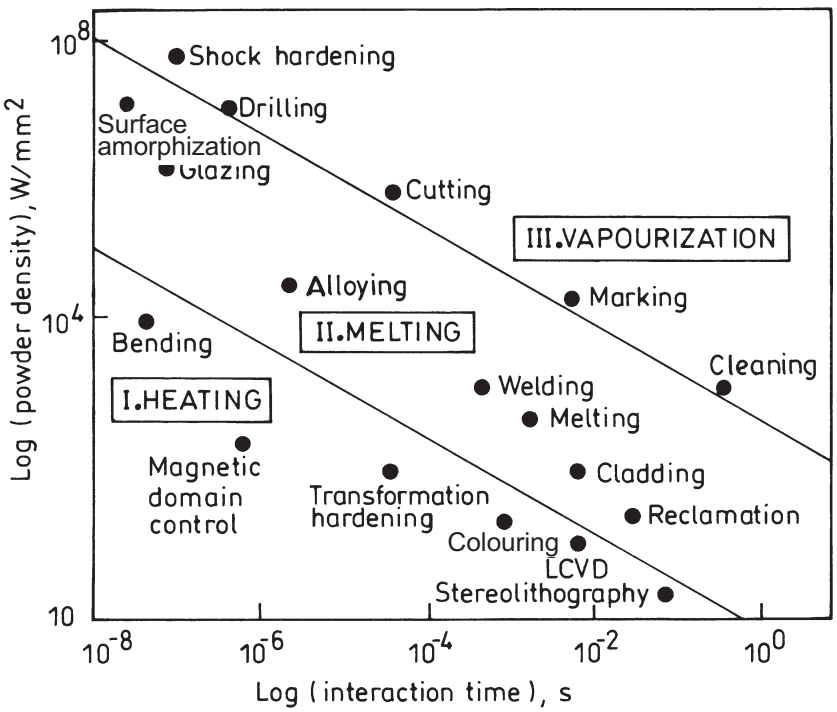

Figure 7. Process map (schematic) in terms of laser power density as a function of interaction time for different examples of laser material processing.

The domain for different laser material processing techniques as a function of laser power and interaction time is illustrated in figure 7 [1]. The processes are divided into three major classes, namely involving only heating (without melting/vapourizing), melting (no vapourizing) and vapourizing. Obviously, the laser power density and interaction/pulse time are so selected in each process that the material concerned undergoes the desired degree of heating and phase transition. It is evident that transformation hardening, bending and magnetic domain control which rely on surface heating without surface melting require low power density. On the other hand, surface melting, glazing, cladding, welding and cutting that involve melting require high power density. Similarly, cutting, drilling and similar machining operations remove material as vapour, hence need delivery of a substantially high power density within a very short interaction/pulse time. For convenience, a single scalar parameter like energy density (power density multiplied by time, J/mm^2) is more useful for quantifying different laser assisted processes. However, the practice is not advisable as the specific combination of power and time (rather than their product) can only achieve the desired thermal and material effect.

In the following sections, we review the individual classes of laser material processing and the current status of understanding.

6. Laser forming

One of the major goals of material processing is to produce finished products of correct design, shape, geometry and dimension. Manufacturing a finished product is seldom a one-

step process. On the contrary, developing a final product involves several primary (procuring, winning/extraction, selection, blending), secondary (melting, casting, compaction, sintering) and tertiary (machining, polishing, shaping) steps that are all inter-related, complex and time/energy/manpower intensive. Laser material processing offers a unique possibility of manufacturing finished products directly from the raw materials without any elaborate intermediate operation [1–4,15]. A one-step fabrication is most attractive, obviously for the tremendous economy in time, cost, material and manpower than that necessary for the usual route of fabrication. Though such possibility is not unlimited and rather confined to only a few types of materials and operations, nevertheless, direct fabrication of components using laser as a non-contact tool is obviously a breakthrough that must be vigorously pursued.

Among the several types of laser assisted forming or manufacturing processes in vogue, the major and successful ones include laser assisted bending, colouring, rapid prototyping, fabrication, deposition, and laser reclamation/repairing [1–4]. These processes distinguish themselves from other laser material processing methods in their proclaimed objective of single-step manufacturing of a finished or semi-finished product than serving to any other intermediate processing aim like machining, joining or surface engineering. For brevity, we will address all these laser-assisted versions of otherwise conventional manufacturing processes as laser forming.

Table 2 summarizes the major and representative studies carried out in the broad area of laser forming in the recent past (1995 onwards) [21–38]. These studies are selected primarily to emphasize the variety of possibilities and their status in laser forming of materials.

6.1 *Laser bending*

Laser bending is a newly developed flexible technique capable of modifying the curvature of sheet metal by thermal residual stresses without any externally applied mechanical forces [21–25]. Laser bending may also serve the purpose of straightening thin sheets by a similar laser based non-contact process without mechanical forces. The process assumes significance due to the ease and flexibility of non-contact processing, amenability to materials with diverse shape/geometry, properties and chemistry, and high precision/productivity. Laser bending involves a complex interplay between the thermal profile generated by the laser irradiation and physical/thermal properties and dimension of the material/work-piece. The dimensional accuracy of parts produced by bending processes is a topical issue. In general, the process is influenced by many parameters such as laser parameters (power density and interaction/pulse time), material properties (thermal conductivity, coefficient of thermal expansion, etc.) and target dimensions (thickness, curvature, etc.). Laser bending of high strength alloys has been an important motivation for the increasing interest in laser forming process. However, success in laser bending of thick ($>$ 1–2 mm) high strength steel or superalloy sheets is not yet achieved. The materials mostly amenable to bending are Al/Ti-alloys and stainless or low alloy steels. Apart from metallic sheets, the success of laser bending of semiconductor and polymeric sheets are eagerly awaited by the semiconductor and packaging industry.

Chan & Liang [21] have recently studied the influence of reinforcement volume fraction on the thermal expansion behaviour and bending angle of the Al2024 alloy reinforced with 15–20% SiC in laser bending. Under comparable processing conditions, a larger bending angle is obtained for the composite with 15% reinforcement. The coefficient of thermal expansion of the composite seems to follow different functional relationships with temperature in different temperature regimes. Thus, it is necessary to consider a varying degree of coefficient of thermal expansion of the composite to predict the bending angle as a function of laser power or interaction time. In fact, thermal profile across a dissimilar layer following laser irradiation

Table 2. Summary of selected studies on laser forming of materials in the recent past (1995 onwards).

Process	Year	Material	Laser	Scope	Results	Ref.
Laser bending						
Bending	2001	Al–2024 and 15–20% SiCp composite	Pulsed laser	Study the effect of reinforcement on bending angle and compare the predicted results	The smaller the reinforcement, the higher the bending angle. A single model cannot account for all regimes	[21]
Bending	2000	Stainless steel sheet	Pulsed Nd:YAG	Study the effect of process parameters on bending angle	Bending varies inversely with sheet thickness and directly with power (below a minimum or threshold)	[22]
Bending	1999	Stainless steel sheet	Nd:YLF, line-shaped pulsed	Finite element modelling of thermoelastoplastic mode of deformation	Reflectivity and thermal expansion coefficient influence the bending more than any other parameter	[23]
Bending	1998	AlCuMg-and α/β–Ti alloy	CW–CO_2 and Nd:YAG	Study the effect of laser parameters and analytically determine plain strain	Bend rate/angle primarily depends on temperature and decreases with pulses due to material accumulation at bend	[24]
Ceramic coating on metals	1995	Cr_2O_3 coating on SAF 2205 steel	CW–CO_2	Study the interfacial bonding strength and compatibility between Cr_2O_3 and steel	Up to 200 μm thick Cr_2O_3 cladding on steel possible by laser cladding. Stress at the interface is very high	[25]
Laser manufacturing						
Laser metal forming for repair	2001	Superalloy	CW–CO_2	Epitaxial laser metal forming of single crystal high-pressure high-temperature turbine blade	Microstructural maps predicting (solidification microstructure, growth morphology, composition) constructed	[26]

(Continued)

Table 2. (*Continued*).

Process	Year	Material	Laser	Scope	Results	Ref.
Laser metal forming	1999	Ni-based superalloy	CW–CO_2	Utilize electron back scattered image for orientation determination of laser formed layer	Close control of solidification micro-structure and orientation distribution is possible in epitaxially grown layer	[27]
Laser aided thixotropic casting	1996	Hydroxyapatite + AISI 316 stainless steel	CW–CO_2	Develop funtionally graded clad of ceramic-metal layer by laser aided thixotropic casting	Functionally + compositionally graded layers (ceramic to metal) developed by laser thixo-casting under vibration	[28]
Laser rapid prototyping						
Laser rapid prototyping	2001	Pulsed-CO_2	Polyvinyl chloride	Develop thick (130 μm) masks for electrodeposition of double metallic layers on cylinder/rod	Cu on rotating Pt disc and NiFe criss-cross pattern on cylindrical rods were deposited by pattern transfer	[29]
Stereo-lithography	2001	He–Cd laser (325 nm)	Alumino-slicate ceramic powder	Stereolithographic fabrication of free standing ceramic shapes	The green was successfully developed from ceramics and sintered at 1600°C	[30]
Composite surfacing	2000	CW–CO_2	Cu–Ti–C and Cu–Ti–Ni–C	Develop a TiC dispersed surface composite layer	Addition of Ni helps in better melting and wetting of TiC in the composite	[31]
Laser rapid prototyping	2000	Q-switched Nd:YAG	Li–niobate and K–titanyl phosphate	Rapid prototyping by second harmonic generation (SHG) in suspended nonlinear crystals	SHG, that turns liquid photo-polymer into solid, is a function of particle size and density. SHG is useful in rapid prototyping and 3-D image formation	[32]
Laser rapid prototyping	1997	Pulsed laser	Al_2O_3	Develop photonic band gap structures by laser rapid prototyping	3-dimensional photonic band gap structure was created by vapour deposition of FCT-Al_2O_3 into rods	[33]
3-D micro-strcture	1995	Pulsed laser	$Al + Al_2O_3$	Develop 3-D microstructure by laser driven movement	Thermal expansion by laser irradiation allows 1-step direct-write prototyping	[34]

(Continued)

Table 2. (*Continued*).

Process	Year	Material	Laser	Scope	Results	Ref.
Laser colouring						
Colouring bleaching	2000	Pulsed KrF excimer and Nd:YAG laser	Amorphous WO_3 film	Colouring of laser deposited thin WO_3 film by laser irradiation and study the mechanism	Brown (photo-chemical activation) to purple (photo-thermal oxidation) colours obtained by colouring/bleaching action	[35]
Colouring deforming	2000	Femtosecond pulsed laser	Nano-Ag embedded glass	Study mechanism of colouring by laser induced deformation of nano-Ag particles	Time frame for transient extinction dynamics changes (along with colour) due to surface plasmon resonance	[36]
Colouring	1996	Excimer laser	Stainless steel	Restore colour (and avoid discolouration) of stainless steel	Thermochemical reaction between Fe and O_2 produce different oxides/colours	[37]
Colouring	1995	Femtosecond red/UV laser	Copper	Study the photoemission process in ultra-short pulses	Three-(red) and two-photon (UV) emission process occur when Cu-cathode is irradiated by red/UV pulses	[38]

may generate a large residual stress gradient and cause delaminating or cracking of Cr_2O_3 ceramic cladding on steel sheet [25].

Laser bending is possible only above a threshold heat input. With sufficient thermal input, bending angle decreases significantly with increasing material thickness. However, bending angle no longer increases with increasing heat input beyond an upper critical value of energy input. The decreasing bend rate with increasing irradiation over the same track may be attributed to increase in elastic modulus due to the thickening of the material along the bending edge [24]. A two-dimensional plane strain numerical analysis to calculate the bending angle in pulsed laser irradiation of stainless steel sheet has shown that both optical reflectivity and thermal expansion coefficient constitute the most important considerations that influence the precision of the predicted bending angle [23]. However, suitable correlation between bending dimension and laser parameters would require proper estimation of the effect of relevant material properties at high temperature on the laser bending.

6.2 *Laser manufacturing*

Laser manufacturing is a new materials-processing technique that utilizes the high-power lasers to induce controlled thermal changes of shape/dimension/geometry, phase (solid/liquid/gas) or function (end use) of a given material or component to manufacture a

semi-finished/finished product/component with a unique precision, versatility and novelty [26–28].

A very recent application of laser forming with a far-reaching industrial significance concerns laser deposition and repair of single-crystal high-pressure high-temperature gas turbine blades. The process combines the advantages of a near net-shape manufacturing with the close control of the solidification microstructure in laser forming. Recently, Gaumann *et al* [26] have demonstrated the feasibility of this proposition by a process called epitaxial laser metal forming that may be useful in repair of cracked or worn parts of single crystal turbine blades and extending the engine life. Through a careful study of the solidification microstructure under different laser forming regimes, the processing windows for generation and repair of single crystal superalloy turbines by laser deposition have been proposed. If the deposited or cladded layer is polycrystalline, the orientation of the epitaxially grown grains can be determined by electron back scattered diffraction and mechanical property of the layer correlated with orientation of the grains [27].

Functionally graded materials are a recent development in composite materials that consist of a continuously graded interface between two or more component phases. Such heterogeneous structure or assembly can be developed by vapour deposition, plasma spraying, electrophoretic deposition, controlled powder mixing, slip casting, sedimentation forming, centrifugal forming, metal infiltration, controlled volatilization and self propagating high-temperature synthesis. A laser-based approach may be more versatile than the above mentioned routes in developing functionally graded materials [28].

6.3 *Laser rapid prototyping*

One of the most recent applications of laser in material processing is development of rapid prototyping technologies, where, lasers have been coupled with computer controlled positioning stages and computer aided engineering design to enable new capability [1,15,29–34]. This development implies that manufacturers are no longer constrained to shape metals by removal of unwanted material. Instead, components can now be shaped into near-net shape parts by addition-building the object in lines or layers one after another. Rapid prototyping relies on ‘slicing’ a 3-dimensional computer model to get a series of cross-sections that can then be made individually. The major techniques for making the slices are stereolithography, selective laser sintering, laminated object manufacturing and fused deposition modelling.

Figures 8 a & b schematically show basic processes involved in stereolithography and selected laser sintering processes, respectively. In stereolithography, the solid object is made by scanning an ultraviolet (UV) laser beam over the surface of a bath of epoxy resin that hardens on exposure to the UV light (figure 8a). Once a layer is complete, the base plate moves down a little in the bath, and a new layer of liquid flows in over the top to enable the next layer to form on top. The layer building continues until the component is ready in the desired dimension. In selective laser sintering, instead of liquid resin, a fluidized powder bed or sheet is used that is heated to close to its melting point (figure 8b). The carbon dioxide laser beam scans over the powder and heats the grains so that they undergo incipient on skin melting and sinter. Subsequently, the base plate moves down slightly, and the next layer of powder is spread across the surface by a rotating roller. The process continues until the desired shape or object is ready.

Figures 9 a & b present the scheme of laminated object manufacturing and fused deposition process of prototyping, respectively. In laminated object manufacturing, the preform is built from the layers by pulling long and thin sheets of pre-glued paper/plastic across the base plate and fixing it in place with a heated roller that activates the glue (figure 9a). A computer

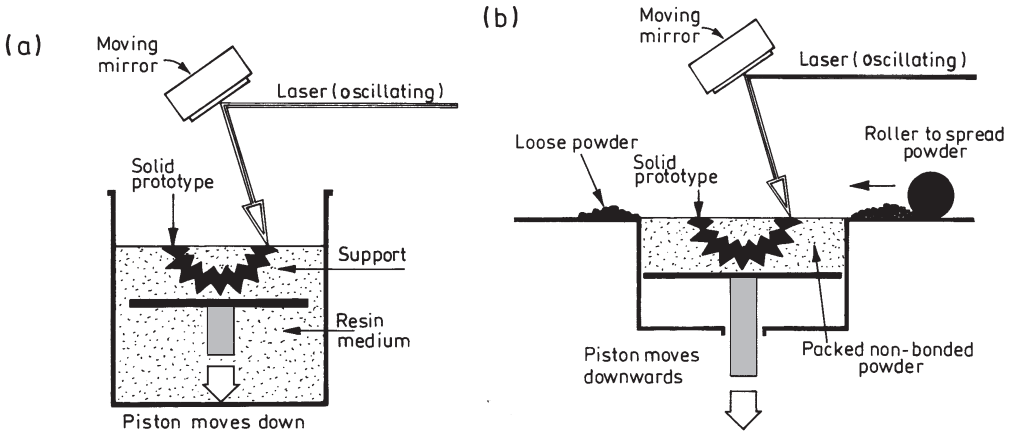

Figure 8. Schematic set-up for laser rapid prototyping by **(a)** stereolithography and **(b)** selected laser sintering.

controlled laser head scans the surface and cuts out the outline of the desired object. As the base plate moves down, the whole process starts again. At the end of the build process, the little crosshatched columns are broken away to free the object. In fused deposition process, the object is made by squeezing a continuous thread of the material through a narrow nozzle (heated by laser) that is moved over the base plate (figure 9b). As the thread passes through the nozzle, it melts only to harden again immediately as it touches (and sticks to) the layer below. For certain shapes, a support structure is needed, and this is provided by a second nozzle squeezing out a similar thread, usually of a different colour to make separating the two easier. At the end of the build process, the support structure is broken away and discarded, freeing the object/model. The models made from wax or plastics in this method are physically robust. This new fabrication concept allows construction of complex parts, starting from a 3D–CAD model without a mould.

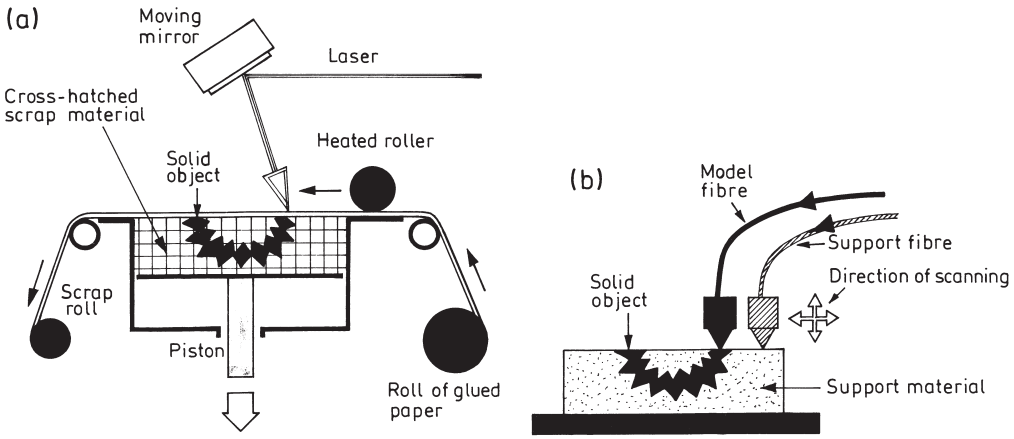

Figure 9. Schematic set-up for laser rapid prototyping by **(a)** thin laminated object manufacturing (for laminates or sheets), and **(b)** fused laser deposition technique (for solid objects).

Most of these additive processes produce polymeric objects and only recently laser sintering of metal powders has been commercially introduced. In a similar laser based additive rapid prototyping approach, it is possible to fabricate free form alumino-silicate ceramic parts by stereolithography starting from the UV curable pre-ceramic suspension [30]. The final components are obtained by pyrolysis of the organic binder and sintering at 1600°C.

Laser can be a useful tool for *in situ* rapid prototyping fabrication of composite components like cutting tools, shear blades, etc. Lu *et al*, [31] have fabricated TiC dispersed Cu–Ti–C and Cu–Ni–Ti–C composites by laser scanning of ball milled powder mixtures. It is felt that addition of Ni improves the integrity and surface quality of the laser-fabricated parts because of improved melting and wettability of Cu with *in situ* TiC.

Second harmonic generation using a 1·06 mm Q-switched Nd:YAG beam in powdered nonlinear crystals suspended in a photopolymeric solution could be useful in high resolution rapid prototyping [32]. Since efficient second harmonic generation occurs for very small powder grain size, this technique may provide a way of realizing high resolution three dimensional imaging in which the feature size could be only a few microns in dimension. Laser rapid prototyping enables fabrication of 3-D solid freeforms by material deposition in successive layers made of adjacent beads. One such structure developed in this method was a 3-D periodic photonic band-gap structure of aluminum oxide that consisted of layers of parallel rods forming a face-centered tetragonal lattice with lattice constants of 66 and 133 μm [33]. A similar laser-driven direct-write deposition technique (from trimethylaminealane and oxygen precursors) was successfully utilized to fabricate a 3-D microstructure consisting of aluminum oxide and aluminum [34]. These laser deposited rapid prototype ceramic components are useful as micromechanical actuators like microtweezers and micro-motors.

6.4 *Laser colouring*

A thin oxide layer on the surface developed by controlled laser irradiation may produce a particular colour or luster. Lu & Qiu [35] have investigated laser-assisted colouring/discolouring and bleaching of amorphous WO_3 thin film during pulsed laser deposition. The original films could be coloured from light brown to purple by a single pulse of KrF excimer laser irradiation at 248 nm and subsequently bleached to brown by a single pulse of Neodynium–yttrium–aluminum–garnet laser at 1·06 μm in air. It is suggested that colouring is due to polaron transition or photochemical activation, while photothermal oxidation is responsible for the bleaching process. In stainless steel, a thermochemical reaction between oxygen and stainless steel is believed responsible for colouring during excimer laser irradiation in air [37]. With increasing laser fluences, the temperature rise in the irradiated area of stainless steel surface increases, which enhances oxygen diffusion into the surface and oxidation reaction within the irradiated area. Thus, laser irradiation in vacuum is an easy way to avoid discolouration of stainless steel.

In order to identify the electronic process involved in colouring, Seifert *et al* [36] have carried out single-colour femtosecond pump-probe experiments to investigate the time dependence of laser-induced ultrafast desorption and deformation processes of silver nanoparticles in glass. Muggli *et al* [38] have reported that a single-colour illumination of a copper surface by a red or an ultraviolet femtosecond laser pulse yields a three-photon (red) or a two-photon (UV) photoemission process. On the other hand, a multicolour and multiphoton process ensues when the red and the UV pulses overlap both in space and in time on the photocathode. It is shown that this emission process results from the absorption by an electron of one red and one UV photon.

6.5 *Summary and future scope*

Laser forming offers a range of direct, contact-less and novel fabrication possibility of finished products/components of metallic, ceramic and polymeric origin. Laser bending is attractive to automobile and aircraft industry both for the precision and productivity involved in the process. Laser bending is routinely applied in tailoring the curvature of aluminum, iron and titanium based metals and alloys. The main mechanisms for bending are identified as 'temperature gradient' and 'buckling' mechanisms. However, these macroscopic approaches fail to identify or address the microstructural changes that accompany or cause bending. There are several questions that remain to be addressed/answered: (a) Does bending necessitate local/global melting? (b) Why does thickness increase along the bend edge? (c) Why does bending rate decrease with number of pass? (d) What microstructural features (grain size, texture etc.) accompany and affect bending?

Laser colouring is a relatively new technique introduced mainly for aesthetics as an offshoot of laser cleaning or marking practices. While colour depends on the thin oxide layer on metals, similar effect on polymers and ceramics may need introduction of pigments at the surface. However, the feasibility and durability of laser colouring strictly depends on the material chemistry and laser parameters (principally, wavelength). The process promises a great market if success is achieved in colouring not only metals, but ceramics, polymers and semiconductors alike. In this regard, the main open questions concern the mechanism, reproducibility and economics of the process.

Both laser-assisted manufacturing and rapid prototyping are the major laser forming processes that have found commercialization in many applications. The main reasons for interest in these processes stem from the scope of direct (one-step) manufacturing of round or square sections, hollow tubes and more complex geometry with the same machine and identical fixture. Solid parts are usually made in layers. Thus, the interfaces of the consecutive layers remain the weakest point. Investigations are warranted to predict the stresses generated at the edges and corners, surface roughness/contour and compositional distribution in the solid object. Development or epitaxial-repair of single crystal superalloy component will be a real breakthrough. In this regard, more comprehensive treatments of heat and mass transfer in specific applications are warranted to establish the reproducibility of the laser forming processes.

7. Laser joining

One of the earliest and most widely practiced applications of laser material processing was joining of metallic sheets using a continuous wave laser [1,16,17]. Today, the automobile and aerospace industry relies on lasers for a clean and non-contact source of heating and fusion for joining of sheets. More than on any other conventional process. Laser joining is applicable to inorganic/organic and similar/dissimilar materials with an extremely high precision, versatility and productivity that can only be matched by electron beam welding. Moreover, laser welding can be done in air, unlike the vacuum processing needed in electron beam welding. In comparison to conventional or arc welding, laser welding scores several advantages like narrow welds with controlled bead size, faster welding with a higher productivity, less distortion, narrow heat affected zone, amenability to welding Al/Mg alloys and dissimilar materials, and minimum contamination [39,40].

Laser joining encompasses welding, brazing, soldering and even, micro welding, sintering, etc. Joining of materials on a commercial basis requires a laser source of a high power level, high reliability, easy operation and low cost. Hence, pulsed or continuous wave Nd:YAG or

CO_2 laser (very seldom ruby laser, too) are the commonly used lasers for joining. The main process variables in laser welding are laser power, beam diameter, beam configuration, travel speed of the work-piece, substrate condition (roughness, temperature), filler type/feed rate, alloy composition and thermophysical properties of the work piece. Table 3 presents a ready reference for the most recent and representative studies on laser joining of materials (1995 onwards) [41–70]. These studies are selected primarily to emphasize recent advances and outline the outstanding issues in using laser as a tool for joining materials.

7.1 *Laser welding*

Laser welding, because of the sheer volume/proportion of work and advancement over the years, constitutes the most important operations among the laser joining processes [1,17,41–59]. Figure 10 shows the front view of the schematic set-up for laser welding without a filler rod. The focused laser beam is made to irradiate the work piece or joint at the given level and speed. A shroud gas protects the weld pool from undue oxidation and provides with the required oxygen flow. Laser heating fuses the work piece or plate edges and joins once the beam is withdrawn. In case of welding with filler, melting is primarily confined to the feeding wire tip while a part of the substrate being irradiated melts to insure a smooth joint. In either case, the work piece rather than the beam travels at a rate conducive for welding and maintaining a minimum heat affected zone (HAZ).

There are two fundamental modes of laser welding depending on the beam power/configuration and its focus with respect to the work piece: (a) conduction welding and (b) keyhole or penetration welding (figures 11 a,b). Conduction limited welding occurs when the beam is out of focus and power density is low/insufficient to cause boiling at the given welding speed. In deep penetration or keyhole welding, there is sufficient energy/unit length to cause evapouration and hence, a hole forms in the melt pool. The 'keyhole' behaves like an optical black body in that the radiation enters the hole and is subjected to multiple reflections before being able to escape. The transition from conduction mode to deep penetration mode occurs with increase in laser intensity and duration of laser pulse applied to the work piece.

Welding efficiency can be defined as a power (or energy) transfer coefficient (η) where η is the ratio between laser power absorbed by the work piece and incident laser power. η is usually very small but can approach unity once a keyhole has been established. The melting efficiency or melting ratio (ε) is given by,

$$\varepsilon = [vdW\Delta H_m/P]\,.$$

Equation (7) relates the rate of melting (ε) to incident laser power, P, where v is welding speed, d is sheet thickness, W is beam width and ΔH_m is the heat content of the metal at the melt temperature. The maximum value of ε is 0·48 for penetration welds and 0·37 for conduction welds [17]. It is apparent that ε never approaches unity even when $\eta \simeq 1$. Both h and ε can be enhanced under the keyhole welding condition if the absorption coefficient can be increased. This can be accomplished by application of absorbent coating, surface roughening or texturing, preheating, tailoring of temporal irradiation profile and/or oxidation/nitriding.

Among various process parameters, the quality and properties of laser weld depend on laser pulse time and power density, laser spot diameter/penetration, melt area, melting ratio and material properties like absorptivity, specific heat, density, etc. Wang *et al* [41] have demonstrated the versatility of laser welding by carrying out *in-situ* weld-alloying and laser beam welding to join SiC reinforced 6061Al metal matrix composite with titanium. Microstructural

Table 3. Summary of selected studies on laser joining of materials in the recent past (1995 onwards).

Process	Year	Material	Laser	Scope	Results	Ref.
Laser welding of Al-alloys						
Welding/ alloying	2000	SiC+Al–6061 composite + Ti	CW–CO_2	Study feasibility of alloying + welding and microstructure	Harmful needle-like carbide formation is avoided. Central fusion zone consists of TiC, Ti_5Si_3 and Al_3Ti	[41]
Welding	2000	C95800 Ni–Al bronze	Diode pumped Nd:YAG	Study the influence of laser and process parameters	Effect of welding speed on weld quality and microstructure determined	[42]
Welding	1999	6061–T6 Al–Mg–Si alloy	2·5 kW CW–CO_2 laser	Study the microstructure and property of the HAZ	A kinetic equation for dissolution of Mg_2Si is proposed. Welding at high speed and energy density is preferred	[43]
Welding	1997	AA 1100 Al alloy	Pulsed Nd:YAG laser	Study the effect of laser parameters on welding	Conditions for pore free, conduction pool geometry welding were defined	[44]
Welding	1996	8090 Al–Li alloy	3 kW CW–CO_2 laser	Microstructure and mechanical characterization of weldment	Fusion zone dimension, solute evapouration, hardness, porosity and tensile properties were evaluated	[45]
Welding	1995	Al–Fe–V–Si alloy	CW–CO_2	Study the effect of welding parameters on microstructural characteristics of weld zone	Si/Fe/V rich Al_4Fe type precipitates were detected. A Si/Fe rich phase formed on boundaries	[46]
Laser welding of steel						
Welding	2001	Ni + Au–Ni plated steel	Pulsed Nd:YAG	Study effect of Ni or Au/Ni plating on welding products	Au/Ni plating does not affect the strength of welded steel sheets	[47]
Welding	2001	Steel	CW-laser	Theoretical study on influence of Marangoni effect in welding	Temperature dependence of surface tension plays a significant role	[48]

(Continued)

Table 3. (*Continued*).

Process	Year	Material	Laser	Scope	Results	Ref.
Bright welding	2000	AISI 304 stainless steel	Photolytic iodine laser	Study welding characteristics of new PIL laser (1315 nm)	Extremely narrow welding seam with very fine fully austenitic microstructure is produced with minimum HAZ	[49]
Penetration welding	1999	High carbon steel	CW–CO_2 and diode laser	Study the influence of laser parameters on weld quality	CO_2 laser welding gives crack free, stronger and wider weld pool	[50]
Welding	1997	Austenitic stainless steel	CW–CO_2	Study the effect of welding parameters on fusion zone	Microstructure was mostly austenitic (2–3% ferrite). Higher speed and lower power produce better welding	[51]
Welding	1997	Stainless steel and titanium	CW–CO_2	Study the plasma plume characteristics in welding	Plasma plume maintains local thermal equilibrium and reaches 11000 K	[52]
Spot welding	1996	Stainless steel, Kovar, Gold	Semiconductor laser	Study the defect formation mechanism in packaging	Defect/hole and center line cracks disappear below a given power density and air gap, respectively	[53]
Micro-gra-vity welding	1995	Stainless steel	70 W CW–CO_2	Study the welding characteristics in varying gravity	Significant variation of Cr-distribution is noted in different gravity conditions	[54]
Laser welding of Ti-alloys						
Welding	2001	TiNi shape memory alloys	CW–CO_2	Study corrosion, mechanical and shape memory properties of weldments	Decrease in M_s-start temperature and ductility, and increase in amount of B2 phase and strength, but no change in shape memory effect are observed	[55]
Melting	2001	Ti–6Al–4V alloy	Pulsed Nd:YAG laser	Study (in-situ X-ray) the key hole formation and correlate melt depth with laser power	Keyhole formation is time dependent and its bottom matches with melt pool. Melt depth depends on power density	[56]

(Continued)

Table 3. (*Continued*).

Process	Year	Material	Laser	Scope	Results	Ref.
Welding	1997	Ti–6Al–4V	CW–CO_2	Study fatigue and tensile properties of weldments	Crack initiates at base metal due to martensite. Aging reduces crack growth rate and produces mixed mode	[57]
Welding	1995	SiC-fibre reinforced Ti-alloy	CW–CO_2	Study feasibility and mechanical property of weldment	Butt and scarf joints were successful. Scarf angle $< 12^\circ$ produced fracture	[58]
Laser welding of Mg-alloys						
Key-hole welding	2001	AZ91 and AM50 alloys	6 kW CW–CO_2 laser	Study the feasibility and welding characteristics	Welding morphology and quality are correlated to energy/heat input	[59]
Laser brazing						
Hard soldering	2001	Diamond film	High power diode laser	Micro-thermal management of high power diode lasers	Hard soldering on chemical vapour deposited diamond film is possible	[60]
Joining	2001	Ni + Au–Ni plated Al, kovar, steel	Pulsed Nd:YAG	Study brazing characteristics, microstructure and inter-diffusion products	Au/Ni braze improves the adhesion of Au/Ni-plating on Ni and other base metals (Al, Kovar, steel)	[47]
Brazing, cladding	1999	Metals	High power 808 nm diode laser	Study the capability of diode lasers in material joining	Diode lasers are useful for brazing and cladding of metallic thin sheets	[61]
Micro-patterning	1997	Si_3N_4 ceramic sheet	KrF excimer laser	Study the effect of laser parameters on micro-patterning	The optimum power level for smooth surface finish is determined	[62]
Laser sintering						
Sintering	2001	AISI 304 stainless steel	High power laser	Mathematical modelling to predict residual stress	Energy transfer through plume and molten metal considered, and strength of sinter joints determined	[63]
Sintering	2000	Nano zirconia particles	High power lasers	Study the microstructure, densification and grain growth	Different crystalline phases evolve during fast/slow sintering	[64]

(Continued)

Table 3. (*Continued*).

Process	Year	Material	Laser	Scope	Results	Ref.
Sintering	2000	$BaTiO_3$ ceramics	CW–CO_2	Study the micro/domain structure of sintered $BaTiO_3$	Both conventional/non-conventional domain structures are observed	[65]
Laser soldering						
Soldering	2001	Sn–Ag and Sn–Ag–Cu solders	Excimer laser	Study the creep property of laser ablated composite solders	Nano-Cu particles improve the creep properties of solders at 25–105°C	[66]
Soldering	2000	Copper alloys	Diode laser	Determine process window of laser soldering	Temperature measured at lased spots to compare that predicted by models	[67]
Soldering	1997	SMT device material	CW-diode laser	Study the effect of process parameters	The laser parameters for good quality and uniform solders are determined	[68]
Micro-soldering	1996	Automatic tape bonding device	Diode pumped Nd:YAG laser	Study feasibility of laser soldering of lead frames	Good soldering is obtained by 98 ms lasing with 5·8 W/lead power	[69]
Laser tissue soldering						
Tissue soldering	1999	Indocyanine green, bovine serum albumin	808 nm diode laser	Study the photothermal effects in laser tissue soldering and process optimization	LS is effective in repairing damaged tissues with better tensile strength and minimum lateral thermal damage	[70]

studies show that the detrimental needle-like aluminum carbides are completely eliminated. The central fusion weld joint consists of TiC, Ti_5Si_3 and Al_3Ti along with some large pores.

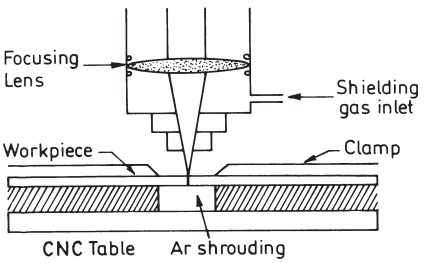

Figure 10. Schematic of laser welding without a filler rod (front view) (after [1]). The argon shroud removes heat and prevents undue oxidation. The relative position of the laser focus determines the quality and configuration of the weld.

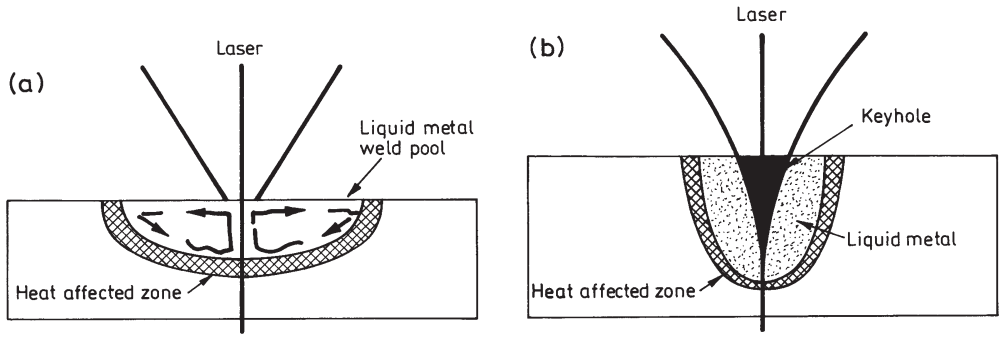

Figure 11. Schematic view of **(a)** conduction melt pool (semi-circular), and **(b)** deep-penetration (key hole) welding mode (after [1]). The surface boiling and marangoni effect are more in **(a)**.

Penetration depths of 17–35 μm were obtained in deep penetration welding of C95800 nickel–aluminum–bronze using a 3 kW diode pumped Nd:YAG laser [42]. The softened zone in laser welding of 6061-T6 Al-alloy could be 1/7th of that obtained in tungsten inert gas welding [43].

Both conduction-mode and keyhole-mode welding are possible in aluminum [44]. Weld pool shapes in aluminum depend on the mean power density of the laser beam and the laser pulse time. The transition from conduction- to keyhole-mode welding occurred in aluminum at a power density of about 10 GW/m^2, compared to about 4 GW/m^2 for stainless steel. In both materials, large occluded vapour pores near the root of keyhole-mode welds are common at higher power density. The pores are due to hydrogen that can be significantly eliminated by surface milling and vacuum annealing [44].

Autogenous "bead-on-plate" laser-beam welding of Al-alloys by a 3 kW CO_2 laser under Ar or N_2 atmosphere is possible in the range 700 to 1300 W power, 1500 to 9000 mm/min scan speed and focus located at 1 to 3 mm below the surface, respectively [45]. The effects of using different gases were evaluated in terms of weld-line appearance, fusion-zone dimension, solute evapouration, microhardness, post-weld tensile properties, as well as porosity distribution. In comparison to electron beam welding, laser welding yielded a higher fusion-zone depth/width ratio, cooling rate and porosity amount, and a lower solute loss and post-weld tensile strain. A similar investigation on microstructural evaluation following autogenous bead-on-plate CO_2 laser welding of an Al–8·5Fe–1·2V–1·7Si alloy (in wt. %) on 2 mm thick sheet showed that the fusion zone microstructure consisted of faceted precipitates around 10 μm in size, embedded in a cellular-dendritic α-Al matrix with a sub-micrometre intercellular phase [46]. Detailed electron microscopy showed that the faceted precipitates in the fusion zone have the Al_mFe-type crystal structure ($m \approx 4$) enriched in Si, Fe and V and a crystalline Fe- and Si-rich phase formed at the cell boundaries.

Compositional variation or segregation and related temperature-dependent coefficient of surface tension (Marangoni effect) have significant effect on the quality of the conduction or deep-penetration welding geometry [48]. However, Ni and Au/Ni plating has marginal or no influence on laser welding of thin steel sheets except raising the hardness of the weld [47]. However, laser power, welding speed, defocusing distance and the type of shielding gas combinations should be carefully selected so that weld joints having complete penetration, minimum fusion zone size and acceptable weld profile are produced [51]. Heat input as a function of both laser power and welding speed has almost no effect on both the type of microstructure and mechanical properties of welds.

Spectroscopic measurement of laser-induced plasma in welding of stainless steel and titanium has shown that the plasma-plume over the keyhole consisted of metal vapours diluted by argon shielding gas and reached a maximum temperature of 11,000 K [52]. Cheng *et al* [53] have studied the defect formation mechanisms in spot-welding during semiconductor laser packaging and concluded that the dimension of hole-formation depends on the laser power density. The hole disappeared as the power density is below 3×10^5 W/cm^2.

Hsu *et al* [55] have studied the effect of CO_2 laser welding of binary $Ti_{50}Ni_{50}$ and $Ti_{49{\cdot}5}Ni_{50{\cdot}5}$ on shape-memory and corrosion characteristics of these alloys. Though martensite start (MS) temperature was slightly lowered, no deterioration in shape-memory character of both alloys was observed. The welded $Ti_{50}Ni_{50}$ alloy consisted of an increased amount of B2 phase, showed higher strength and considerably lower elongation than the base metal. The same alloy registered satisfactory performance in potentiodynamic corrosion tests in 1·5 M H_2SO_4 and 1·5 M HNO_3 solutions. However, a significantly higher corrosion rate and a less stable passivity was noted in artificial saliva. On the other hand, the pseudoelastic behaviour of the laser weld of $Ti_{49{\cdot}5}Ni_{50{\cdot}5}$ alloy (in cyclic deformation) indicated that the stress required to form stress-induced martensite (σ_m) and permanent residual strain (ε_p) were higher after welding due to more inhomogeneous nature of the weld metal.

Perret *et al* [56] have reported a novel X-ray based study to characterize the keyhole formed during pulse Nd–YAG laser interaction with a Ti–6Al–4V metallic target. The keyhole formed during the laser–matter interaction is not instantaneous but grows linearly with the laser irradiation time. The keyhole depth is nearly the same as the melt-zone depth. An approximate estimation of melt depth can be made simply from the ratio of the power density for melting to that of a reference metal. However, the proper microstructural control in laser welding of Ti–6Al–4V is needed as tensile fracture of laser-welded specimens usually occurs in the base metal due to the presence of martensite in the narrow fusion zone [57].

To fabricate practical engineering structures with composites, a technique for joining the metal matrix composites to themselves and to monolithic metals is essential. Hirose *et al* [58] have compared the joining processes (e.g., laser welding, diffusion bonding and transient liquid phase bonding) for structural applications of continuous fiber reinforced metal matrix composites like continuous SiC fiber reinforced Ti–6Al–4V composites. Both butt and scarf joints were successful by laser welding to join the composites to themselves or to Ti–6Al–4V plate without degrading the microstructure. Fracture usually occurred in base the metal.

In laser welding with power density beyond 10^4 W/mm^2, the formation of plasma cavity, commonly referred to as keyholes, leads to deep penetration welds with high aspect ratio. Marya & Edwards [59] have identified the major factors controlling the magnesium weld morphology in deep penetration welding of AZ 91 and AM 50 alloys by a CO_2 laser. Though irregular weld cross-section profiles were consistently observed on each material, bead dimensions often varied with the welding variables in contrasting ways. These variations could arise from base metal vapourization and characteristic radiation.

7.2 *Laser brazing*

Like welding, laser is widely used in brazing non-ferrous metals/alloys and ceramics/glasses [60–62]. Lorenzen *et al* [60] have demonstrated the possibility of performing hard soldering on a chemical vapour deposited diamond film using a new technique based on high-power diode laser. Similarly, Schubert *et al* [61] have shown that a 1·4 kW diode laser (808 nm) and a rectangular spot can be very useful in cladding and brazing.

Biro *et al* [47] have studied the effects of Ni and Au/Ni plating on laser brazing/welding of 200 μm thick aluminum, nickel, Kovar, and cold-rolled steel sheet in the lap-joint config-

uration using a pulsed Nd:YAG laser and a range of weld process conditions. The strength of the joint was equivalent to that of the annealed base material. Significant gas porosity was observed at the interface between the Al weld pool and the unmelted Ni and Au/Ni plating layers. However, porosity did not affect the tensile shear strengths of the Al joints. Au/Ni braze increased the strength of the Au/Ni-plated Ni specimens to that of the base material. Heitz *et al* [62] have reported a detailed investigation on KrF excimer-laser ablation and micro patterning of Si_3N_4 to identify the ablation threshold in air. The surface morphology was flat or cone-type at 4 J/cm^2. Typical ablation rates for obtaining smooth surfaces free from pores, scratches, and cracks lie between 0·1 to 0·2 μm/pulse.

7.3 *Laser sintering*

Though sintering is not a true bulk joining process, laser assisted sintering involves localized incipient fusion and joining of particles spread over a thin section thickness (unlike conventional sintering by bulk heating), and hence, is included in the present discussion. Instead of direct synthesis of a component, laser irradiation may be useful to develop a desired shape with adequate strength by laser assisted sintering of a pre/directly deposited green compact. For instance, laser may be useful in sintering/densification of sol-gel processed nano-ZrO_2 ceramic coatings [64] and pressure-less sintering of ferroelectric domains in barium titanate [65]. In sintering of $BaTiO_3$, typical herringbone, square net, and watermark morphologies are noted. Furthermore, the wedge-shape and overlapped microtwin domains characterize the delta-fringes.

The advances in miniaturization and ever increasing complexity of integrated circuits frequently mean an increase in the number of connections to a component with simultaneous reduction in pitch. For this emerging smaller contact geometry, micro-laser connection technologies are required. The reliability of the connection plays a decisive role. The implementation and reproducibility of laser connection technology in microelectronics depend on good thermal contact between the two parts and high quality absorption of the material surface used. Laser energy can cause local melting due to overheating of the lead because of the low distance between lead and bump. This effect influences the reproducibility of the contacts. Even the slightest interruption in the thermal contact of the parts can cause non-reproducibility of the contacts. Materials with a higher quality of absorption, for example Sn (32%), can be soldered with a good level of reproducibility unlike that for gold (4%) or copper (7%) surfaces. Due to the low absorption of these materials it is necessary to use a laser with a higher intensity or lower wavelength to produce the same energy. In this regard, reproducibility depends on irregularity in absorption, laser instability and thermal contact.

7.4 *Laser soldering*

Laser soldering of semiconductor devices needs extreme care and perfection. However, the precision of laser soldering is far superior to conventional soldering. For instance, 215 μm-width tape-automated bonding leads could be soldered to with a device with 430 μm center-to-center spacing by 98 ms diode-pumped Nd:YAG laser at 5·8 W/lead laser power. Like conventional soldering, one of the major concerns about laser soldering remains the mechanical property, particularly creep resistance at elevated temperatures. Guo *et al* [66] have studied the creep behaviour in Cu and Ag particle-reinforced composite and eutectic Sn–3·5Ag and Sn–4·0Ag–0·5Cu non-composite Pb-free solder joints at 25, 65 and 105°C (representing homologous temperatures ranging from 0·61 to 0·78). Creep resistance in composite solder joints was significantly improved with Cu particle reinforcements, but not with Ag-reinforcement.

The strain at the onset of tertiary creep for Cu- and Ag-reinforced composite solder joints was typically lower compared to non-composite solder joints. The activation energies for creep were similar for all the solder materials. Brandner *et al* [67] have explored soldering of thin or narrow Cu-based electrical joints with solid state (1064 nm) and diode (808 nm) lasers to identify the mechanism of energy coupling, mode the temperature rise and determine the process window. Laser soldering may be more beneficial for secondary flux-less re-flow solder bumping than that in a furnace.

Berkowitz & Walvoord [68] have studied laser soldering of fine pitch printed wiring boards using a continuous wave diode laser. The success of laser soldering of such semiconductor devices depends on selection of laser, optimization of laser parameters, surface preparation/cleaning, lead form configuration, solder selection/ application and soldering process control. It may be noted that solder inter-diffusion in die bonding is important for good bonding and hence, high power devices must be mounted in the epitaxy-side down configuration for good heat transfer in the well-controlled, high yield and void-free die-attach method.

7.5 *Laser tissue soldering*

Laser has now opened new possibilities in joining organic substances including human and animal tissues and organs. Laser tissue welding uses laser energy to induce thermal changes in the molecular structure of the tissues. In laser tissue welding, low-strength anastomoses and thermal damage of tissue are major sources of concerns. On the other hand, laser tissue soldering is a bonding technique in which a protein-solder is applied to the tissue surfaces to be joined, and laser energy is used to bond the solder to the tissue surfaces. The addition of protein solders to augment tissue repair procedures significantly reduces the problems of low strength and thermal damage associated with laser tissue welding techniques. McNally *et al* [70] have attempted to determine optimal solder and laser parameters for tissue repair in terms of tensile strength, temperature rise and damage and the microscopic nature of the bonds formed. An in vitro study was performed using an 808 nm diode laser in conjunction with indocyanine green (ICG)-doped albumin protein solders to repair bovine aorta specimens. Liquid and solid protein solders prepared from 25% and 60% bovine serum albumin (BSA), respectively, were compared. Increasing the BSA concentration from 25% to 60% greatly increased the tensile strength of the repairs. A reduction in dye concentration from 25 to 0|.25 mg/ml was also found to result in an increase in tensile strength. Increasing the laser irradiance or surface temperature resulted in an increased severity of histological injury. The strongest repairs were produced with an irradiance of 6·4 W/cm^2 using a solid protein solder composed of 60% BSA and 0·25 mg/ml ICG with a surface temperature around $85 \pm 5^\circ$C and thermal gradient of about 15°C across 150 μm thick solder strips. Post soldering histological examination showed negligible evidence of collateral thermal damage to the underlying tissue. Microstructural study revealed albumin intertwining within the tissue collagen matrix and subsequent fusion with the collagen as the mechanism for laser tissue soldering. Thus, laser tissue soldering may be effective for producing repairs with improved tensile strength and minimal collateral thermal damage over conventional tissue welding.

7.6 *Summary and future scope*

Laser joining is one of the earliest recorded applications of laser material processing. That laser can heat a material irrespective of its chemistry, state, bonding or size/geometry, is obviously a big advantage in joining a component with another of the same type or not by using laser a clean source of heating. Obviously, joining special steels and alloys constitutes the main

demand for laser welding or joining. Apart from routine joining, laser is useful in joining dissimilar materials like steel-Al, steel-alumina, polymer-metal and so on. Even, joining of tissues and organic substances is now commonplace using laser. The main issues for future research concern joining materials with dissimilar physical (melting point, density, diffusivity) and mechanical (hardness, strength) properties and bonding (e.g., metallic to covalent). While several attempts have been made to develop mathematical models to predict the microstructure and width of the joint with similar materials, similar approaches now need to be extended for dissimilar materials. In this regard, capability to predict the microstructure and strength of the joints would be the core issues. In particular, investigations on the changes in microstructural and mechanical properties across the weldment as a function of the selected process/laser parameters are needed. Perhaps, using filler rods can be dispensed with if mechanism for brittleness of the joints in certain combinations is well understood. Apart from welding, attempts must be made to develop useful localized joining methods like sintering and brazing to fabricate finished products of greater variety and challenges. For further details about the technology and mechanism of laser joining, several recently published text books may be consulted [16,17,39].

8. Laser machining

Laser machining refers to controlled removal of material by laser induced heating from the surface or bulk of the work piece and includes laser assisted drilling, cutting, cleaning, marking, scribing and several other forms of material removal/shaping [1,2,6]. Laser cutting is the most common industrial application of laser in material machining. Metals, ceramics, polymers and composites may be laser cut or drilled irrespective of the hardness. Processing is easily automated for speed and accuracy giving clean edges with minimum heat affected zone. The advantages of laser cutting over other techniques are: flexibility and automation-worthiness, easy control of depth of cut, cleanliness, non-contact processing, speed, amenability to a wide variety of materials (ductile/brittle, conductor/non-conductor, hard/soft), negligible heat affected zone, narrow kerf, and so on [1].

Table 4 provides a summary of the most recent (1995 onwards) and representative studies on laser machining of materials [71–91]. The areas covered under laser machining include cutting, drilling, cleaning (or paint stripping), marking and scribing. These processes are applicable to very soft polymers to most hard ceramics, normal incidence to oblique/inclined irradiation, ultra-thin semiconductor chips to multi-layer metallic films/sheets, and simple/curved surfaces to complex geometry. The discussion in this section will highlight the scope/versatility of laser machining and emphasize the recent advances and outstanding issues in using laser as a non-contact and non-contaminating tool for machining all kinds of materials.

8.1 *Laser cutting*

The general arrangement for cutting with a laser is shown in figure 12 (a,b) [1]. The cutting is done either using a transmissive (glass) or reflecting (metal mirror) optics. The transmissive optics is made of ZnSe, GaAs or CdTe lenses for CO_2 lasers or quartz lenses for YAG or excimer lasers. The reflective optics consists of parabolic off-axis mirrors. The main constituents for control and monitoring are the lasers with shutter control, beam guidance train, focusing optics and a computer controlled translation stage to move the work-piece. The shutter is usually a retractable mirror, which blocks and guides the beam into a water-cooled

Table 4. Summary of selected studies on laser machining of materials in the recent past (1995 onwards).

Process	Year	Material	Laser	Scope	Results	Ref.
Laser cutting						
Cutting	2001	Microelectronic packaging materials	CO_2 and YAG (frequency multiplied)	Direct pattern processing, image transfer, contour cutting/trimming	LM is useful for fine scale direct patterning and drilling of Cu-clad glass fiber reinforced epoxy laminates	[71]
Modelling of laser cutting	2000	Metals	Theoretical study – pulsed lasers	Finite element two stage laser cut simulation model that considers stress relief effect and cut mechanism	Cutting is efficient in a specific energy window. Upper and lower corner stress depends on passivation break-through due to upper corner crack	[72]
Modelling of laser cutting	1998	Metals	CW–CO_2	Model laser machining as a process of reaction and energy-absorption	Effect of absorptivity, mass diffusion rate, exothermic reaction, cutting speed, and geometry are considered	[73]
Cutting	1996	Al–Li + SiC metal matrix composite	Pulsed Nd:YAG	Predict empirical relation between laser parameters and cut shape/depth and HAZ	Proper choice of laser parameters minimize HAZ, improve cut quality and efficiency, and surface finish	[74]
Modelling, cutting	1995	Mild and stainless steel	CW–CO_2	Study the laminar boundary layer of O_2-assisted LM	Cutting includes reaction/ evapouration. The model excludes shock-effects	[75]
Laser drilling						
Drilling	2001	Stainless steel	Dual pulse Nd:YAG	Improve drilling quality by two synchronized laser pulses without coaxial gas flow	Drilling improves due to melting by the first and evaporation and recoil process during the second pulse	[76]
Drilling	1999	Al,W,Mo,Ti, Cu,FeAg,Au	Femtosecond Ti-sapphire	Study the effect of laser parameters on drill quality	800 nm short pulses produce good quality holes. A model is proposed	[77]

(Continued)

Table 4. (*Continued*).

Process	Year	Material	Laser	Scope	Results	Ref.
Precision machining	1999	Stainless steel	Pulsed laser	Create photonic band gap metal crystals by precision laser machining	Cut-off frequency lies in 8–18 GHz that can be tuned by varying the hole size and interlayer distance	[78]
Machining/ Metallization	1997	Al-nitride	Excimer laser	Drill high aspect ratio 60–300 μm via-holes in AlN without / with metallization	A bottom substrate can considerably reduce back-surface damage. Shock-wave analysis and resistance reported	[79]
Laser cleaning						
Cleaning	2000	Stainless steel – 3 compositions /history.	Pulsed Nd:YAG	Study the mechanism and influence of laser parameters on oxide removal	Laser ablation expels the oxide laser without damaging/removing the underlying metal layer	[80]
Polymer coating, removal/ cleaning	1998	Polymer on TiN coated Al–Cu alloy	Pulsed 248 nm excimer (23 ns) and Nd:YAG (7 ns) lasers.	Study the influence of laser parameters in removing polymer layer on sub-micron TiN coated Al–Cu alloy	Sub-threshold ablation by oblique irradiation may improve cleaning efficiency and depth. YAG causes more surface damage	[81]
Paint stripping	1996	Metal surfaces	Pulsed TEA–CO_2 laser	Explore complete removal of resin/paints from metal surface	Surface condition is important for effective paint removal	[82]
Laser marking						
Marking	2001	Polypropylene	Pulsed Nd:YAG (532 nm)	Use frequency doubled YAG laser for surface marking	Laser marking on polymers offers more benefit than usual processes	[83]
Marking Cutting	2000	Thin sheets	CO_2 laser	Use hollow glass waveguide or Ag-halide fibers for marking	The system is capable of cutting, heating and marking	[84]
Etching	1999	Polyethylene Polypropylene	Pulsed Nd:YAG (532 nm)	Explore non-contact and dry etching of polymers	Reaction of laser pulses with polymers and compounds investigated	[85]

(Continued)

Table 4. (*Continued*).

Process	Year	Material	Laser	Scope	Results	Ref.
Data storage	1997	Polyethylene terephthalate	Infrared laser	Use laser lithography for optical storage of data	Marking is based on radiation induced crystallization, melting and ablation	[86]
Marking	1996	Organo-metallic films	Ar^+ ion laser (514 nm)	Explore marking with organo-metal film on ceramics/plastics	Optimum power/time, etc. for marking by photothermal deposition outlined	[87]
Cracking Marking	1995	Sodalime/boro–silicate glass	CW–CO_2 laser	Investigate marking/cracking of glass by laser ablation	Marking occurs by surface crazing and boiling. Residual stress causes cracks	[88]
Laser scribing						
Scribing	2001	Textured Si–steel	KrF excimer laser (248 nm)	To reduce core-loss of transformer steel by scribing	Core loss reduces due to domain refinement, stress relaxation and domain wall pinning	[89]
Scribing	2000	CdTe, ZnO, $CuInGaSe_2$, etc	YAG, Cu-vapour, Excimer	Investigate the feasibility and mechanism of scribing plastics	The optimum conditions for scribing avoiding ridge formation are defined	[90]
Scribing	1998	Soft-magnetic ribbon	Excimer and YAG lasers	To reduce magnetic losses of amorphous ribbons	Scribing at optimum distances reduces core losses by 29–50%	[91]
Scribing	1997	Al–nitride (AlN)	Excimer laser	Machining and metallization of high aspect ratio vias in AlN	Straight wall through hole vias (60–300 μm) drilled with back up substrate	[79]

device that measures the input power. During cutting, the mirror rapidly moves out and allows the beam to be directed on to the work piece after passing through the beam guide that directs the beam to center on a focussing optic. The focussed beam then passes through a nozzle from which a coaxial jet flows. The gas jet is needed both to aid the cutting operation and to protect the optics from spatter. For cutting processes which rely on melt removal by the gas jet there is a problem for the metal optics system. To achieve a gas jet suitable for cutting (> 20 m/s and reasonably well focussed) without interposing a transmissive elements, a set of centrally directed nozzles or a ring jet can be used. For cutting non-conducting materials like wood, carbon and plastics, the focussed beam heats up the surface to boiling point and generates a keyhole. The keyhole causes a sudden increase in absorptivity due to multiple reflections and the hole deepens quickly [14]. The parameters controlling the laser cutting operation are

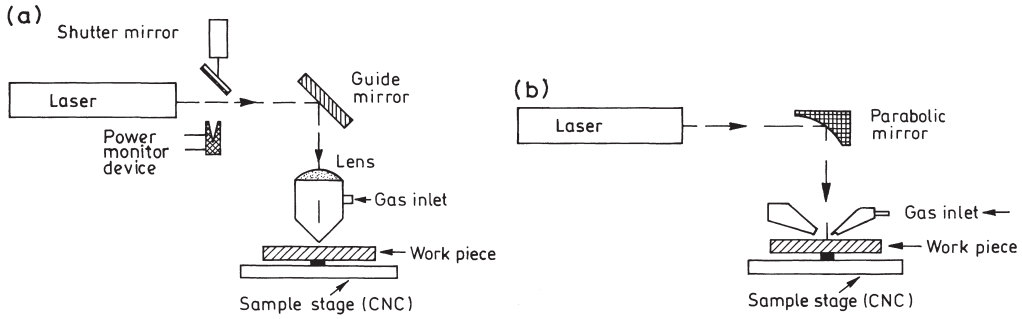

Figure 12. General arrangement for laser assisted cutting using **(a)** transmissive optics, and **(b)** reflective optics (after [1]). Selection of the optics is based on considerations related to beam power vis-à-vis thermal stress limit and operational safety.

beam diameter, laser power, traverse speed, gas composition, material thickness, reflectivity and thermo-physical properties.

Laser cutting does have a diversified application starting from thin sheet metal cutting for general purpose equipment, such as household appliances, electrical cabinets, automotive components, thick section metal cutting for trucks, buildings, stoves, construction equipment, shipbuilding etc. Titanium alloys cut in an inert atmosphere are used in airframe manufacture. Aluminum alloys have similar advantages in cutting by using the laser, which has to be well turned and of higher power. Cutting of radioactive material is another important area of application of laser cutting. Cutting of wood up to 1" thick for the die-board industry, furniture industry, puzzle and gift industry, crafts and trophies, etc. Textile cutting examples include plastics, rubbers, composites, cloth, ceramics, etc. Hard brittle ceramics such as SiN can be cut ten times faster by laser than by diamond saw.

Laser cutting is equally useful in manufacturing special materials including laser cutting of circuit boards, resistance trimming of circuits, functional trimming of circuits and microlithography. The growing use of the excimer laser is of current interest. Hole drilling thorough circuit boards to join circuits mounted on both sides has advantages. The excimer laser can do this without risk of some form of conductive charring.

The microelectronics industry is moving toward smaller feature sizes so as to improve performance and lower cost. Small distances between chips together with the short interconnection routes are conducive for faster operation. Laser processing for via generation, direct pattern processing, image transfer, contour cutting and trimming now find increasing application in microelectronics packaging industry. On the other hand, smaller spaces between conductive patterns increases the risk of short circuits (caused by pattern faults, solder bridges, migration, etc.), that emphasizes the need to ensure reliability of laser processing. Illyefaalvi-Vitez (2001) has attempted utilization of CO_2 and frequency-multiplied Nd:YAG lasers (using five wavelengths, i.e. 10600, 1064, 532, 355 and 266 nm) for drilling and direct patterning of copper clad glass fiber reinforced epoxy laminates, polyester foils and similar packaging structures. Laser processing was combined with through contacting of the generated vias by screen printing with polymer thick films, by wet chemical direct plating and by evapouration of thin metal layers. The results show promising opportunities for laser processing of metal layers and polymeric materials in microelectronics packaging.

Analysis of laser metal-cut energy process window is important to predict or develop a useful strategy for cutting or machining operation for any engineering material (Bernstein

et al 2000). A laser-energy window exists for each cut structure under a specified laser pulse. Experimental observations showed that the differences between upper and lower corner stress is temporarily dependent on the passivation breakthrough caused by upper corner cracks. In a recent model on metal cutting with a gas assisted CO_2 laser, laser cutting is considered as a surface reaction and absorption process that needs an adjusting parameter to represent the absorptivity for different materials at different incident angles [73]. The computation of the mass diffusion rate at the gas/solid boundary of the cutting front includes the exothermic heat released during cutting. It is shown that a very small level of impurity in oxygen exerts a significant influence on the cutting performance. Earlier, the combined effect of chemical reactions taking place between a gas jet and molten metal was considered adopting a laminar boundary layer approach [75]. These models seem to work well for cutting speed of up to 30 mm/s and all jet velocities up to sonic speed (as the effect of shock is ignored).

Yue & Lau [74] have studied the pulsed laser cutting of an Al–Li/SiC metal matrix composite to examine the influences of laser cutting parameters on the quality of the machined surface. Proper process control may minimize the heat-affected zone, improve the quality of the machined surface and predict the maximum depth-of-cut for the composite. Finally, the optimum condition for achieving high cutting efficiency with minimum material damage was recommended.

8.2 *Laser drilling*

High power CO_2 lasers or Nd:YAG lasers may also be used to drill holes. Figure 13 shows the basic set used in laser drilling, which is not very different from that used for other laser machining processes. Laser drilling can be done in both pulse and continuous wave modes with suitable laser parameters. The advantage of the laser is that it can drill holes at an angle to the surface – fine lock pinholes in Monel metal bolts is an example. Mechanical drilling is slow and causes extrusions at both ends of the hole that have to be cleaned. Mechanical punching is fast but is limited to holes further than 3 mm diameter. Electro chemical machining is too slow at 180 s/hole but does give a neat hole. Electro discharge machining is expensive and

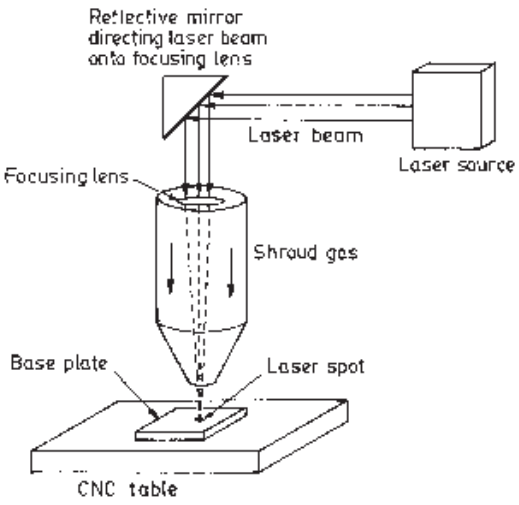

Figure 13. Basic system hardware for pulse laser drilling of thin sheets of metal, semiconductor or polymers. The beam focus coincides with the surface. Argon shroud may be need to avoid/minimize thermal damage.

slow at 58 s/hole. Electron beam drilling is fast at 0·125 s/hole but needs a vacuum chamber and is more expensive than a YAG laser processing. In comparison, a YAG laser takes 4 s/hole to outsmart all other methods [1].

The ability to machine very small features like holes into a metal or polymer sheet/film by laser ablation with an unmatched precision, accuracy and speed has opened a very useful scope of application of laser material processing in microelectronic industry. For instance, holes with a diameter of 300 nm and depth of 52 nm could be drilled in metal films with minimum distortion and heat affected zone using 200 fs and 800 nm pulses from a Ti:sapphire laser focused to a spot size of 3000 nm. Lehane & Kwok [76] have developed a novel method for improving the efficiency of laser drilling using two synchronized free-running laser pulses from a tandem-head Nd:YAG laser capable of drilling through 1/8-in-thick stainless-steel targets at a standoff distance of 1 m without gas-assist. The combination of a high-energy laser pulse for melting with a properly tailored high-intensity laser pulse for liquid expulsion results in the efficient drilling of metal targets. The improvement in drilling is attributed to the recoil pressure generated by rapid evapouration of the molten material by the second laser pulse. Similarly, Zhu *et al* [77] have carried out a detailed experimental study of drilling sub-micron holes in thin aluminum foils with thickness ranging from 1·5 to 50 μm, and W, Mo, Ti, Cu, Fe, Ag, Au and Pb foils of 25 μm thickness with femtosecond Ti:sapphire laser pulses of 800 nm width. The influence of laser parameters and material properties on hole drilling processes at sub-micron scale has been examined and a simple model to predict the ablation rate for a range of metals has been developed.

Laser precision machining has been applied to fabricate metallic photonic band-gap crystals (consisting of stainless steel plates with a tetragonal lattice of holes and a lattice constant of 15 mm) operating in the microwave frequency [78]. Transmission measurements showed that the periodic crystals exhibited a cutoff frequency in the 8–18 GHz range allowing no propagation below this level. Furthermore, the cutoff frequency could be easily tuned by varying the interlayer distance or the filling fraction of the metal. Combinations of plates with different hole-diameters create defect modes with relatively sharp and tunable peaks.

8.3 *Laser cleaning*

Removal of small particles or continuous layers from a metal surface can be carried out by laser beam using a selected area irradiation at an optimum combination of incident power, interaction/pulse time and gas flow rate (that sweeps the dislodged atoms from the surface). Figure 14 shows the schematic mechanism of laser cleaning. At the initial stage, a plasma plume is formed due to ionization of the atoms vapourized from the surface and blocks the beam-surface contact (figure 14a). As the irradiation stops, the temporary compression on the surface changes into tension and causes spallation of the oxidized layer (figure 14b). A dramatic improvement of cleaning efficiency in terms of area and energy is possible when the laser irradiates the work-piece at an oblique or glancing-angle of incidence rather than direct or perpendicular irradiation of the surface. Furthermore, substrate damage is greatly reduced and probably eliminated at glancing angles.

Psyllaki & Oltra [80] have investigated the influence of pulsed laser irradiation on the removal of the oxide layer from the surface of stainless steels developed by high temperature oxidation using a pulsed Nd:YAG laser. At 1·0–2·0 J/cm^2, irrespective of the composition and thickness of the surface layer, the laser irradiation resulted in the expulsion of the oxide layer without any material removal from the underlying metal.

The demand for new wafer cleaning technology after plasma etching increases as the industry enters into submicron processes. The success of low-resistance interconnecting high-

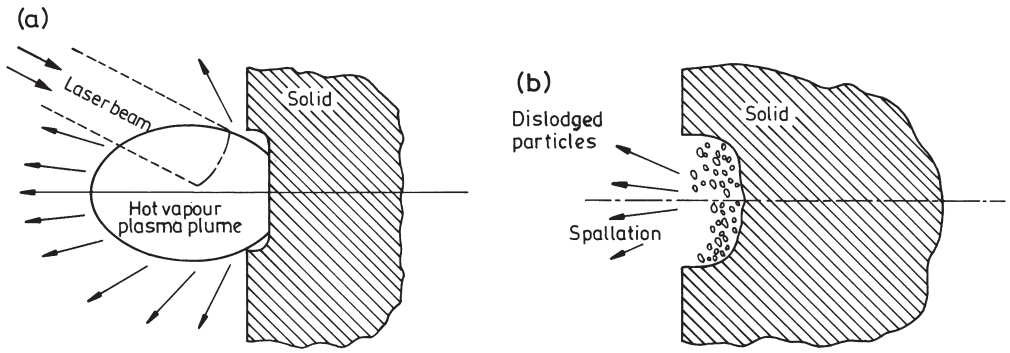

Figure 14. Mechanism of laser cleaning of solid surface with a thin oxide or undesirable layer **(a)** Formation of plasma plume due to ionization of the vapour (at very high laser power for a short time), and **(b)** spallation of the oxidized layer when surface residual stress changes from compressive to tensile.

density ultralarge-scale integrated devices depends on the cleanliness of via holes. The side wall and bottom polymers resulting from reactive ion etching of via holes can be removed by a non-contact dry laser-cleaning technique using pulsed excimer laser irradiation [81]. Similarly, laser cleaning is capable of removing the polymers by sub-threshold ablation, even at fluences limited by the damage threshold ($= 250$–$280\,\mathrm{mJ/cm^2}$) of the underlying Al–Cu metal film with titanium nitride (TiN) antireflective coating. Comparing ablation results obtained using Nd–YAG laser and excimer laser shows that although the shorter 7 ns Nd–YAG laser pulse gives a greater etch thickness than the 23 ns excimer laser pulse, it also tends to damage the metal films and the silicon substrates of the via wafers more easily.

Tsunemi *et al* [82] have demonstrated that pulsed laser irradiation of oxidized metallic surfaces in an electrolytic cell under proper voltage conditions could be a promising new approach for effective removal of oxide films. Systematic measurements on simulated corrosion-product films by optical reflectance profile and energy dispersive X-ray spectroscopy showed that the utilization of a basic electrolyte solution and imposition of a certain cathodic potential prior to laser irradiation were essential for a high removal efficiency. This new technique should find potential applications in paint removal metallurgy, semiconductor fabrication technology, de-contamination of nuclear power plants and mask-less patterning of oxidized surfaces.

8.4 *Laser marking*

Laser ablation can be applied as a means of direct marking on plastics or polymer compounds as it is fast, economical and eco-friendly compared to the conventional marking processes [83]. Besides embossing a mark/design on a surface for identification or aesthetics, laser marking is useful in non-contact and dry etching and printing of polypropylene or polyethylene plastics using a 532 nm laser pulse [85]. Similarly, laser irradiation can produce controlled micro cracking or fracture of soda lime and borosilicate glasses [88].

Beu-Zion *et al* [84] have designed and constructed a CO_2 laser marking system based on a scanned flexible wave guide (silver halide infrared optical fiber or a hollow glass wave guide) capable of cutting, heating or marking on various surfaces. Recently, permanent markings of various colours on different ceramic and plastic substrates (with orasols dispersed palladium acetate organometallic films) have been made by a photothermal deposition process using an argon ion laser (514 nm) [87].

Buckley & Roland [86] have developed a thermal method for lithography on polymer films based on selective exposure of the films to infrared laser radiation passing through a mask. A high contrast between the image and background is essential in optical data storage processes. In this regard, the non-linear response of laser/thermal-marking is inherently advantageous. Laser irradiation leads to crystallization, melting and ablation of the polymer and produces high-resolution images with excellent edge acuity and minimal interference from diffraction. The absence of diffraction effects is due to the nonlinear response of the polymer film to the radiation. In this technique, the best resolution achievable is limited by the size of the smallest features present on the masks used to create the pattern.

Recently, attempts have been made to develop a dual-laser-writing scheme in which an un-modulated short-wavelength read laser augments the writing process effected by a longer-wavelength laser. Apart from increasing the thermal efficiency of the laser marking process itself, the dual-beam-writing scheme may decrease the mark width and the recorded mark length variability. Coupled with the increased resolution of the short wavelength read spot, these enhancements could improve the performance.

8.5 *Laser scribing*

Laser machining of ceramics is used extensively in the microelectronics industry for scribing and via-hole drilling. Scribing is a process for making a groove or line or line of holes either fully penetrating, or not, but sufficient to weaken the structure so that it can be mechanically broken. The quality, particularly for silicon chips and alumina substrates, it is measured by the lack of debris and low heat affected zone. Thus low energy or high power density pulses are used to remove the material principally as vapour.

Scribing involves laser ablation of a groove or row of holes that form perforation lines to separate a large substrate into individual circuits. Via machining is generally followed by a metallization step to create three-dimensional interconnections in a multilayer circuit board. Lumpp & Allen [79] have drilled high aspect ratio, straight walled 60 and 300 μm diameter via-holes in 635 μm thick aluminum nitride with or without a metallization layer deposited on the via-walls using an excimer laser. Attachment of a second substrate or metal sheet prevents damage to the back surface.

In fabrication of core laminations for motors and transformers, laser scribing may induce reduction in hysteresis and eddy current losses. Laser scribing needs a very low power so as not to melt the surface. For example, pulsed excimer laser (248 nm, 23 ns) irradiation to scribe the grain-oriented M-4 electrical steel has resulted in a 26% core loss reduction due to the beneficial thermal stresses that refined the magnetic domains and reduced the eddy current losses [89]. Similarly, 50% reduction in core loss in 50 μm thick amorphous alloy ribbon has been achieved by laser scribing at 2–5 mm line spacing at the same excitation power [91]. The mechanisms responsible for improvement include magnetic domain refinement, stress relaxation and inhibition of domain-wall movement. Laser scribing also relieves the stresses that are induced in the material during manufacture. The scribe lines increase the surface resistivity of the material, resulting in reduced eddy current loss. Laser scribing of polycrystalline thin films used for solar cells can eliminate the frequently observed problem of ridge formation along the edges of scribe lines in the semiconductor films [90].

8.6 *Summary and future scope*

Laser machining requires controlled-removal of material by vapourizing within a narrow dimension with least heating of the surrounding. The process can be extended to cutting,

drilling, scribing, marking or cleaning. In all these processes, material removal without damaging the surrounding is a challenge. The recent advances are now based on selecting appropriate wavelength, using multiple beams, allow inclined/oblique incidence and material removal in stages. A large variety of materials starting from human/animal tissues to diamond can be laser machined, however, an appropriate choice of laser power and wavelength is crucial for the success of the operation. Due to diversity of materials, geometry and conditions for machining, laser machining now often relies on more than one laser for the same operation. Use of advanced optics and better control of the sample stage are the other concerns with regards to improving the quality of the cut. Future challenges include increasing the capability to machine thicker sections, curved surfaces and dissimilar/ heterogeneous materials. Similarly assessment of material damage will need more close control and monitoring of the microstructural change/damage across the cut. Development of intelligent machines for machining diverse materials would require interfacing a vast database with the hardware. Thus, continued efforts are needed to model laser machining processes with suitable experimental validation of the predicted results.

9. Laser surface engineering

Failure of engineering materials due to corrosion, oxidation, friction, fatigue and wear/abrasion is most likely to initiate from the surface because: (i) free surface is more prone to environmental degradation, and (ii) intensity of externally applied load is often highest at the surface [19]. The engineering solution to minimize or eliminate such surface initiated failure lies in tailoring the surface composition and/or microstructure of the near surface region of a component without affecting the bulk [2,3,18–20]. In this regard, the more commonly practiced conventional surface engineering techniques like galvanizing, diffusion coating, carburizing, nitriding and flame/induction hardening possess several limitations like high time/energy/material consumption, poor precision and flexibility, lack in scope of automation/ improvisation and requirement of complex heat treatment schedule. Furthermore, the respective thermodynamic and kinetic constraints of restricted solid solubility limit and slow solid state diffusivity impose additional limitations of these conventional or near-equilibrium processes [18,19].

In contrast, the surface engineering methods based on application of electron, ion and laser beams are free from many of the limitations of equilibrium surface engineering methods. A directed energy electron beam is capable of intense heating and melting the surface of the most refractory metals and ceramics [4]. However, the energy deposition profile in the irradiated zone under electron beam is gaussian, and hence, the latter is more suitable for deep penetration welding or cladding of similar or dissimilar solids (figure 5). Moreover, the scope of generation of X-ray by rapid deceleration of high-energy electrons impinging on a solid substrate poses additional disadvantage of a possible health hazard. As an alternative, ion beam processing offers practically an unlimited choice and flexibility of tailoring the surface microstructure and composition with an implant which has otherwise no or very restricted solid solubility in a given substrate [8,10]. However, the peak concentration of implanted species, like the energy deposition peak in electron beam irradiation, lies underneath and does not coincide with the surface (figures 5b,c). Furthermore, the requirements of an expensive ionization chamber, beam delivery system and ultra-high vacuum level are serious impediments against large-scale commercial exploitation of ion beam assisted surface engineering methods. In comparison, laser circumvents majority of the limitations cited above with regards to both conventional and electron/ion beam assisted surface engineering

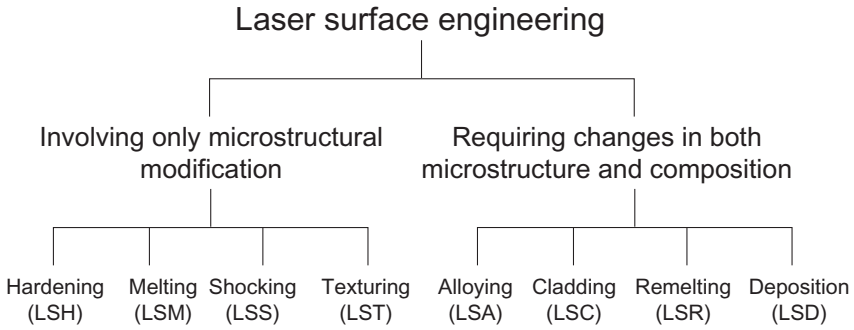

Figure 15. General classification of laser surface engineering.

methods and offers a unique set of advantages in terms of economy, precision, flexibility and novelty of processing and improvement in surface dependent properties concerned [1–4]. One of the major advantage of using laser in surface engineering is its exponential energy deposition profile vis-à-vis the gaussian profile of that in electron or ion beam irradiation (figure 5).

Among the notable advantages, laser surface engineering (LSE) enables delivery of a controlled quantum of energy (1–30 J/cm^2) or power (10^4–10^7 W/cm^2) with precise temporal and spatial distribution either in short pulses (10^{-3} to 10^{-12} s) or as a continuous wave (CW). The process is characterized by an extremely fast heating/cooling rate (10^4–10^{11} K/s), very high thermal gradient (10^6–10^8 K/m) and ultra-rapid resolidification velocity (1–30 m/s) [18–20]. These extreme processing conditions very often develop an exotic microstructure and composition in the near surface region with large extension of solid solubility and formation of metastable even amorphous phases.

Figure 15 presents a brief classification of different LSE methods that involve mainly two types of processes. The first type is meant for only microstructural modification of the surface without any change in composition (hardening, melting, remelting, shocking, texturing and annealing), while the other requires both microstructural as well as compositional modification of the near-surface region (alloying, cladding etc.).

Among the various LSE methods, laser surface alloying (LSA) involves melting of a deposited layer along with a part of the underlying substrate to form an alloyed zone for improvement of wear, corrosion and oxidation resistance. Figure 16a illustrates the scheme of LSA with a continuous wave laser. It includes three major parts: a laser source with a beam focusing and delivery system, a lasing chamber with controlled atmosphere and a microprocessor controlled sweeping stage where the specimen is mounted for lasing. The process includes melting, intermixing and rapid solidification of a thin surface layer with pre/co-deposited alloying elements (figure 16b). The coating material may be pre-deposited by any of the conventional means like electro-deposition, plasma spray and physical/chemical vapour deposition or may be injected in the form of powder or powder mixture into the melt at the time of laser treatment and is termed as co-deposition. In LSA with pre- or co-deposition, a 20–30 % overlap of the successive melt tracks is intended to ensure microstructural/compositional homogeneity of the laser treated surface. The sweeping stage (x-y or x-y-z-θ) allows laser irradiation of the intended area of the sample-surface at an appropriate rate and interaction time/frequency. The irradiation results into transient melting of the deposit with a part of the underlying substrate, rapid mass transfer by diffusion/convection in the melt pool, and ultra-

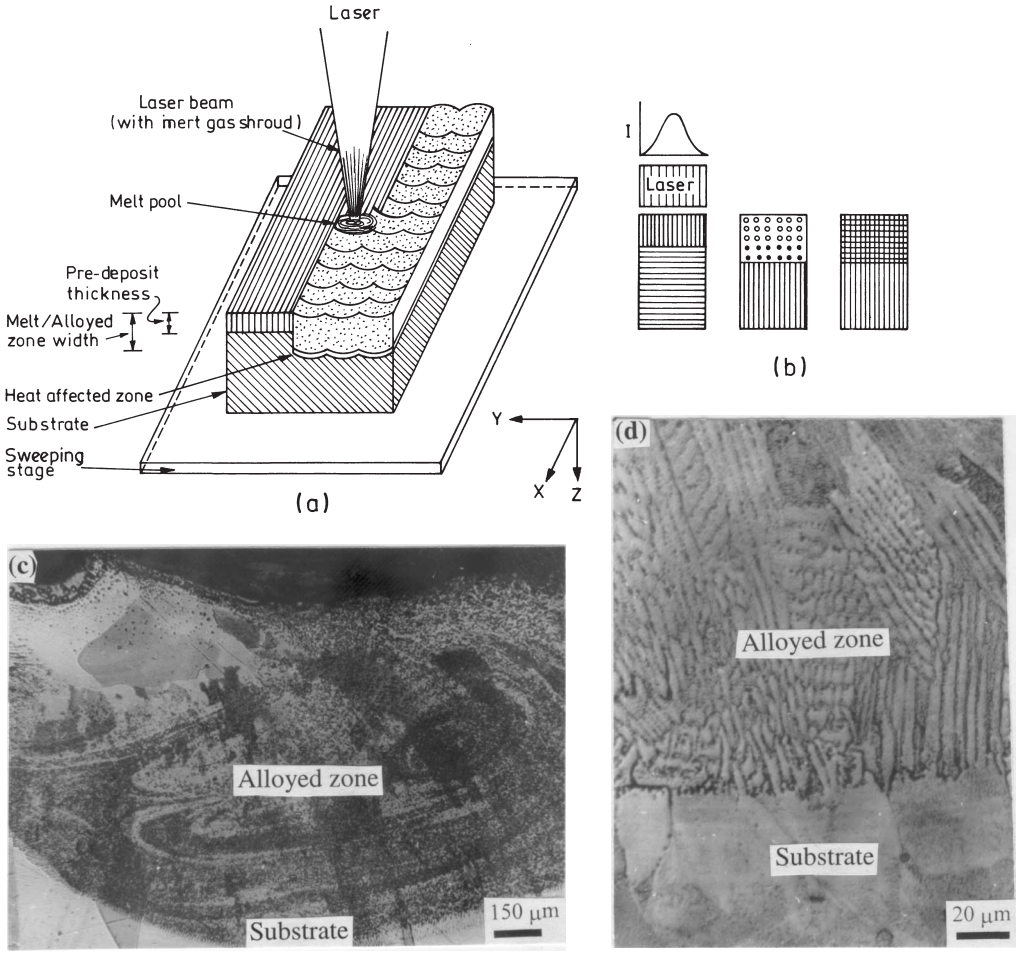

Figure 16. **(a)** Schematic hardware set-up for laser surface alloying (LSA), **(b)** the processes of heating/melting, intermixing and solidification in LSA, and microstructure of **(c)** a typical alloyed zone and **(d)** solid-liquid interface formed in LSA of Cu with Cr [134]. Note that convection dominates mass transfer in the alloyed zone (c), and epitaxial growth marks solidification of the melt pool (d).

fast solidification to form an alloyed zone (figures 16c,d). The depth, chemistry, microstructure and associated properties of the alloyed zone depend on the suitable choice of laser/process parameters i.e. incident power/energy, beam diameter/profile, interaction time/pulse width, pre or co-deposition thickness/ composition and concerned physical properties like reflectivity, absorption coefficient, thermal conductivity, melting point and density.

9.1 *LSE of ferrous alloys*

As already mentioned, LSE is mostly utilized to enhance resistance to corrosion, oxidation, wear and similar surface degradation of engineering materials. In this section, we will review the scope and current status of understanding about LSE of Fe-based or ferrous alloys. A summary of the major studies carried out in the recent past in this direction is provided in table 5 [92–150].

Table 5. Summary of selected studies on laser surface engineering of materials in the recent past (1995 onwards).

System	Year	LSE	Property	Scope	Results	Ref.
LSE of ferrous alloys						
AISI 316 stainless steel	2001	LSM	Corrosion	Improve intergrannular corrosion and intergrannular stress corrosion	LSM is effective in de-sensitization	[92]
AISI 304 stainless steel	2001	LSM	Pitting	Role of LSM in N_2 or Ar atmosphere in enhancing pitting corrosion resistance	Tendency for pitting decreases due to dissolution of nitrogen and formation of nitrides	[93]
AISI 1040 (NiCoCrB) AISI 316L	2001	LSA	Corrosion, erosion	Improve both corrosion and erosion by LSA	Corrosion resistance improves in mild steel but deteriorates in stainless steel	[94]
17-4 PH stainless steel	2001	LSAn	Fatigue, stress corro-sion	Reduce tendency for fatigue crack growth and stress corrosion cracking	Laser annealing produces duplex microstructure that retards crack growth in quasi-cleavage fracture	[95]
G 10380 steel G 41400 martensitic AISI 316L austenitic	2000	LSS	Corrosion, stress corro-sion	Introduce compressive residual stress and suppress crack growth by laser assisted shot peening	Corrosion current decreases in martensitic steel. Laser peeling is more effective in reducing stress corrosion	[96]
UNS–S31603 auste-nitic stainless steel (Co,Ni, Mn,Cr,Mo)	2000	LSA	Corrosion, erosion	Improve both corrosion and cavitation erosion corrosion by LSA	Resistance to erosion improves due to dispersed ceramic/intermetallic phase but pitting resistance decreases	[97]
AISI 304 stainless steeel (Si)	2000	LSA	Corrosion	Investigate the role of Si in improving corrosion resistance	Si turns the matrix ferritic and segregates. Post LSA homogenization improves corrosion resistance	[98]
AISI 304 stainless steeel (Mo)	1999	LSA	Pitting, ero-sion	Attain AISI 316-SS equivalent corrosion property on 304-SS	Mo improves pitting and erosion corrosion resistance of 304-SS	[99]

(Continued)

Table 5. (*Continued*).

System	Year	LSE	Property	Scope	Results	Ref.
AISI 304 stainless steeel (Si)	2000	LSA	Corrosion	Investigate the role of Si in improving corrosion resistance	Si turns the matrix ferritic and segregates. Post LSA homo-genization improves corrosion resistance	[98]
AISI 304 stainless steeel (Mo)	1999	LSA	Pitting, erosion	Attain AISI 316-SS equivalent corrosion property on 304-SS	Mo improves pitting and erosion corrosion resistance of 304-SS	[99]
AISI 316L	1998	LSM	Pitting corro-sion	De-sensitization of nitrogen bearing stainless steel	LSM eliminates the sensitized zones and significantly improves pitting corrosion resistance	[100]
ASTM S31254 stain-less steel on mild steel	1997	LSC	Corrosion	Improve pitting corrosion resistance of mild steel by LSC	Pits following LSC are smaller in size and number	[101]
AISI 304 stainless steel (Mo, Ta)	1995	LSMLSA	Corrosion, wear	Improve corrosion and wear resistance by LSM or LSA	LSM produces δ-ferrite and deteriorates corro-sion. LSA with Mo is useful. Not much change in wear	[102]
Mild steel (Fe,Cr,Si,N)	1995	LSA	Corrosion	Utilize LSA to improve corrosion resistance of mild steel	LSA with Fe–Cr–Si–N produces a fine duplex microstructure and greatly increases corrosion resistance	[103]
Oxidation properties						
Steel (Al)	2001	LSA	Oxidation	Improve oxidation resistance by LSA with predeposited Al	LSA with Al forms several aluminides that imparts good oxidation resistance at 600°C up to 200 h	[104]
Stainless steel	2000	LC	Cleaning	Remove oxide layers by laser assisted vapourization	Thin oxide layers could be removed irrespective of chemical composition and history in a narrow energy band	[105]

(Continued)

Table 5. (*Continued*).

System	Year	LSE	Property	Scope	Results	Ref.
Plain carbon steel (TiB_2)	2000	LSA	High temperature oxidation	Impart oxidation resistance by alloying with borides	Complex oxide layers develop on steel surface exposed to 600–1000°C following parabolic growth rate	[106]
AISI 304 stainless steel (Ni–Cr–Al–Y and ZrO_2+Y_2O_3)	1998	LSR	Oxidation	Improve oxidation resistance of 304-SS by LSR of prior twin (bond + top) coated ceramic layers	Double remelting produces better oxidation resistance at 1200°C than single-remelted/plasma-coated sample	[107]
Inconel 800H (Al)	1997	LSA	Oxidation	Improve high temperature oxidation resistance	LSA with Al develops an Al-rich surface that considerably improves resistance to oxidation up to 1000°C	[108]
AISI 316L (Fe–Cr–Al–Y)	1996	LSC	Oxidation	Develop thermal barrier coating for enhanced oxidation resistance	Rhombohedral-Al2O3 and mixed Fr + Cr or Ni + Cr oxides offer enhanced oxidation resistance at 1100–1200°C	[109]
Wear properties						
S 31603 stainless steel (CrB_2, Cr_3C_2, SiC,TiC,WC, Cr_2O_3)	2001	LSA	Cavitation erosion resistance	Enhance erosion resistance by developing a ceramic dispersed composite surface layer	Erosion resistance improves considerably for all carbides and borides except Cr_2O_3	[110]
Austenitic stainless steel (Nano-Zr)	2000	LSA	Hardness, Erosion	Develop amorphous dispersed composite layer to improve resistance to erosion and wear	Hardness and wear/erosion resistance improves significantly due to dispersion of Zr-rich amorphous phase	[111]
Austempered ductile iron (Cr)	2001	LSALSH	Hardness, Wear	Improve adhesive/abrasive wear resistance of austempered ductile iron by LSA or LSH	LSH (than LSA) is more effective in improving wear resistance and developing compressive residual stress	[112]

(Continued)

Table 5. (*Continued*).

System	Year	LSE	Property	Scope	Results	Ref.
AISI 1040 (TiB_2)	2000	LSA	Tribology, Wear	Develop boride coated/dispersed surface layer and improve wear resistance of low-carbon steel	LSA improves resistance to adhesive/ abrasive wear and reduces friction coefficient	[113]
Mild steel (FeCr–TiC)	2000	LSR,SHS	Wear	Utilize SHS and LSR to develop a TiC dispersed surface composite	LSR homogenizes the microstructure and improves wear resistance	[114]
Mild steel (Hadfield, Fe–Mn–C)	1999	LSC	Wear	Improve hardness, wear and bulk mechanical properties	LSC improves wear resistance and bulk mechanical properties of the clad	[115]
Pearlitic rail steel	1998	LSM	Wear	Improve mechanical and tribological properties by LSM	LSM produces a thin glazed layer with better hardness and lower friction rate	[116]
EN31 bearing steel	1997	LSH	Wear, Friction	Improve wear and friction properties by LSH	Single or double glazed LSH tracks have better wear and friction property	[117]
A 7 tool steel (Ti)	1997	LSA	Wear, Friction	LSA with excimer laser to improve wear/friction property	LSA reduces friction coefficient but does not affect wear properties	[118]
Medium carbon steel (Stellite 6)	1996	LSC	Wear	Improve wear resistance by LSC with stellite coating	Wear against 4140/4340 steels considerably improves due to LSC	[119]
Mild steel (WC)	1995	LSR, SHS	Hardness	Improve hardness and wear resistance by SHS and LSR		[120]
2. LSE of superalloys and special steels						
Cr–Mo steel (Cr)	2000	LSA	Oxidation	Improve high temperature oxidation resistance	LSA enhances oxidation resistance in 800–1000°C due to Cr_2O_3 rich scale	[139]
Martensitic steel (Ni-alloy)	1999	LSC	Hardness, Wear	Improve wear and erosion resistance of the base steel	LSC significantly increased hardness and erosion resistance	[140]

(Continued)

Table 5. (*Continued*).

System	Year	LSE	Property	Scope	Results	Ref.
AISI 304 stainless steel (Ni–Cr–Al–Y and ZrO_2+Y_2O_3)	1998	LSR	Oxidation	Improve oxidation resistance by LSR of bond (Ni–Cr–Al–Y) and top ($ZrO_2 + Y_2O_3$) coat layers	Double remelting produces better oxidation resistance at 1200°C than single-remelted/ plasma-coated sample	[107]
Si-steel (Ni + Cr)	1998	LSC	Oxidation	Improve oxidation resistance	LSC with high Ni–Cr alloy (with Si) improves oxidation resistance at 900°C. Si content is important	[141]
Inconel-600	1997	LSM	Oxidation	Enhance oxidation resistance	LSM improves oxidation resistance due to microstructural homogeneity	[142]
Inconel 800H (Al)	1997	LSA	Oxidation	Improve high temperature oxidation resistance	Al-rich surface by LSA improves oxidation resistance up to 1000°C	[108]
35 NCD 16 ferritic steel (Cr_3C_2/SiC)	1996	LSA	Hardness, oxidation	Enhance hardness and high temperature oxidation resistance	Hardness increased, Oxidation resistance increased due to Si containing complex oxides	[143]
3. LSE of non-ferrous alloys						
Al and its alloys – Corrosion properties						
Al–6013 + SiC_p composite	1999	LSM	Corrosion	Improve pitting and general corrosion properties by LSM	Rapid solidification of LSM refines the surface microstructure and improves the corrosion resistance	[121]
2014 Al alloy (Cr, W, Zr–Ni,Ti–Ni)	1998	LSA	Corrosion	Study the corrosion behaviour of Al-alloy surface after LSA	Overlapping regions are more prone to pitting corrosion due to segregation	[122]
Al-alloy ($Zr_{60}Al_{15}Ni_{25}$)	1997	LSCLSR	Corrosion	Surface amorphization of Al by LSC/LSR to improve pitting corrosion resistance	Amorphous phase dispersion (function of LSC/LSR parameters) produces an improved corrosion resistance	[123]

(Continued)

Table 5. (*Continued*).

System	Year	LSE	Property	Scope	Results	Ref.
2014 Al alloy (Cr, W, Zr–Ni,Ti–Ni)	1998	LSA	Corrosion	Study the corrosion behaviour of Al-alloy surface after LSA	Overlapping regions are more prone to pitting corrosion due to segregation	[122]
Al-alloy ($Zr_{60}Al_{15}Ni_{25}$)	1997	LSCLSR	Corrosion	Surface amorphization of Al by LSC/LSR to improve pitting corrosion resistance	Amorphous phase dispersion (function of LSC/LSR parameters) produces an improved corrosion resistance	[123]
Al–Si (Ni–Cr–B–Si)	1997	LSR	Micro-structure	Study microstructural evolution in LSR of plasma coating on Al–Si	Ultrafine Ni_3Al and amorphous phase with very high hardness form by LSR	[124]
Al–SiC composite	1996	LSM	Corrosion	Improve corrosion resistance by LSM with excimer laser	Microstructural homogeneity by LSM improves corrosion resistance	[125]
Al and its alloys – Oxidation properties						
6061 Al alloy (Al + TiC)	2001	LSCLSA	Oxidation	Improve oxidation resistance of Al-alloy by LSC/LSA	TiC + Al composite coating improves oxidation resistance in 200–600°C	[126]
Al–Cu–Li	1997	LSM	Oxidation	Improve oxidation resistance by LSM assisted surface treatment	LSM produces adherent scale and improves oxidation resistance at 450°C	[127]
AlGaAs and AlAs layers	1996	LSM	Oxidation	Study wet oxidation characteristic of buried thin film for laser device	Oxidation of AlGaAs provides suitable apertures for surface lasers	[128]
Al and its alloys – Wear properties						
Al + SiC	1999	LSS	Hardness, wear	Improve oscillating wear property by LSS of HVOF coated composite surface layer	Both hardness and wear resistance improve by LSS due to residual compressive stress	[129]
Al (Al_3Ti)	1999	LSC	Wear	Improve wear resistance	Composite intermetallic layer on surface enhances wear resistance	[130]

(Continued)

Table 5. (*Continued*).

System	Year	LSE	Property	Scope	Results	Ref.
Al (AlN)	1998	LSA	Hardness	Synthesize AlN layer by excimer laser irradiation in nitrogen	LSA produces adherent AlN layer on Al with high hardness	[131]
AlSi (Ni–WC)	1997	LSC	Hardness	Develop carbide/amorphous dispersed high hardness layer	Microstructure of cladded layer consists of aluminides + amorphous phases and has high hardness	[132]
Cu and its alloys						
Cu–Cr–Fe	2000	LSR	Hardness, Wear	Improve tribological properties of powder compacts by LSR	LSR improves hardness and wear resistance and reduces friction	[133]
Cu (Cr)	1999	LSA	Wear, erosion	Improve wear/erosion resistance of Cu by LSA with Cr	LSA enhances resistance to adhesive/ abrasive wear and erosion due to solid solution and dispersion hardening	[134]
Mg and its alloys						
Mg + SiC (Al–Si)	2001	LSC	Corrosion	Improve corrosion resistance by LSC with Al + Si alloy	LSC improves corrosion resistance. LSC parameters have strong influence	[135]
AZ91D and AM60B Mg alloys	2001	LSM	Corrosion	Improve corrosion resistance by LSM	Uniform and refined microstructure improves corrosion resistance	[136]
AZ91 Mg alloy	1999	LSM	Corrosion	Enhance corrosion resistance	Pulsed excimer laser irradiation improves corrosion resistance	[137]
Mg – ZK60 + SiC composite	1997	LSM	Corrosion	Enhance corrosion resistance	Uniform and refined microstructure produced by excimer laser improves corrosion resistance	[138]

(Continued)

Table 5. (*Continued*).

System	Year	LSE	Property	Scope	Results	Ref.
Ti and its alloys						
Ti–6Al–4V (TiN)	2001	LSA	Wear	Enhance wear resistance by LSA with nitrogen	TiN forms by LSA and improves wear resistance that occurs in 3 stages	[144]
Ti (Si,Al, Si + Al)	2000	LSA	Wear, friction	Improve wear resistance by LSA	LSA with Si is more effective than Al/Si + Al to improve wear resistance	[145]
Ti (Si,Al, Si + Al)	1999	LSA	Cyclic oxidation	Improve oxidation resistance by LSA with Si/Al	LSA with Si/Si + Al is more effective than Al in enhancing cyclic oxidation resistance between ambience/750oC	[146]
Ti–6Al–4V (WC,TiC)	1998	LSA	Corrosion	Enhance corrosion resistance	LSA with TiC improves, but that with WC deteriorates corrosion resistance	[147]
Ti (Ti + TiC)	1997	LSA	Hardness, wear	Increase hardness by developing a composite surface layer	LSA with TiC significantly enhances the hardness of substrate Ti	[148]
Ti and Ti–IMI829 alloy (N_2)	1996	LSA	Hardness, corrosion	Study microstructure and enhance hardness and corrosion resistance	LSA enhances hardness and corrosion resistance	[149]
Ti alloy (WC, TiC)	1996	LSA	Hardness	Improve wear/galling resistance	LSA significantly enhances hardness	[150]

9.1a *Corrosion resistance by LSE:* Parvathavarthini *et al* [92] have attempted to eliminate the susceptibility to inter-granular corrosion of the cold worked and sensitized AISI 316 stainless steel by laser surface melting (LSM). Similarly, Mudali *et al* [100] have found LSM could be useful in de-sensitization of nitrogen bearing 316L stainless steel. The improvement by LSM is attributed to complete dissolution of $M_{23}C_6$ type of carbides and suppression of re-precipitation due to rapid quenching. LSM in nitrogen atmosphere or of nitrogen bearing steel is reported to improve the resistance to pitting corrosion of AISI 304 stainless steel [92,93]. In either case, this improvement may arise due to the presence of chromic oxide and nitrogen compound on the surface and consequent reconstruction of the passive layer or barrier to the electrolyte. Potentiodynamic polarization and ultrasonic vibration studies with

stainless hard-facing NiCoCrB alloy coated mild steel have shown that LSM could markedly improve the resistance to corrosion and cavitation erosion-corrosion of the substrate [94]. However, attempts to simultaneously improve electrochemical and mechanical properties by LSE may be counter-productive as presence of ceramic or intermetallic phases on the surface may provide initiation sites for pitting [97].

Dutta Majumdar & Manna [99] have investigated the effect of LSM and LSA of plasma spray deposited Mo on AISI 304 stainless steel (304-SS). Figure 17a shows the optimum conditions (shaded region) for the formation of a homogeneous microstructure and composition in this study for improvement in pitting corrosion and mechanical property. Potentiodynamic anodic polarization tests of the substrate and laser surface alloyed samples (SS(Mo)) in 3·56 wt. % NaCl solution (both in forward and reverse potential) showed that the critical potential for pit formation (E_{PP1}) and growth (E_{PP2}) have significantly (2–3 times) improved from 75 mV(SCE) in 304-SS to 550 mV(SCE) (figure 17b). E_{PP2} has also been found to be nobler in as lased specimens than that in 304-SS. The poor pitting resistance of the plasma sprayed 304-SS samples (without laser remelting) was probably due to the presence of surface defects present in plasma deposited layer. Standard immersion test was conducted in a 3·56 wt. % NaCl solution to compare the effect of laser surface alloying on

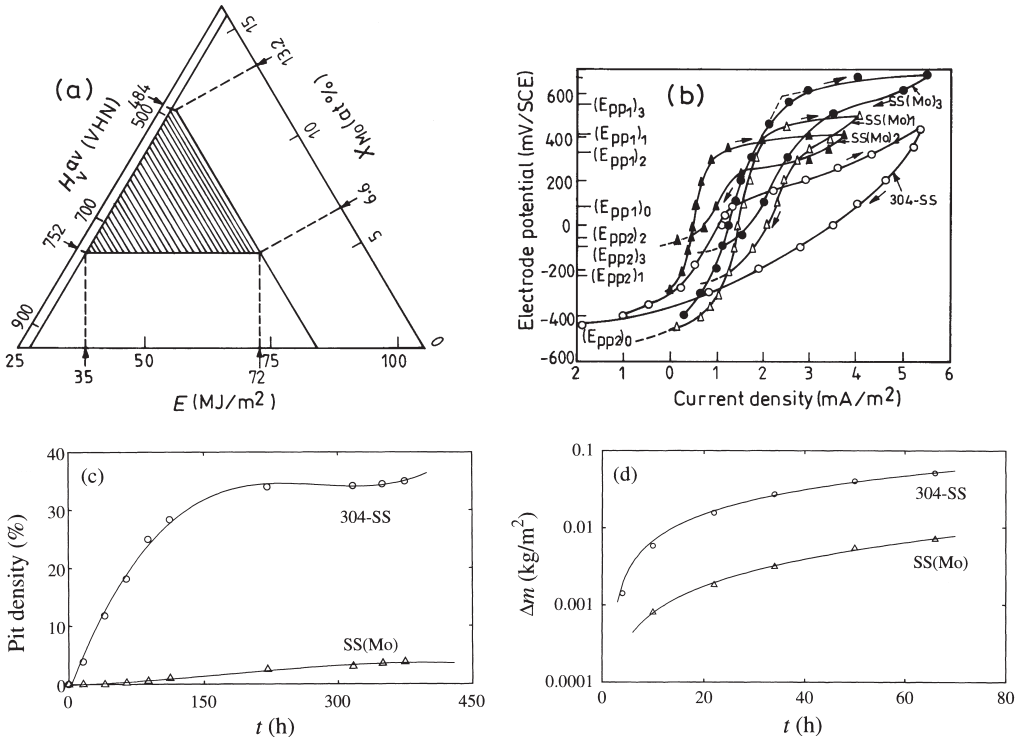

Figure 17. **(a)** Process optimization diagram for selecting the necessary energy density (E) for LSA of 304-SS with Mo to achieve the desired composition (X_{Mo}) and hardness (H_v^{av}) in the alloyed zone (shaded region), **(b)** cyclic potentiodynamic polarization behaviour of 304-SS and SS(Mo) in 3·56 wt. % NaCl solution, **(c)** variation of pit density in 304-SS and SS(Mo) as a function of time (t) in a 3·56 wt. % NaCl solution, and **(d)** comparison of material loss per unit area (Δm) due to erosion as a function of t for 304-SS and SS(Mo). For details, please see [99,197].

the pitting corrosion resistance. Figure 17c compares the kinetics of pit formation in terms of area fraction of pits determined by standard immersion test in a 3·56 wt.% NaCl solution as a function of time (t) between 304-SS and SS(Mo) lased with 1210 MW/m^2 power density and 31·7 mm/s scan speed for deposit thickness of 250 μm (corresponding to highest E_{PP1}). It is evident that both the extent and rate of pitting were significantly reduced in the SS(Mo) as compared to that in 304-SS. Furthermore, the process of pitting in 304-SS follows a sigmoidal nature marked by a substantially rapid initial stage than that of the later stage with no incubation time. In comparison, pits were noticed in SS(Mo) only after 50 h of immersion, and the number increases linearly following a much slower kinetics as compared to that in 304-SS. Continuous circulation of the samples at 750 rpm for 10 to 75 h in a medium containing 20 wt. % sand in 3·56 wt. % NaCl solution showed significant decrease in the kinetics of erosive-corrosion loss in SS(Mo) than that in 304-SS. It was thus concluded that LSA is capable of imparting an excellent superficial microhardness and resistance to corrosion and erosion-corrosion properties to 304-SS due to Mo both in solid solution and as precipitates.

In an attempt to develop stainless mild steel by coating ASTM S31254 stainless steel powder on plain carbon steel, Anjos *et al* [101] have noted that the anodic polarization behaviour following LSE is similar to the bulk stainless steel even in very aggressive solution. Similar efforts of surface alloying of Fe–Cr and Fe–Cr–Si–N layers on plain carbon steel to improve corrosion resistance led to development of a Fe–Cr–Si–N surface layer with a fine duplex microstructure that showed a higher pitting potential than that of the Fe–Cr layer [103]. The passive film resistance increased and passive current density decreased with the increasing Cr content.

9.1b *Oxidation resistance by LSE:* Oxidation is another serious mode of surface degradation that gets aggravated under unabated counter ionic transport of cations and anions at elevated temperature. Unlike electrochemical corrosion, oxidation occurs through dry reaction and solid state ionic transport through the oxide scale. In the past, several attempts have been made to enhance resistance to oxidation by LSA, LSC and similar LSE techniques [104–109]. Recently, Pillai *et al* [104] have obtained enhanced oxidation resistance (at 873 K for up to 200 h) of plain carbon steel following LSA with Al due to several intermetallic phases like $Al_{13}Fe_4$ and Al_2Fe_2. Agarwal *et al* [106] used a composite boride (TiB_2) coating to enhance oxidation resistance of steel in the range 600–1000°C. Thermal barrier coatings could also be effective for improving oxidation resistance of stainless steel [107]. However, such coatings are brittle and hence are applied with a favorable composition gradient like applying a bond coat (Ni–22Cr–14Al–1Y) between the topcoat ($ZrO_2 + 7{\cdot}5\ wt\%Y_2\ O_3$) and stainless steel substrate before single or multi pass LSM treatments. Oxidation tests at 1200°C indicated that double pass LSM was more effective to impart a better oxidation resistance [107]. Similar attempts of improving oxidation resistance have been made with Incoloy 800 H by LSA with Al [108] and by LSC of 316 L stainless steel with Fe–Cr–Al–Y alloy coatings [109]. In all these cases, it appears that the degree of enhancement of oxidation resistance by LSE primarily depends on stability, adherence, imperviousness and strength of the complex oxide scale comprising multiple oxide on top of the base metal.

Manna *et al* [139] attempted to enhance the high temperature oxidation resistance (above 873 K) of 2·25Cr–1Mo ferritic steel by laser surface alloying (LSA) with co-deposited Cr using a 6 kW continuous wave CO_2 laser. The main process variables chosen for optimizing the LSA routine were laser power (from 2 to 4 kW), scan speed of the sample-stage (150 to 400 mm/min) and powder feed rate (16 to 20 mg/s). Isothermal oxidation studies in air by thermogravimetric analysis at 973 and 1073 K for up to 150 h revealed that LSA had

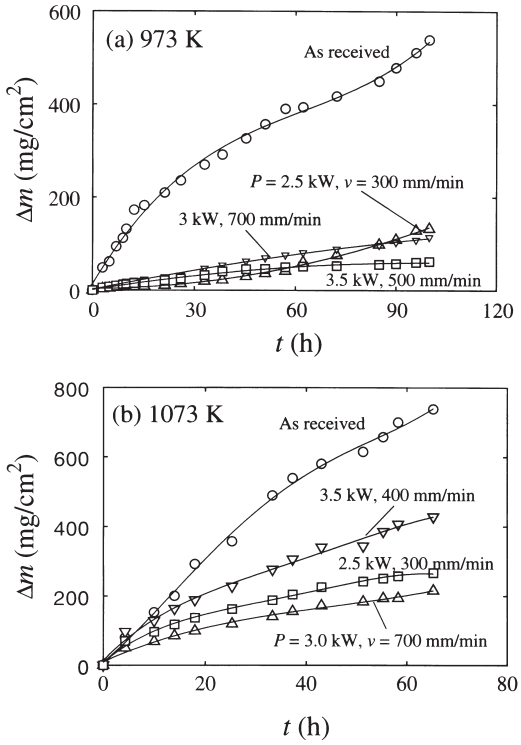

Figure 18. Kinetics of isothermal oxidation of 2·25Cr–1Mo ferritic steel laser surface alloyed with Cr and exposed to **(a)** 973 and **(b)** 1073 K in air, respectively [139].

significantly enhanced the oxidation resistance of ferritic steel during exposure to 973 and 1073 K (figures 18a,b). Post oxidation microstructural analysis suggests that an adherent and continuous Cr_2O_3 layer is responsible for the improvement in oxidation resistance [139].

Similar improvement in oxidation resistance has been obtained by LSR of bond (Ni–Cr–Al–Y) and top ($Zr\,O_2 + Y_2O_3$) coated stainless steel [107], LSC of Si-steel with Ni + Cr [141], LSM of inconel 600 [142] and LSA of inconel 800 H with Al [108].

9.1c *Wear resistance by LSE:* Attempt to improve wear resistance of steel by LSE seems to be more effective than the attempts to enhance the resistance to corrosion and oxidation. Cheng *et al* [110] have added a mixture of WC–Cr_3C_2–SiC–TiC–CrB_2 and Cr_2O_3 to produce a metal matrix composite surface on stainless steel UNS-S31603. Following LSM, cavitation erosion resistance improved in all cases except for Cr_2O_3. Wu & Hong [111] have attributed the improvement in hardness and corrosion/wear resistance of stainless steel to the presence of amorphous phase in the Zr-rich surface (with 7·8–14·5 at. % Zr) following LSA of stainless steel with Zr nano-particles. Roy & Manna [112] have demonstrated that laser surface hardening (LSH), instead of LSA or LSM is more effective in enhancing hardness and wear resistance of unalloyed austempered ductile iron (ADI). Figures 19 a,b show the typical martensitic microstructure developed by LSH and significant improvement in adhesive wear of laser hardened vis-à-vis as-received and laser surface melted ADI samples, respectively. Adhesive wear of austempered ductile iron consists of three distinct stages: the initial rapid, subsequent steady state and final accelerated (abrasive) wear. The improvement in wear resistance following LSH is attributed to the martensitic surface with residual compressive stress [112].

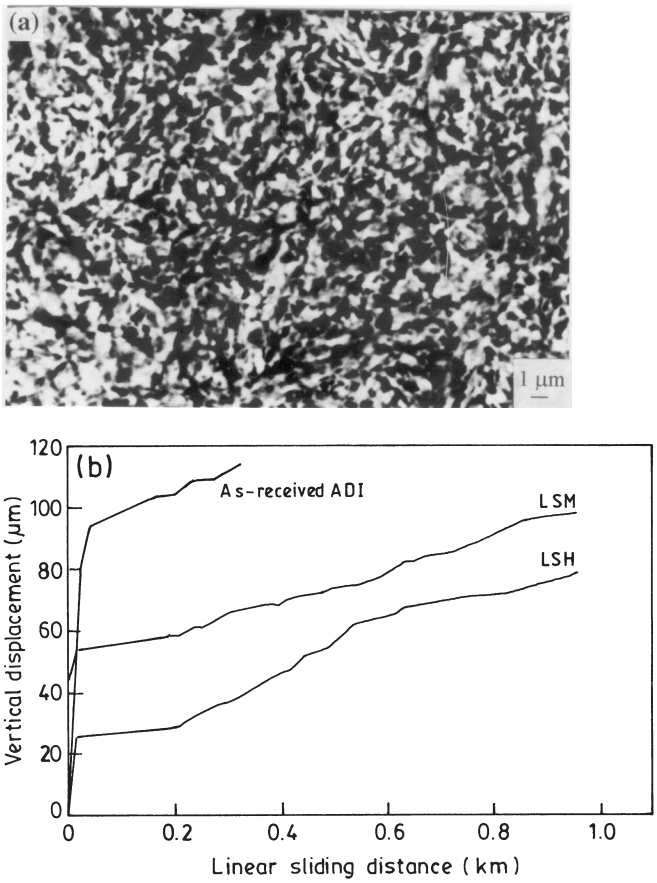

Figure 19. **(a)** A predominantly martensitic microstructure of the laser hardened sample surface, and **(b)** kinetics of wear in terms of vertical displacement of the pin-head as a function of sliding distance during adhesive wear testing of austempered ductile iron (ADI) subjected to LSM and LSH with a pin-on-disc machine in dry condition at 5 kg load. For details, please see [112,191,202].

Agarwal & Dahotre [113] have reported a substantial improvement in resistance to adhesive/abrasive wear of steel following LSA with TiB_2. The surface composite layer containing about 69 vol. % TiB_2 particles recorded an elastic modulus of 477·3 GPa. Similar improvement in wear resistance of mild steel was reported by Tondu *et al* [114] due to formation of a FeCr + TiC composite coating formed by laser assisted self propagating high temperature synthesis. Earlier, Zhukov *et al* [120] achieved a similar carbide dispersed composite coating on steel by laser assisted self-propagating high temperature synthesis.

Instead of composite coating, Pelletier *et al* [115] applied a Fe–Mn–C hadfield steel coating by LSC on steel and achieved significant improvement in hardness (over 800 VHN) elastic modulus (210 GPa) and yield strength (1200 MPa) mostly due to deformation induced twinning transformation. A signification mitigation of subsurface crack propagation in pearlitic rail steel was achieved following LSM without any change in surface chemistry [116]. Similar improvement in wear and friction properties of En 31 steel was obtained by LSH without melting or any change in surface chemistry [117]. However, the methods that involve change in surface composition seem more popular or effective in enhancing wear resistance of ferrous alloys. For instance, LSA of A7 tool steel with Ti was reported to reduce the dry sliding friction coefficient due to the formation of a low-friction transfer film [118].

Similarly, Stellite coating by LSC is a standard method of reducing wear loss of ferrous substrate [119]. Besides providing with a harder and tougher surface, stellite coating develops

a tougher oxide scales and reduces wear under severe condition. Improvement in hardness and wear resistance has been achieved by LSC of martensitic steel with Ni alloy [140] and LSA of ferritic steel with Cr_3C_2 + SiC [143]. Several other examples are cited in table 5.

9.2 *LSE of non-ferrous alloys*

Surface dependent degradation by wear, oxidation and corrosion is as much a problem in nonferrous metals and alloys as that in ferrous alloys. Thus LSE in widely applied to Al, Ti, Cu, Mg and other important nonferrous metals and alloys to extend the service life of components subjected to severe conditions of wear, oxidation and corrosion. In this section, we will briefly review the scope and current status of understanding regarding the application of LSE to enhance surface dependent properties of non-ferrous alloys. For ready reference, table 5 summarizes the major work done in the recent past in this area [92–150].

Several attempts have been made to improve corrosion resistance of Al-based alloys by LSM [121,125], LSA [122] and LSC/LSR [123,124]. While grain refinement and microstructural homogeneity are responsible for better corrosion resistance in LSM dispersion of intermetallic and/or amorphous phases are considered crucial for corrosion resistance following LSC/LSR. Katipelli & Dahotre [126] have achieved considerable improvement in oxidation resistance of 6061 Al alloy by LSA with Al + TiC. On the other hand, improved scale adherence is believed responsible for enhanced oxidation resistance of Al–Cu–Li and Al–Ga–As following LSM [127,128].

Improvement in wear resistance of Al alloys seems to necessitate addition of ceramic or intermetallic particles by LSC or LSA [129–132]. Usually, the alloyed or cladded layer possesses a high hardness and consists of intermetallic or amorphous phases [131,132]. Schnick *et al* [129] induced residual compressive stress by laser surface shocking and achieved a significant improvement in wear resistance in HVOF spray coated SiC on Al.

Manna & Dutta Majumdar [134] attempted to enhance the wear and erosion resistance of Cu by laser surface alloying with Cr (electrodeposited with 10 and 20 μm thickness, t_z). Total Cr content (X_{Cr}), Cr in the form of precipitates (f_{Cr}) and Cr in solid solution with Cu (Cu_{Cr}) were determined by energy dispersive spectrometry, optical microscope and X-ray diffraction technique respectively. LSA extended the solid solubility of Cr in Cu as high as 4·5 at. % as compared to 1 at. % under equilibrium condition. Figure 20a expresses the variation of X_{Cr}, Cu_{Cr}, and f_{Cr} as a function of E for $t_z = 20\,\mu$m. The higher the E, the smaller the X_{Cr}, Cu_{Cr}, and f_{Cr} in the alloyed zone. The microhardness of the alloyed zone was found to improve significantly (as high as 225 VHN). Since hardness is related to Cr present in solid solution and dispersed as precipitates in the matrix, the variation of average microhardness of the alloyed zone (H_v^{av}) as a function of the X_{Cr}, Cu_{Cr}, and w_{Cr} shows that hardness increases for all these microstructural factors, especially for Cu_{Cr} (figure 20b). f_{Cr} was converted to the corresponding weight fraction (w_{Cr}) by the simple relation: $w_{Cr} = X_{Cr} - Cu_{Cr}$. Thus, suitable LSA parameters must be chosen to obtain the desired hardness.

Figure 21a shows the variation of scratch depth (z_{sc}) as a function of load (L) for pure Cu as well as laser surface alloyed Cu with Cr [Cu(Cr)] subjected to scratching with an oscillating steel ball in a computer controlled scratch tester. It is evident that the rate of increase of z_{sc} with both load and number of scratches is much higher in pure Cu than that in Cu(Cr). Figure 21b compares the kinetics of material loss (Δm) of Cu(Cr) lased with 1590 MW/m^2 and 0·08 s power and interaction time, respectively ($t_z = 20\,\mu$m) with that of Cu as a function of time (t) under an accelerated erosive wear condition conducted both at room and high temperature in a slurry bath containing 20 wt. % sand. In addition to reducing the magnitude of Δm by over an order of magnitude, LSA has significantly decreased the kinetics of erosion loss in Cu(Cr)

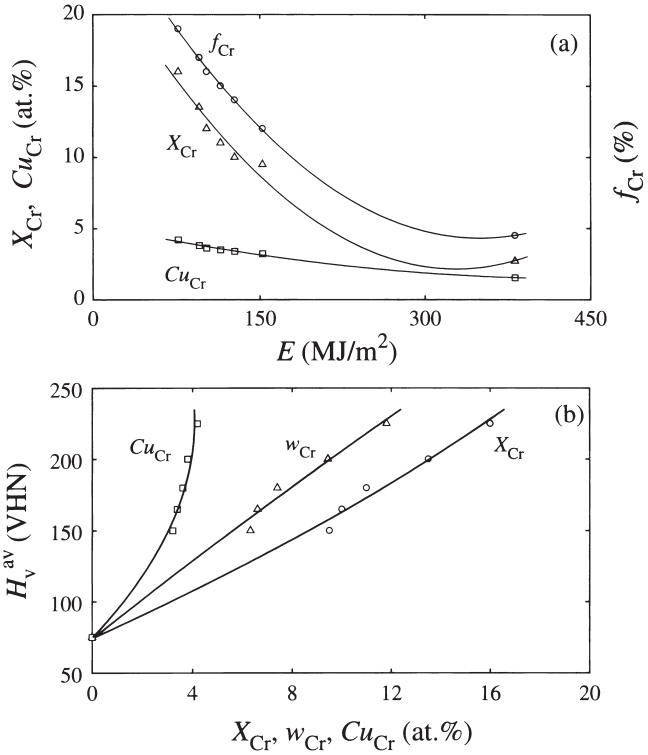

Figure 20. **(a)** Variation of Cr-content (X_{Cr}), dissolved Cr in solid solution (Cu_{Cr}) and volume fraction of Cr-precipitates (f_{Cr}) as a function of energy density (E), and **(b)** variation of H_v^{av} as a function of X_{Cr}, Cu_{Cr} and $w_{Cr}(= X_{Cr} - Cu_{Cr})$. For details, please see [134,195].

than that in Cu under comparable conditions. Though the extent of material loss increases with an increase in T for both pure Cu and Cu(Cr), the rate of erosion loss for Cu(Cr) is negligible as compared to a substantial change in Δm with T for pure Cu, especially beyond 370 K.

Uniform and refined surface microstructure by LSM seems quite effective in improving corrosion resistance in AZ91D/AM60B [136], AZ91 [137], Mg–ZK60 [138] and other commercial Mg-based alloys. Recently, Wang & Wue [135] have achieved significant improvement in corrosion resistance of SiC dispersed Mg by LSC with Al–12Si alloy layer.

Laser surface alloying of Ti with Si, Al and Si + Al (with a ratio of 3:1 and 1:3 respectively) was conducted to improve the wear and high temperature oxidation resistance of Ti by LSA [145,146]. Figure 22a reveals a typical hyper-eutectic microstructure on the top surface of the alloyed zone in Ti with Si consisting of faceted Ti_5Si_3 uniformly distributed in a two-phase eutectic aggregate of α-Ti and Ti_5Si_3 [146]. The high volume fraction of the primary phase and degree of fineness of the eutectic products signify complete dissolution and uniform intermixing of Si in the alloyed zone, and a rapid quenching experienced by the latter, respectively. Subsequent oxidation studies conducted at 873–1023 K showed that LSA of Ti with Si and Si + Al significantly improved the isothermal oxidation resistance (figure 22b).

In addition to oxidation, the effect of LSA of Ti with Si or Si + Al on wear resistance was also studied. Figure 22c shows the variation of depth of scratching (z_w) with load (L) due to scratching of pure Ti, Ti(Si), Ti(Al) and Ti(3Si + Al) with a hardened steel ball. It may be noted that z_w varies linearly with L for all the cases. The effect of L on z_{sc} is more prominent at higher number of scratching ($n_{sc} \geq 1000$) than that at a lower value of the same ($= 25$). Under comparable conditions of scratching, Ti undergoes the most rapid wear loss followed

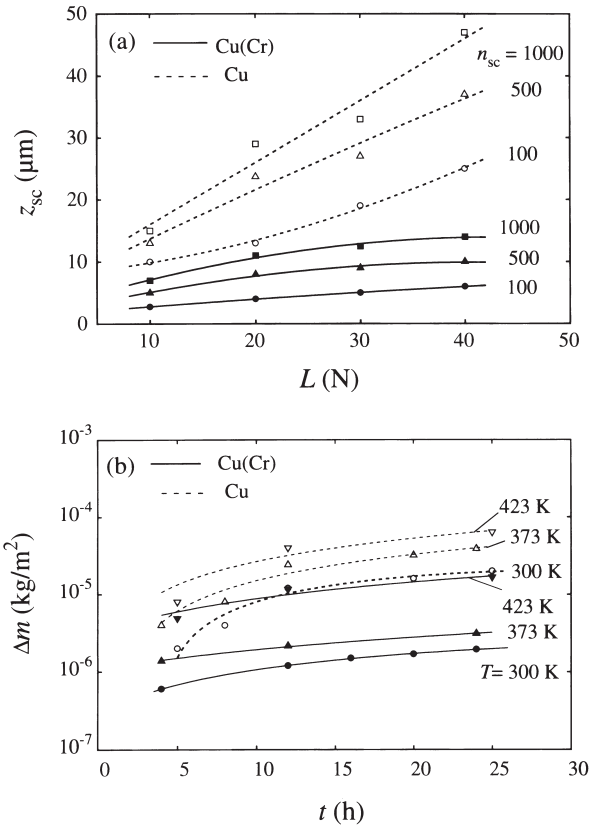

Figure 21. **(a)** Variation of scratch depth (z_{sc}) with load (L) for different numbers of oscillations (n_{sc}) for pure Cu and laser alloyed Cu(Cr), and **(b)** comparison between of material loss per unit area (Δm) due to erosion of Cu(Cr) and Cu as a function of time (t) at different temperature (T) due to erosion in flowing SiO_2 dispersed oil medium. For details please see [134,195].

by that in Ti(Al), Ti(3Si + Al) and Ti(Si). Ti(Si) undergoes the minimum wear loss. The improved wear resistance of laser surface alloyed Ti with Si was attributed to the formation of a hard Ti_5Si_3 precipitates in the alloyed zone [145].

Manna *et al* [199–201] made a novel attempt to develop the material for neural stimulation electrode by LSA of Ti with Ir that can mimic the normal spatio-temporal pattern of neuronal activation by reversible charge transfer. The usual electrode made of iridium is expensive, brittle and not amenable to miniaturization by plastic deformation. On the other hand, titanium is cheaper, bio compatible and amenable to drawing/etching. Figure 23a shows the indigenous set-up used for fabricating the electrode by LSA. Intelligent combination of laser parameters, powder composition and post LSA etching was used to develop the desired microstructure (figure 23b). Though charge density could not be measured due to exceedingly uneven surface intentionally developed by special etching (meant for increasing the surface area), the total charge was comparable to that of pure iridium in appropriate solution [201].

9.3 *Mathematical modelling on correlation between microstructure and LSE*

Studies on mathematical modelling of LSE mostly focus on predicting the thermal profile and composition in the laser irradiated volume. While the knowledge on thermal history and solute distribution is essential for predicting the properties, attempts have seldom been made to correlate the microstructure and property of the laser treated zone with the LSE parameters. Manna & Dutta Majumdar [198] developed a one dimensional heat transfer model based on

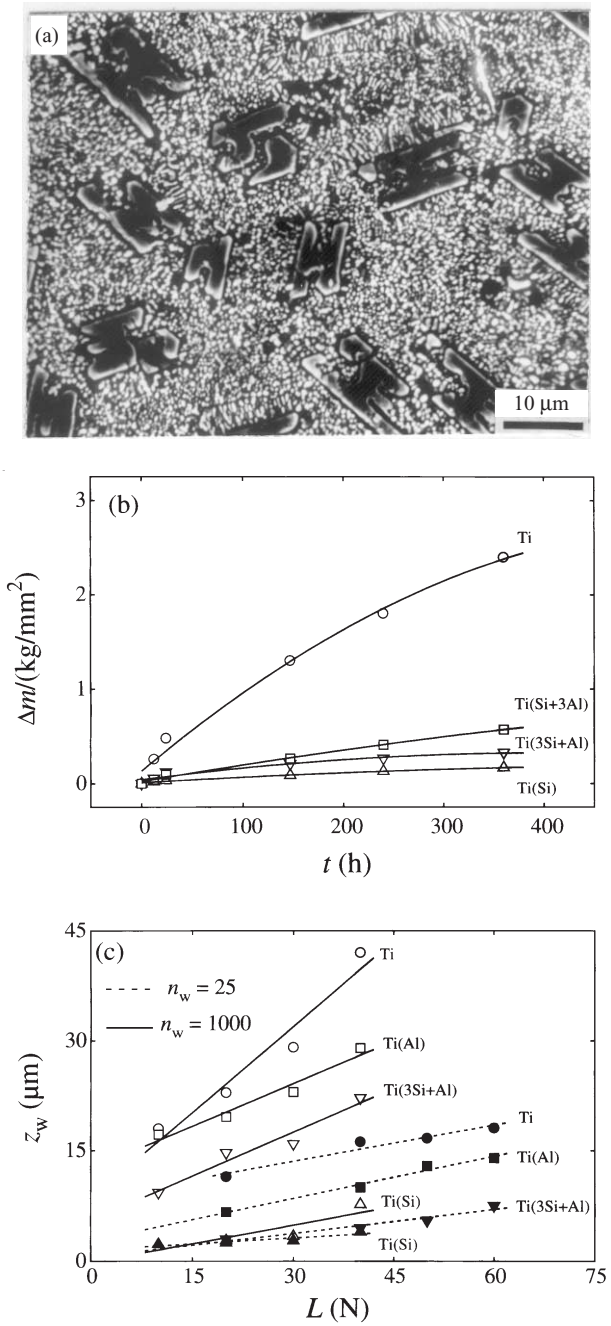

Figure 22. **(a)** Scanning electron micrograph of the top surface of laser surface alloyed Ti with Si, and **(b)** kinetics of oxidation expressed as total weight gain per unit area (Δm) as a function of time (t), and **(c)** kinetics of wear in scratch test expressed as depth of scratch (z_w) as a function of load (L) for Ti, Ti(Si), Ti(Al) and Ti(3Si + Al). For details about LSA, oxidation and wear test, please see [145,194].

explicit finite difference method to predict the thermal history (i.e. temperature profile, thermal gradient, cooling rate and solid–liquid interface velocity) and hence, the microstructure of the alloyed zone developed by laser surface alloying. Figure 24a shows the temperature (T) profile as a function of time (t) during LSA of AISI 304 stainless steel with 100 μm thick pre-deposited Mo using a CW–CO_2 laser delivering 1800 MW/m^2 power irradiation with a

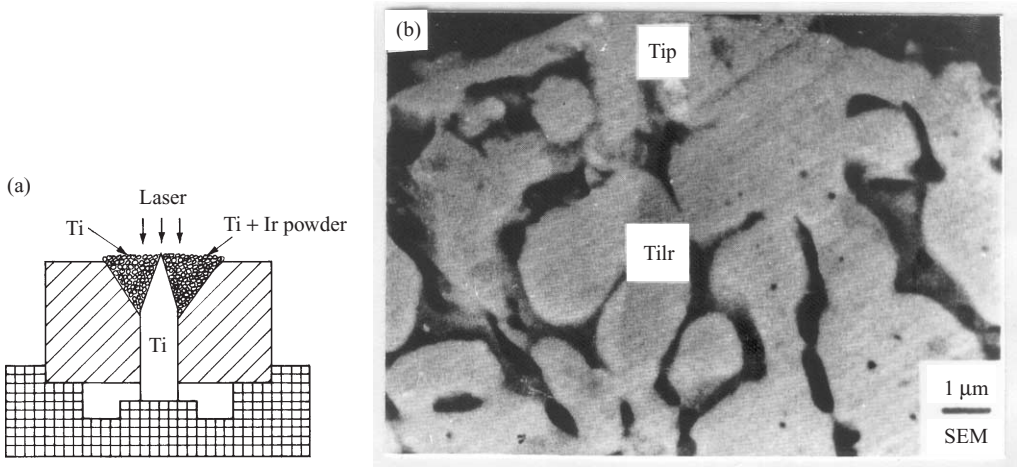

Figure 23. **(a)** Schematic diagram showing the set-up used for LSA of Ti with Ir (or Ti + Ir) by CO_2 laser pulse for developing neural stimulation electrode, and **(b)** microstructure of the alloyed zone showing a 3 fold increase in surface area following special etching [199,200].

25 ms interaction time. The calculation considered the effect of intermixing between the bi-metallic layer after melting and temperature dependence of concerned material properties. The corresponding thermal quenching rate has been shown in figure 24b. The model allows calculation of other thermal parameters like thermal gradient, solidification velocity, etc. that are useful in predicting the microstructure [204]. Similar model could be extended to two-dimensional radially symmetric heat transfer condition [205].

Roy & Manna [191] have used a simple analytical approach, based on the treatment of Ashby & Easterling [188], to predict the thermal profile in LSH of austempered ductile iron and explain the phenomenon of partial or complete 'localized melting' of graphite nodules without liquefaction of the surrounding ferritic matrix. This phenomenon was first reported by Fiorletta *et al* [206]. Figure 25a reveals that a graphite nodule has undergone partial melting during LSH of austempered ductile iron with 650 W power and 60 mm/s scan speed. Note that melting initiates at the graphite-matrix interface and assumes only a part of the nodule leaving the core unaffected. The extent or width of this incipient fusion primarily depends on the thermal cycle and concomitant carbon diffusion profile from the nodule into the matrix. The mathematical model to predict the thermal and composition profile, and hence, the width of annular molten region by Roy & Manna [191] could establish a fair-correlation between the melt width (y_m) and laser parameters used for LSH. Figure 25b shows the variation of y_m as a function of depth (z) from the surface predicted for two predetermined conditions of laser surface hardening. It is evident that y_m decreases as z increases bearing a linear relationship between them. The experimental data (open symbols) are fairly close to the predicted trend of the model, particularly for higher laser power.

9.4 *Summary and future scope*

Laser surface engineering encompasses several applications that are mainly related to enhancing one of the surface dependent properties like hardness, friction, fatigue and resistance to wear, corrosion, etc. There are several books [1–4,8–10,19] and review articles [18,20,180–184] exclusively dealing with this subject. The present section thus made an attempt mainly

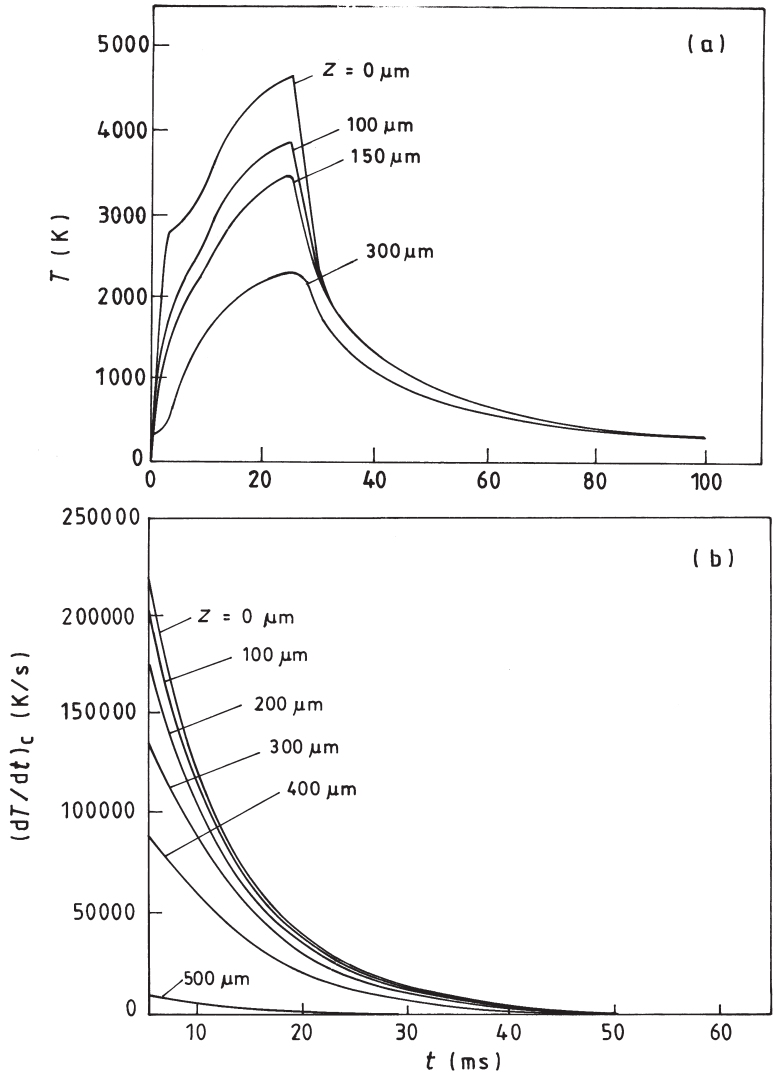

Figure 24. **(a)** Temperature (T) distribution as a function of time (t) for SS(Mo) at different levels of depth (z), and **(b)** variation of corresponding cooling rate $(\mathrm{d}T/\mathrm{d}t)_C$ as a function of time (t) at different z during LSA of AISI 304 stainless steel with Mo. For details, please see [198,204].

to review the recent developments and highlight the important issues concerning them. An important aspect purposely avoided in this contribution, obviously to avoid exceeding the prescribed length, concerns mathematical modelling of LSE. For this, readers may see references [5–6,185–186] and obtain most of the necessary data on material properties from the references [189–190]. The current trend appears to suggest that the excimer and diode lasers with shorter wavelengths may soon substitute CO_2 even YAG lasers for LSE applications. Sustained efforts will then be needed to establish the microstructural evolution and scope of improvement following LSE with those new lasers.

Apart from structural applications, LSE could be equally useful in enhancing functional properties like magnetism, emission/absorption characteristics, sensors, microelectronic

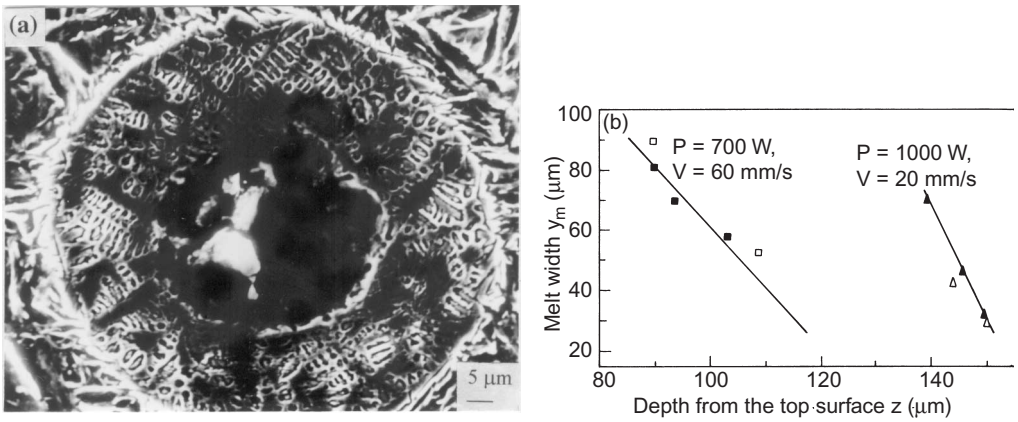

Figure 25. **(a)** Partial melting of a graphite nodule embedded in the ferritic/martensitic matrix following LSH with 650 W power and 60 mm/s scan speed. Note that melting initiated at the graphite-matrix interface and consumed nearly half the nodule from the circumference, and **(b)** variation of predicted melts widths (y_m) around graphite nodules as a function of depth (z) from the surface. Open and solid symbols represent experimental and predicted data, respectively [191].

devices and several other applications requiring monolithic or functionally/ compositionally graded microstructures confined to smaller dimensions. The LSE processes described in this section are equally applicable to such functional application, provided the correct laser parameters (wavelength, mode, energy etc.) are selected for the given materials (semiconductor, polymer etc.).

The major outstanding issues concerning LSE are: (a) utilization of shorter wavelengths for more precise surface engineering, (b) developing compositionally and functionally graded microstructure, (c) elimination or minimization of structural/coefficient mismatch and combining dissimilar materials. In the next section, we shall introduce a major challenge concerning LSE that might prove a technological breakthrough if it is possible to convert the scientific feasibility into commercial reality.

10. Laser surface vitrification – A challenge

It is known that environmental degradation by corrosion and oxidation alone accounts for more than 30% discard and loss of engineering components of all dimensions from bridges/railway-carriages to needles/bolts made of metals and alloys. While replacing a bolt/structural member in a bridge or painting a carriage is neither too expensive nor difficult, an early malfunction of a heart valve, orthopedic implant or aeroturbine engine component may pose threat to the human life, cause tremendous trauma and lead to catastrophic failure respectively.

One or higher dimensional structural defects in a polycrystalline aggregate like dislocations, homo/heterophase boundaries, voids and inclusions constitute the higher energy hence preferred nucleation sites for materials degradation by oxidation and corrosion. On the other hand, an amorphous state is devoid of both crystalline anisotropy and intercrystalline defects, and thus, does not provide the nucleation sites and short-circuiting diffusion path for such environmental degradation. However, an amorphous or glassy material, more often than not, is brittle and not amenable to material processing/shaping to develop a large component of complex geometry. Thus, a crystalline solid with an amorphous surface or over-layer is

obviously superior to a usual crystalline engineering component for applications in hostile environment where aqueous corrosion and high temperature oxidation are anticipated.

Since the maiden success of Klement *et al* [151] in 1960 in developing Au–Si metallic glass by rapid quenching from the liquid stage, considerable research efforts have been devoted in the past few decades to form metallic glasses with other metals/alloys. It is now generally accepted that all liquid metals/alloys may be transformed to the glassy state provided crystallization is overridden during solidification [152]. The cooling rate required to retain the glassy state, which is the maximum for monoatomic pure metals [153], is a strong function of the melt composition. Rapid solidification processing (RSP) including splat cooling is by now an established technology in producing metallic glasses. However, limitation in the maximum cooling rate achievable ($< 10^5$–10^8 K/s), stringency of melt composition amenable to amorphization and constraints of physical dimensions of the amorphous ribbons/products have severely restricted the scope of RSP to produce metallic glasses.

In this regard, the landmark discovery of Lin & Spaepen [154] to form metallic glasses from compositionally modulated Fe–B thin film sandwich using pico-second pulse laser irradiation pioneered a unique possibility of laser assisted surface vitrification or amorphization. Suppression of partition-less crystallization was attributed to both the ultra-high quenching rate achieved ($10^{10} - 10^{13}$ K/s) and preference to collision-limited transformation over the interface or diffusion-limited mechanism due to the slow kinetics of the latter. The results assumed particular significance because amorphization of only the surface of a crystalline material was earlier believed not feasible due to the scope of epitaxial growth of partitionless or partition-involved crystallization from the underlying solid substrate.

Table 6 presents an exhaustive list of systems known to have undergone laser assisted surface amorphization. Snezhnoi *et al* [155] were the first to report the presence of an amorphous phase on the laser remelted chilled (ledeburitic) cast iron surface showing an average hardness of 1200 H_V. Subsequently, Bergmann & Mordike [156,157] were successful in developing dispersion of Fe–B based amorphous phases in laser surface quenched cast tool steel, Cr-steel

Table 6. Summary of work done on laser surface vitrification (LSV).

Year	Substrate/deposit	Laser	Ref.
1980	Chilled cast iron	Nd: Glass pulsed	[155]
1980	Cast tool steel/Fe–B (sprayed)	CW–CO_2	[156]
1981	Fe–2C–12Cr/Fe–B Nb-alloy	CW–CO_2	[157]
1981	Fe–C/Si–P–B (ternary/quaternary)	TEA–CO_2 Pulsed	[158]
1982	Fe–Fe_3B (modulated thin film)	Nd:YAG Pulsed	[154]
1984	Fe-4 at.% B	Nd:YAG Pulsed	[160]
1984	Mo/Ni (30–60 at%) Mo/Co (45 at%) Co/Nb (40 at%)	Nd:YAG mode locked	[161]
1984	Ni–Nb thin film	Nd:YAG	[160]
1984	Zr/Cu	Nd:YAGQ-switched	[162]
1984	Au–Ti, Co–Ti, Cr–Ti, Zr–Ti	Pulsed	[159]
1984	Pd–6Cu–16Si	CW–CO_2	[166]
1986	Fe–10Si–15B	Pulsed CO_2	[168]
1987	Fe–10Cr–5Mo/12–14 P, C	CW–CO_2	[169]
1985	Pure Ga	KrF excimer	[171]
1987	Mild steel/Ni–Cr–16P–4B	CW–CO_2	[169]
1989	Ni, Cu(Ni), Ti(Ni)/Pd–25Rh–10P–9Si	CW–CO_2	[170]
1988	Nb/Ni–Pt–Pd–Rh	CW–CO_2	[165]
1988	Fe–Cr–P–C–Si	CW–CO_2	[174]
1990	Review-paper		[163]

and Nb-alloys. Borodina [158] met with similar success of amorphizing the surface of several ternary and quaternary Fe-metalloid (B/C/Si) compositions up to 7–20 μm depth. Affolter & von Allmen [159] attempted to establish the criteria for surface amorphization by laser irradiation with Au–Ti, Co–Ti, Cr–Ti and Zr–Ti binary systems. While surface amorphization was achieved in Au–Ti, Co–Ti and Cr–Ti systems, failure to convert Zr–Ti couple into the glassy state was attributed to the scope of easy partitionless crystallization enabled by complete mutual solubility both in liquid and solid state in Zr–Ti.

Lin & Spaepen [160] extended their earlier approach to produce amorphous layers in Ni–Nb [160], and Mo–Ni, Mo–Co and Co–Nb couple [161]. A systematic study on the genesis of surface amorphization appears to suggest that impurity stabilization of short-range order in the liquid state is primarily responsible to prevent diffusion controlled or partitionless crystallization during laser quenching. For instance, the formation of the metallic glass in Cu–Zr by den Broeder *et al* [162] is a typical case of impurity stabilized surface amorphization. Hashimoto *et al* [163] have reviewed a number of experimental studies [164–170] by their own group to emphasize that laser assisted surface amorphization is a feasible method of improving corrosion resistance of bulk crystalline alloys.

Thus, a sizable number of experimental studies seem to evidence that surface amorphization of laser irradiation is feasible under a chosen composition range and optimum LSE condition. In this regard, the extreme heating/cooling rates, thermal gradient and resolidification-velocity may aid the collision controlled partitionless amorphization of the melt. However, Kear *et al* [172] and Bergmann & Mordike [156,157] pointed out that suppression of epitaxial nucleation and prevention of growth of crystallites from the underlying solid substrate must be insured to achieve this laser assisted surface amorphization.

Spaepen [173] has worked out the thermodynamic and kinetic criteria for surface amorphization for picosecond pulse laser irradiation of metals. It is suggested that partitionless crystallization may occur at an interface velocity (v_i) of 100 m/s so long as the isotherm velocity (v_T) coincides with v_i. When $v_i < v_T$, the liquid may be quenched as glass. The time (t) for a monolayer (say, $z = 0{\cdot}3$ nm) crystallization is approximately 3 ps. The corresponding diffusion distance $(D_l t)^{1/2}$ is less than an interatomic distance (D_l = liquid diffusivity, $\sim 10^{-8}$ m^2/s). Hence, the liquid may undergo only partitionless solidification either as a crystal or glass.

Thermodynamically, partitionless solidification occurs only below the T_0-curve, as shown in figure 26. The solidified structure is crystalline at either A-rich or B-rich ends of the hypothetical phase diagram. Since the T_0-curves are of 'deep-plunging' type [9], it is likely that the atomic transport rate at sufficiently low temperature (say, below T_g) is too sluggish to nucleate a crystalline phase. As a result, the liquid may be configurationally frozen to a supercooled liquid or glassy structure. Suppression of crystallization is likely in the shaded composition range. However, the criterion illustrated in figure 26 is only an essential but not sufficient condition for surface amorphization.

Thus, interface velocity in metals for heat flow limited condition ($v_{i,th}$) is given by:

$$v_{i,th} = nz(T_m - T_i)/T_i,$$

where, n is atomic jump frequency across the solid–liquid interface, z is the distance or depth, and T_m and T_i are melting and interface temperatures. The resolidification rate is also governed by the rate of removal of down the thermal gradient across the interface. Thus, $v_{i,th}$ may be obtained as:

$$v_{i,th} = (\mathrm{k}\mathrm{V}_m \Delta T)/\Delta H_c,$$

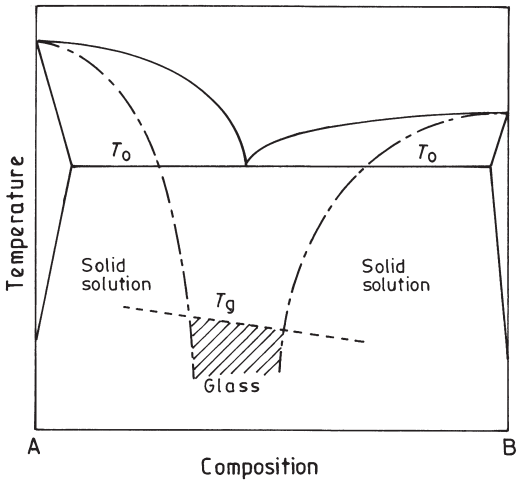

Figure 26. A schematic binary phase diagram showing the plunging T_o-curves for the terminal solid solutions. The shaded region represents the composition range (below T_g) in which partition-less solidification may lead to amorphization or vitrification.

where k is the thermal conductivity, ΔT is the thermal gradient, V_m is the molar volume, and ΔH_c is the latent heat of crystallization.

The solidification is 'heat flow limited' when $v_{i,th} \ll nz$ and $T_i \simeq T_m$. This is the case for usual solidification and crystal growth. However, $v_{i,th} \gg nz$ and $T_m > T_i$ in LSE such that the growth is 'interface-limited' leading to the formation of metastable phases and glassy state. Furthermore, depending on the magnitude of the product nz, solidification may either belong to collision controlled (when $n \simeq$ thermal vibration frequency) or diffusion controlled (when $n =$ diffusion jump frequency) regime. While the former process (applicable to pure metals, dilute alloys and intermetallic compounds) is difficult (or impossible) to suppress, the latter mechanism may easily be overridden if ΔT is large or $T_i \ll T_m$ and $T_i < T_g$. This criterion may be applicable for amorphization at $T_i < T_0 < T_g$ even for systems not having a plunging T_0-curve if, and only if, the concerned partitionless solidification is diffusion controlled and considerable change in short range order in the liquid is necessary for crystallization.

The theoretical analysis presented above is primarily applicable to surface amorphization by picosecond pulsed laser treatment. For practical applications as an industrial process, particularly for large-sized and complex-shaped components, pulsed laser is not quite suitable. Instead, a CW–CO_2 laser with suitable scope of surface scanning/integration is required for that purpose. If CW–CO_2 laser is to be utilized for laser assisted surface amorphization, the following difficulties and hurdles are likely to be encountered:

(a) Epitaxial nucleation and growth of crystalline phases from the well compatible liquid-substrate interface as a competitive process to partitionless amorphization.
(b) Recrystallization or nucleation of crystalline phase at the overlap regions between adjacent laser tracks due to thermal activation.
(c) Possibility of diffusion-controlled partial crystallization from the melt or adjacent amorphous regions due to a relatively longer interaction time necessary for a CW–CO_2 laser assisted LSE process.
(d) Deviation from the intended melt composition due to a possible compositional dilution effect in the melt arising out of a higher interaction time and hence higher melt depth.

To achieve LSV, it is necessary to suppress the scope of epitaxial nucleation/growth, and overcome the difficulty of maintaining collision controlled interface limited growth. It is predicted (by the applicant) that kinetic barrier at $T_i < T_o < T_g$ may suppress nucleation

of crystalline phases due to poor atomic mobility and high viscosity. However, attaining this glassy state will crucially depend upon the melt composition, heat and mass transfer condition and suppression of epitaxial nucleation that primarily depends on the ability of maintain the condition: $T_i < T_o < T_g$. This is usually not possible through any of the known LSE techniques/routines.

11. Concluding remarks

Lasers are a clean source of heating with a unique set of optical properties that allow a wide range of material processing methods from mere heating to synthesis of finished components. In this article, we have reviewed the major material processing routines that are either routinely used in the industry or are slated for future exploitation. The processes discussed are broadly categorized into laser-assisted forming (bending, colouring, rapid prototyping etc.), joining (welding, soldering, brazing etc.), machining (cutting, drilling, cleaning etc.) and surface engineering (hardening, annealing, alloying etc.). The materials considered include metallic, polymeric, ceramic, semiconductor and various combinations thereof. Comprehensive lists of notable and current studies in the relevant areas are documented in separate tables for ready reference. The focus of this review centres on the basic principles, scope and mechanism/methodology of a given process. Conscious effort has been made to outline the outstanding issues and define the future scope of research and development in some selected areas. However, the discussion is intentionally made succinct in order to restrict the length of the article.

The major hurdles that restrict wider use of lasers in routine material processing applications are limitation of beam size with respect to the component size/dimension, high installation and replacement cost, additional and expensive accessories, and need for skilled manpower. However, the high productivity, precision and versatility of laser material processing can easily overcome the above limitations, if areas are identified where laser offers unmatched advantages in terms of end properties and product quality in comparison to those achieved by other conventional techniques. It is hoped that the present review would provide an impetus in that direction.

The authors wish to record their deep appreciation and gratitude to their collaborators in India (Drs A K Nath, G L Goswami, S V Joshi, A Bharti) and abroad (Profs W M Steen, B L Mordike, K G Watkins, N B Dahotre). Useful discussion with their colleagues (Profs U K Chatterjee, S K Roy and S K Pabi) and contributions of the former students are sincerely acknowledged. Partial financial support from the Council of Scientific and Industrial Research and Department of Science and Technology, New Delhi is duly acknowledged. One of the authors (I M) would like to thank the Alexander von Humboldt Foundation, Bonn for financial support during the preparation of the manuscript.

References*

1. Steen W M (ed.) 1991 *Laser material processing* (New York: Springer Verlag)
2. Duley W W 1986 *Laser surface treatment of metals: NATO-ASI Series (E) No.: 115* (eds) C W Draper, P Mazzoldi (Boston: Martinus Nijhoff) p. 3

*References are not in journal format

3. Mordike B L 1993 *Materials science and technology* (eds) R W Cahn, P Haasen, E J Kramer (Weinheim: VCH) 15: 111
4. Draper C W 1980 *Laser and electron beam processing of materials* (eds) C W White, P S Peercy (New York: Academic Press) p. 721
5. Mazumdar J 1983 *Lasers for materials processing* (ed.) M Bass (New York: North Holland) p. 113
6. Rykalin N N, Uglov A, Kokora A 1978 *Laser machining and welding* (Moscow: Mir)
7. von Allem M 1982 *Laser annealing of semiconductors* (eds) J M Poate, J W Mayer (New York: Academic Press) p. 43
8. White C W, Aziz M J 1987 *Surface alloying by ion, electron and laser beams* (eds) L E Rehn, S T Picraux, H Wiedersich (Metals Park O: ASM) p. 19
9. Perepezko J H, Boettinger W J 1987 *Surface alloying by ion, electron and laser beams* (eds) L E Rehn, S T Picraux, H Wiedersich (Metals Park, Ohio: ASM) p. 51
10. Picraux S T, Follstaedt D M 1983 *Laser–solid interactions and transient thermal processing of materials* (eds) J Narayan, W L Brown, R A Lemons (New York: North-Holland) p. 751
11. Einstein A 1917 *Z. Phys* 18: 121
12. Kopfermamm H, Ladenburg R 1928 *Phys. Chem. Abt.* A139: 375
13. Maiman T H 1960 *Nature (London)* 187: 493
14. Andrews J G, Atthey D R 1976 *J. Phys.* D9: 2181
15. Laeng J, Stewart J G, Liou F W 2000 *Int. J. Prod. Res.* 38: 3973–3996
16. Dawas C (ed.) 1992 *Laser welding* (New York: McGraw-Hill)
17. Duley W W (ed.) 1999 *Laser welding* (New York: John Wiley & Sons) p. 1
18. Draper C W, Poate J M 1985 *Int. Met. Rev.* 30: 85–108
19. Molian P A 1989 *Surface modification technologies-An engineers guide* (ed.) T S Sudarshan (New York: Marcel Dekker) p. 421
20. Draper C W, Ewing C A 1984 *J. Mater. Sci.* 19: 3815
21. Chan K C, Liang J 2001 *Compos. Sci. Technol.* 61: 1265–1270
22. Chan K C, Yau C L, Lee W B 2000 *J. Laser Appl.* 12: 34–40
23. Chen G, Xu X, Poon C C, A C 1999 *J. Appl. Mech.* 66: 772–779
24. Magee J, Watkins K G, Steen W M, Calder N J, Sidhu J, Kirby Jn 1998 *J. Laser Appl.* 10: 149–155
25. van den Burg M, De-Hosson J T M 1995 *Interface Sci.* 3: 107–118
26. Gaumann M, Bezencon C, Canalis P, Kurz W 2001 *Acta Mater.* 49: 1051–1062
27. Cleton, Jouneau P H, Henry S, Gaumann M, Buffat P A 1999 *Scanning* 21: 232–237
28. Ruys A J, Kerdic J A, Sorrell C C 1996 *J. Mater. Sci.* 31: 4347–4355
29. Wiehua- Wang W, Holl M R, Schwartz D T, 2001 *J. Electrochem. Soc.* 148: C363–C368
30. Greco A, Licciulli A, Maffezzoli A 2001 *J. Mater. Sci.* 36: 99–105
31. Lu L, Fuh J Y H, Chen Z D, Leong C C, Wong Y S 2000 *Mater. Res. Bull.* 35: 1555–1561
32. Daneshvar K, Raissi M, Bobbio S M 2000 *J. Appl. Phys.* 88: 2205–2210
33. Wanke M C, Lehmann O, Muller K, Qingzhe W, Stuke M 1997 *Science* 275: 1284–1286
34. Lehmann O, Stuke M 1995 *Science* 270: 1644–1646
35. Lu Y F, Qiu H 2000 *J. Appl. Phys.* 88: 1082–1087
36. Seifert G, Kaempfe M, Berg K J, Graener H 2000 *Appl. Phys.* B71: 795–800
37. Lu Y F, Song W D, Hong M H, Chong T C, Low T S 1997 *Appl. Phys.* A64: 573–578
38. Muggli P, Brogle R, Joshi C 1995 *J. Optical Soc.* B12: 553–558
39. Parmar R S 1999 (ed.) *Welding engineering and technology* (New Delhi: Khanna)
40. Lancaster J F (ed.) *Metallurgy of welding* (London: George Allen and Unwin)
41. Wang H M, Chen Y L, Yu L G 2000 *Mater. Sci. Eng.* A293: 1–6
42. Leong K H, Kirkham P A, Jr Meinert K C 2000 *J. Laser Appl.* 12: 181–184
43. Hirose A, Todaka H, Yamaoka K, Kurosawa N, Kobayashi K F 1999 *Metall. Mater. Trans.* A30: 2115–2120
44. Weckman D C, Kerr H W, Liu J T 1997 *Metall. Mater. Trans.* B28: 687–700
45. Lee M F, Huang J C, Ho N J 1996 *J. Mater. Sci.* 31: 1455–1468

46. Whitaker I R, McCartney D G 1995 *Mater. Sci. Eng.* A196: 155–163
47. Biro E, Zhou Y, Weckman D C, Ely K J 2001 *J. Laser Appl.* 13: 96–104
48. Fuhrich T, Berger P, Hugel H 2001 *J. Laser Appl.* 13: 178–186
49. Farid M, Molian P A 2000 *J. Mater. Sci.* 15: 3817–3826
50. Ng E S, Watson I A 1999 *J. Laser Appl.* 11: 273–278
51. El-Batahgy A M 1997 *Mater. Lett.* 32: 155–63
52. Szymanski Z, Kurzyna J, Kalita W 1997 *J. Phys.* D30: 3153–62
53. Cheng W H, Wang W H, Chen J C 1996 *IEEE Trans. Components, Packaging Manu. Technol.* 19: 764–769
54. Wang G, Tandon K N 1995 *Microgravity Sci. Technol.* 8: 131–133
55. Hsu T T, Wang Y R, Wu S K, Chen C 2001 *Metall. Mater. Trans.* A32: 569–576
56. Perret O, Bizouard M, Naudy Ph, Pascal G, Nore D, Horde Y, Delaisse Y 2001 *J. Appl. Phys.* 90: 27–30
57. Tsay L W, Tsay C Y 1997 *Int. J. Fatigue* 19: 713–720
58. Hirose A, Fukumoto S, Kobayashi K F 1995 *Key Eng. Mater.* 104–107:853–872
59. Marya M, Edwards G R 2001 *J. Mater. Eng. Performance* 4: 435–443
60. Lorenzen D, Bonhaus J, Fahrner W R, Kaulfersch E, Worner E, Koidl P, Unger K, Muller D, Rolke S, Schmidt H, Grellmann M 2001 *IEEE Trans. Ind. Electron.* 48: 286–297
61. Schubert E, Seefeld T, Zerner I, Grupp M, Sepold G 1999 *Laser Opt.* 31: 75–77
62. Heitz J, Pedarnig J D, Baeuerle D, Petzow G 1997 *Appl. Phys.* A65: 259–261
63. Kahlen F J, Kar A 2001 *J. Laser Appl.* 13: 60–69
64. De-Hosson J T M, Hooijmans J, Popma R 2000 *Surface Eng.* 16: 245–249
65. Chou J F, Lin M H, Lu H Y 2000 *Acta Mater.* 48: 3569–3579
66. Guo F, Lucas J P, Subramanian K N 2001 *J. Mater. Sci.* 12: 27–35
67. Brandner M, Seibold G, Chang C, Dausinger F, Hugel H 2000 *J. Laser Appl.* 12: 194–199
68. Berkowitz H, Walvoord J 1997 *Soldering Surface Mount Technol.* 9: 41–43
69. Yamaguchi S, Chiba K, Saito Y, Kobayashi T 1996 *Opt. Eng.* 35: 3585–3590
70. McNally K M, Sorg B S, Welch A J, Dawes J M, Owen E R 1999 *Phys. Med. Biol.* 44: 983–1002
71. Illyefaalvi-Vitez Z 2001 *Microelectron. Reliab.* 41: 563–570
72. Bernstein J B, Joo-Han-Lee, Gang-Yang, Dahmas T A 2000 *IEEE Trans. Semiconductor Manuf.* 13: 228–234
73. Chen S L 1998 *Proc. Inst. Mech. Eng., B (J. Eng. Manuf.)* 212: 113–128
74. Yue T M, Lau W S 1996 *Mater. Manuf. Process.* 11: 17–29
75. Yilbas B S, Sahin A Z 1995 *Opt. Laser Technol.* 27: 175–184
76. Lehane C, Kwok H S 2001 *Appl. Phys.* A73: 45–48
77. Zhu X, Villeneuve D M, Yu A Naumov, Nikumb S, Corkum P B 1999 *Appl. Surf. Sci.* 152: 138–148
78. Katsarakis N, Chatzitheodoridis E, Kiriakidis G, Sigalas M M, Soukoulis C M, Leung W Y, Tuttle G 1999 *Appl. Phys. Lett.* 74: 3263–3265
79. Lumpp J K Allen S D 1997 *IEEE Trans. Components, Packaging Manuf. Technol.* 20: 241–246
80. Psyllaki P, Oltra R 2000 *Mater. Sci. Eng.* A282: 145–52
81. Lu Y F, Lee Y P, Zhou M S 1998 *J. Appl. Phys.* 83: 1677–1684
82. Tsunemi A, Hagiwara K, Saito N, Nagasaka K, Miyamoto Y, Suto O, Tashiro H 1997 *Appl. Phys.* A63 435–439
83. Feng Y, Liu Z Q, Yi X S 2001 *J. Mater. Sci. Lett.* 20: 517–519
84. Beu-Zion D, Inberg A, Croitoru N, Shalem S A, Katzir 2000 *Opti Eng.* 39: 1384–1390
85. Xiao Y S, Yi F 1999 *J. Mater. Sci. Lett.* 18: 245–247
86. Buckley G S, Roland C M 1997 *Polym. Eng. Sci.* 37: 138–142
87. Alexander D R, Khlif M S 1996 *Opt. Lasers Eng.* 25: 55–70
88. Allcock G, Dyer P E, Elliner G, Snelling H V 1995 *J. Appl. Phys.* 78: 7295–7303
89. Ponnaluri S V, Cherukuri R, Molian P A 2001 *J. Mater. Proc. Technol.* 112: 199–204; and Patri S, Gurusamy R, Molian P A, Govindaraju M 1996 *J. Mater. Sci.* 31: 1693–1702
90. Compaan A D, Matulionis I, Nakade S 2000 *Opt. Lasers Eng.* 34: 15–45

91. Raybould D, Meola M, Bye R, Das S K 1998 *Mater. Sci. Eng.* A241: 191–201
92. Parvathavarthini N, Subbarao R V, Kumar S, Dayal R K, Khatak H S 2001 *J. Mater. Eng. Performance* 10: 5–13
93. Conde A Garcia I, Damborenea J J 2001 *Corrosion Sci.* 43: 817–828
94. Kwok C T, Cheng F T, Man H C 2000 *Surf. Coat. Technol.* 145: 206–214
95. Tsay L W, Yang T Y, Young M C 2001 *Mater. Sci. Eng.* A311: 64–73
96. Peyre P, Braham C, Ledion J, Berthe L, Fabbro R 2000 *J. Mater. Eng. Performance* 9: 656–662
97. Kwok C T, Cheng F T, Man H C 2000 *Mater. Sci. Eng.* A290: 74–88; and Kwok C T, Cheng F T, Man H C 2000 *Mater. Sci. Eng.* A290: 55–73
98. Isshiki Y, Shi J, Nakai H, Hashimoto M 2000 *Applied Physics* A70: 651–656; and Isshiki Y, Shi J, Nakai H, Hashimoto M 2000 *Appl. Phys.* A70: 395–402
99. Dutta Majumdar J, Manna I 1999 *Mater. Sci. Eng.* A267: 50–59
100. Mudali U K, Pujar M G, Dayal R K 1998 *J. Mater. Eng. Performance* 7: 214–220
101. Anjos M A, Vilar R, Qiu Y Y 1997 *Surf. Coat. Technol.* 92: 142–149
102. Akgun O V, Inal O T 1995 *J. Mater. Sci.* 30: 6105–6112
103. Chong H C, Wen T T, Ju L T 1995 *Mater. Sci. Eng.* A190: 199–205
104. Pillai S R, Shankar P, Subba-Rao R V, Sivai N B, Kumaravel S 2001 *Mater. Sci. Technol.* 17: 1249–1252
105. Psyllaki P, Oltra R 2000 *Mater. Sci. Eng.* A282: 145–152
106. Agarwal A, Katipelli L R, Dahotre N B 2000 *Metal. Mater. Trans.* A31: 461–473
107. Chang K C, Wei W J, Chen C 1998 *Surf. Coat. Technol.* 102: 197–204
108. Gutierrez A, Damborenea J 1997 *Oxid. Met.* 47: 259–275
109. Nagarathnam K, Komvopoulos K 1996 *Metal. Mater. Trans.* A27: 381–390
110. Cheng F T, Kwok C T, Man H C 2001 *Surf. Coat. Technol.* 139: 14–24
111. Wu X L, Hong Y S 2000 *Metal. Mater. Trans.* A31: 3123–3127
112. Roy A, Manna I 2001 *Mater. Sci. Eng.* A297: 85–93
113. Agarwal A, Dahotre N B 2000 *Wear* 240: 144–151; and Agarwal A, Dahotre N B 2000 *Met. Mater. Trans.* A31: 401–408
114. Tondu S, Schnick T, Pawlowski L, Wielage B, Steinhauser S, Sabatier L 2000 *Surf. Coat. Technol.* 123: 247–251
115. Pelletier J M, Sauger E, Gachon Y, Vannes A B 1999 *J. Mater. Sci.* 34: 2955–2969
116. Di-Melfi R J, Sanders P G, Hunter B, Eastman J A, Sawley K J, Leong K H, Kramer J M 1998 *Surf. Coat. Technol.* 106: 30–43
117. Zhang X M, Man H C, Li H D 1997 *J. Mater. Proc. Technol.* 69: 162–166
118. Jervis T R, Nastasi M, Jr. Griffin A J, Zocco T G, Taylor T N, Foltyn S R 1997 *Surf. Coat. Technol.* 89: 158–164
119. So H, Chen C T, Chen Y A 1996 *Wear* 192: 78–84
120. Zhukov A A, Dutta-Majumdar J, Manna I 1995 *J. Mater. Sci. Lett.* 14: 828–829
121. Yue T M, Wu Y X, Man H C 1999 *Surf. Coat. Technol.* 114: 13–18
122. Watkins K G, Liu Z, McMahon M, Vilar R, Ferreira M G S 1998 *Mater. Sci. Eng.* A252: 292–300
123. Carvalhoa D, Cardoso S, Vilar R 1997 *Scr. Mater.* 37: 523–527
124. Wong T T, Liang G Y 1997 *Mater. Characterization* 38: 85–89
125. Zhang X M, Man H C, Yue T M 1996 *Scr. Mater.* 35: 1095–1100
126. Katipelli L R, Dahotre N B 2001 *Mater. Sci. Technol.* 17: 1061–1068
127. Prasad N H, Balasubramaniam R 1997 *J. Mater. Process. Tech.* 68: 117–20
128. Choquette K D, Geib K M, Chui H C, Hammons B E, Hou H Q, Drummond T J, Hull R 1996 *Appl. Phys. Lett.* 69: 1385–1387
129. Schnick T, Tondu S, Peyre P, Pawlowski L, Steinhauser S, Wielage B, Hofmann U, Bartnicki E 1999 *J. Thermal Spray Technol.* 8: 296–300
130. Uenishi K, Kobayashi K F 1999 *Intermetallics* 7: 553–559
131. Boulmer-Leborgne C, Thomann A L, Andreazza P, Andreazza-Vignolle C, Hermann J, Craciun V, Echegut P, Craciun D 1998 *Appl. Surf. Sci.* 125: 137–148

132. Liang G Y, Wong T T 1997 *J. Mater. Eng. Performance* 6: 41–45
133. Geng H R, Liu Y, Chen C Z, Sun M H, Gao Y Q 2000 *Mater. Sci. Technol.* 16: 564–567
134. Dutta-Majumdar J, Manna I 1999 *Mater. Sci. Eng.* A268: 227–235; and Dutta Majumdar J, Manna I 1999 *Mater. Sci. Eng.* A268: 216–226
135. Wang A H, Yue T M 2001 *Composites Sci. Technol.* 61: 1549–1554
136. Dube D, Fiset M, Couture A, Nakatsugawa I 2001 *Mater. Sci. Eng.* A299: 38–45
137. Schippman D, Weisheit A, Mordike B L 1999 *Surf. Eng.* 15: 23–26
138. Yue T M, Wang A H, Man H C 1997 *Scr. Mater.* 38: 191–198
139. Manna I, Kondala Rao K, Roy S K, Watkins K G 2000 In *Surface engineering in materials science I* (Conf. Proc.) (eds) S Seal, N B Dahotre, J J Moore, B Mishra (Warandale, PA: TMS) pp. 367–376
140. Zhang D W, Lei T C, Zhang J G, Ouyang J H 1999 *Surf. Coat. Technol.* 115: 176–83
141. Shyh A L, Tung T L, Wen T T 1998 *Scr. Mater.* 38: 559–563
142. Ghosh S, Goswami G L, Biswas A R, Venkataramani R, Garg S P 1997 *Trans. IIM* 50: 287–290
143. Gemelli E, Galerie A, Caillet M 1996 *J. Mater. Sci.* 31: 6627–6630
144. Yilbas B S, Hashmi M S J, Shuja S Z 2001 *Surf. Coat. Technol.* 140: 244–250
145. Dutta Majumdar J, Mordike B L, Manna I 2000 *Wear* 242: 18–27
146. Dutta-Majumdar J, Weisheit A, Mordike B L, Manna I 1999 *Mater. Sci. Eng.* A266: 123–134
147. Cooper K P, Slebodnick P L, Lucas K E, Hogan E A 1998 *J. Mater. Sci.* 33: 3805–3816
148. Fouilland-Paille L, Ettaqi S, Benayoun S, Hantzpergue J J 1997 *Surf. Coat. Technol.* 88: 204–211
149. Weerasinghe V M, West D R F, de-Damborenea J 1996 *J. Mater. Process. Tech.* 58: 79–86
150. Masse J E, Mathieu J F 1996 *Mater. Manuf. Proc.* 11: 199–206
151. Klement W, Willens R H, Duwez P *Nature (London)* 187: 869
152. Cohen M H, Turnbull D 1959 *J. Chem. Phys.* 31: 1164
153. Turnbull D 1969 *Contemp. Phys.* 10: 473 [cited after ref. 151]
154. Lin C J, Spaepen F 1982 *Appl. Phys. Lett.* 41: 721
155. Snezhnoi R L, Zhukov A A, Kokora A N 1980 *Mater. Sci. Heat Treatment* 22: 900
156. Bergmann H W, Mordike B L 1980 *Z. Metallkde* 71: 658
157. Bergmann H W, Mordike B L 1981 *J. Mater. Sci.* 16: 863
158. Borodina G G 1981 *Sov. Phys. Dokl.* 26: 761
159. Von Allmen M, Affolter K 1984 *Proc. Mater. Res. Soc.* 28: 81
160. Lin C J, Spaepen F 1984 *Proc. Mater. Res. Soc.* 28: 75
161. Lin C J, Spaepen F, Turnbull D 1984 *J. Non-Crys. Solids* 61–62: 767
162. Den Broeder F J A, Vandenberg J M, Draper C W 1984 *Thin Solid Films* 111: 43
163. Hashimoto K, Kumagai N, Yoshioka H, Asami K 1990 *Mater. Manuf. Proc.* 5: 567
164. Kumagai N, Samata Y, Kawashima A, Asami K, Hashimoto K 1986 *J. Non-Cryst. Solids* 93: 78
165. Kumagai S, Samata Y, Jikihara S, Kawashima A, Asami K, Hashimoto K 1988 *Mater. Sci. Eng.* 99: 489
166. Yoshioka H, Asami K, Hashimoto K 1984 *Scr. Metall.* 18: 1215
167. Yoshioka H, Asami K, Kawashima A, Hashimoto K 1985 *Rapidly quenched metals* (eds) S Steels, H Warlimont (Amsterdam: Elsevier) vol. 1, p. 123
168. Kumagai N, Asami K, Hoshimoto K 1986 *J. Non-Cryst. Sol.* 87: 123
169. Yoshioka H, Asami K, Kawashima A, Hashimoto K *Corros. Sci.* 27: 981
170. Kumagai N, Jikihara S, Kawashima A, Asami K, Hashimoto K 1989 In *Proc. of MRS Int. Meeting on Advanced Materials* (Conf. Proc.) vol. 3, p. 267
171. Froehlingsdorf J, Stritzker B 1986 *Laser surface treatment of metals. NATO ASI Series E: Applied Sciences No. 115* (eds) C W Droper, P Mozzoldi (Boston: Martinus Nijhoff)
172. Kear B W, Breinon E M, Greenwald L E *Metals Technol.* 6: 121
173. Spaepen F 1986 *Laser surface treatment of metals. NATO ASI Series E: Applied Sciences No. 115* (eds) C W Droper, P Mozzoldi (Boston: Martinus Nijhoff) p. 81
174. Gaffet E, Deluze G, Martin G, Pelletier J M, Pergue D 1988 *Mater. Sci. Eng.* 98: 291
175. Yablonovitch E, Gmitter T J 1992 *Solid-State Electron.* 35: 261–267

176. Lewis G K, Schlienger E 2000 *Mater. Design* 21: 417–423
177. Skolbelkin O K, Manenkov A A, Litvin G D, Eliseenko V I, Denisov N N, Bagdasarov V K, Starkovsky A M, Yakimenko A P 1993 *Lasers Life Sci.* 5: 243–246
178. Dubrujeaud B, Fontes A, Forget P, Papaphilippou C, Sainte C C, Vardavoulias M, Jeandin M *Surf. Eng.* 13: 461–470
179. Lin L 2000 *Opt. Lasers Eng.* 34: 231–253
180. Mordike B L 1997 *Progr. Mater. Sci.* 42: 357–372
181. Bamberger M 1998 *Int. Mater. Rev.* 43: 189–203
182. Vilar R 1999 *Mater. Sci. Forum* 301: 229–252
183. Peyre P, Merrien P, Lieurade H P, Fabbro R 1995 *Surf. Eng.* 11 1, 47, Peyre P, Fabbro R, Merrien P, Lieurade H P 1996 *Mater. Sci. Eng.* A210: 102
184. Folkes J 1997 *Mater. Sci. Forum* 246: 261–278
185. Mukherjee K, Majumdar J 1985 (eds) *Laser processing of materials* (New York: Am Inst. Mining, Metall. Petroleum Eng.)
186. Mazumder J, Mohanty P S, Kar A 1996 *Int. J. Mater. Product Technol.* 11: 193–252
187. Walker H A, Steen W M, West D R F 1985 *Laser processing of materials* (eds) K Mukherjee, J Mazumder (Warrendale PA: The Metall. Soc. AIME) p. 169
188. Ashby M F, Easterling K E 1984 *Acta. Metall.* 32: 1935
189. Eric A Brandes (ed.) *Smithells metals reference book* (London: Butterworths) pp. 11–379, 940
190. Belforte D, Levitt M (eds), *The industrial annual handbook* (Tulsa: Pennwell) p. 209
191. Roy A, Manna I 2001 *Opt. Lasers Eng.* 34: 369–383
192. Roy A, Manna I 1997 *Indian Foundry J.* 43: 15–22
193. Manna I, Reddy G, Abraham S, Ghosh T B, Bose D N, Pabi S K 1994 *Scr. Metall. Mater.* 31: 713–718
194. Dutta Majumdar J, He X, Weisheit A, Mordike B L, Manna I 1998 *Lasers Eng.* 7: 89–102
195. Manna I, Dutta Majumdar J, Chatterjee U K, Nath A K 1996 *Scr. Mater.* 35: 405–410
196. Manna I, Roy S K 1993 *Indian Foundry Journal* 39: 11–21
197. Manna I, Dutta Majumdar J, Rambabu D, Bharti A, Joshi S V 1995 *Steel India* 18: 1–6
198. Manna I, Dutta Majumdar J 1995 *Z. Metallkde.* 86: 362–364
199. Manna I, Steen W M, Watkins K G 2000 In *Surface engineering in Materials Science I* (Conf. Proc.), (eds) S Seal, N B Dahotre, J J Moore, B Mishra (Warandale, PA: TMS) pp. 377–384
200. Manna I, Steen W M, Watkins K G 1997 *Scr. Mater.* 37: 561–568
201. Watkins K G, Steen W M, Manna I, Williams D F, Rhodes S, Mazzoldi P, Russo S L, Ferreira M G S, Rito J T, Silva T M, Simoes A M P 1996 In *ICALEO'96 – Laser Materials Processing and Surface Modification* (Conf. Proc.), (eds) W Duley, K Shibata, R Poprawe (Laser Inst. of America) vol. A81, pp. 37–46
202. Manna I, Roy A, Watkins K G, Steen W M 1999 In *Proceedings of the 6th Asian Foundry Congress* (Conf. Proc.), (eds) A K Chakrabarti, B K Dhindaw, G L Dutta, C S Sivaramakrishnan (Calcutta: Inst. Indian Foundrymen) p. 153–159
203. Sinha V, Goswami G L, Kale G B, Manna I 2000 In *Surface engineering in materials science I* (Conf. Proc.), (eds) S Seal, N B Dahotre, J J Moore, B Mishra (Warandale, PA: TMS) p. 131–140
204. Dutta Majumdar J, Ashok Kumar B V S, Manna I (unpublished work)
205. Manna I, Dutta Majumdar J, Das P K 1995 In *Int. Conf. Advances in Physical Metallurgy (ICPM)* (Conf. Proc.) (eds) S Banerjee, R V Ramanujan (New York: Gordon & Breach) p. 49–54